UNCLASSIFIED

CRATERING AND PENETRATION

by

E. P. Palmer, N. P. Bailey, G. H. Turner, C. E. McDermott,

S. M. Taylor, and R. V. Bunnag

Final Report and
Fifth Quarterly Program Progress Report
Contract AF 04(694)-259

30 September 1963

Prepared for
Air Force Ballistic Systems Division
Air Force Systems Command
Norton Air Force Base, California

UNCLASSIFIED

UNCLASSIFIED

CRATERING AND PENETRATION

by

E. P. Palmer, N. P. Bailey, G. H. Turner, C. E. McDermott,
S. M. Taylor, and R. V. Bunnag

Final Report and
Fifth Quarterly Program Progress Report
Contract AF 04(694)-259

30 September 1963

Prepared for
Air Force Ballistic Systems Division
Air Force Systems Command
Norton Air Force Base, California

UNCLASSIFIED

TABLE OF CONTENTS

SUMMARY

This Fifth Quarterly Report and Final Report on Contract AF 04(694)-259 summarizes previously reported theoretical and experimental work and includes unreported work on cratering and penetration.

Work is reported in six areas as follows.

1. Energy Partitioning in Impact. Techniques and results are summarized for measurements of target heating, target mass loss, spray energy, and recrystallization and strain energy. Progress is reported on the measurement of transient temperature distributions in impact and on the measurement of energies involved in deformation. The conclusions of a brief theoretical study of shock heating and its comparison with observed target heating are given.

2. Material Properties. The formulation of a general equation describing the relation between pressure, specific volume, and internal energy of a material is reported and the comparison with existing data for gases, for static compression of liquids and metals, and for shock compression of metals is reviewed. New work on energy-storage transitions is reported.

3. Wave Motion in Impact. Theoretical and experimental studies of wave motion in idealized systems which can be described by one space variable are summarized. It is found that the product of stress, velocity, and area is constant at the wave front. Plane shock wave propagation is discussed and plots of pressure-velocity relations for six metals are given and their utility in impact

scaling laws is demonstrated.

4. Transient Measurements in Impact. Work on the measurement of subsurface pressure waves using buried barium-titanate pressure-transducers is summarized along with uncompleted work on surface-wave motion.

5. Spray-Particle Generation. Work on the role of spray particles in impact flash is summarized. A preliminary report is given on the generation of spray particles and material flow in the penetration of thin targets.

6. Impact Theory. Work on correlating impact parameters with material velocity and with the product of pressure velocity and area is reported. The best correlation is with velocity but this is not satisfactory. A kinematic theory of lead cratering is summarized. The need for additional data on material flow properties is pointed out.

It is concluded that significant new information on the details of the impact process has been found and new techniques of measurement developed. Recommendations for future work in the above areas are made.

I. INTRODUCTION

The purpose of work done under Contract No. AF 04(694)-259 has been to develop theory describing the phenomena which occur during high-velocity impact. The theory must be general enough to include all phenomena of importance in target damage and spray particle generation and must be applicable to a wide variety of materials and conditions. The behavior of single and two-layer thin targets was of particular interest, although the actual work concentrated on investigations of cratering in semi-infinite metal targets. This emphasis occurred because of the necessity of building on the great amount of experimental and theoretical material available for thick-target impact. The plan of investigation used in this research has been to begin with simple, idealized models which illustrate various phases of the problem and to study their behavior experimentally and theoretically. These models are then modified and combined in the formulation of more comprehensive models. In carrying out this program, work was done, and progress will be reported in the areas as follows:

1. The investigation of energy partitioning in impact and the development of theory based on this.
2. The investigation of material properties and the formulation of suitable mathematical descriptions of material-property behavior.
3. The investigation of wave propagation in various systems and materials of interest in high velocity impact.
4. Measurements of transient behavior during impact.
5. The investigation of spray-particle generation.

6. The development of theory.

These research projects have resulted in the generation of considerable fundamental information of interest and value. The projects were necessarily limited because of the time and manpower available, and engineering applications of the results, unfortunately, could not be made. The reports prepared during the contract will be listed in Section 2. The individual projects will be described and progress reported in Section 3. Reference will be made to previously published reports and their contents will be briefly summarized. Unreported work in each project will be given.

As with any fundamental research in a new area, much of the work has been exploratory and uncompleted. Recommendations for future work, based on the achievements of this contract, will be made. During the last quarter of the contract, several projects were instituted which could not be completed as far as expected. A recommendation for a brief program to further complete these projects will be made.

2. REPORTS

Five quarterly reports including this one have been published and distributed under the contract. Four technical documentary reports have been prepared and distributed. They are:

Absolute Luminosity, Size, and Velocity of Individual Laboratory Micrometers by J. C. Bryner, E. P. Palmer, and R. R. Kadesch, Technical Report UU-10, BSD-TDR-62-270, July 1962.

Stored Energy of Compressed Metals from Shock and Static Tests by N. P. Bailey, Technical Report UU-11, BSD-TDR-63-112.

Wave Front Solutions in Linear and Nonlinear Media by C. E. McDermott and N. P. Bailey, Technical Report UU-12, BSD-TDR-63-131.

Stress-Time Measurements in High-Velocity Impact by S. M. Taylor, E. P. Palmer, R. R. Kadesch, Technical Report UU-13, BSD-TDR-63-152.

These reports have provided the material for three Ph.D. theses, one Master's thesis, and two Bachelor Theses. It is expected that one additional Ph.D. and one Master's thesis will result from this material. An additional technical documentary report combining and analyzing all the data on energy partitioning is contemplated if the contract can be extended for a three-month period.

3. PROJECTS

3.1 Energy Partitioning in Impact

This project is concerned with determining the distribution of energy among the various competing processes occurring in cratering and penetration and with determining the effects of different material properties, geometry, and impact velocity on this energy distribution. The purpose is to provide information necessary to formulate impact theory from models which adequately describe the physical processes involved.

In the four previous quarterly progress reports, details relating to the experimental determination of energy distribution for the impact of steel spheres into lead targets have been reported. In this work, it was assumed that the kinetic energy of the projectile is partitioned into three categories:

1. Energy appearing as heat in the target.
2. Energy leaving the target with spray-particle material.
3. Energy associated with recrystallization or appearing as "locked-in" strain energy in the target material.

The distribution of energy in these three categories has been determined for

projectile velocities up to 2.0 km/sec.

Target Heating. The method of determining the fraction of the projectile kinetic energy appearing as heat in the target was developed under Contract AF 04(647)-942 and preliminary results were reported in Technical Report BSD-TDR-62-185. Complete results up to date are given in the Third Quarterly Report under this contract. The method used to make these measurements consisted of using a target block as a calorimeter and measuring its temperature rise with a thermocouple imbedded in the target material. This temperature rise was then related to the energy and compared to the projectile kinetic energy.

Spray-Particle Energy. The energy associated with spray particles was measured by using small lead boxes as calorimeters in which the spray material was caught and the energy involved computed from the resulting temperature rise. Again, thermocouples were used to measure the temperature changes. This work is described in the Second Quarterly Report.

The spacial distribution of mass loss in spray particles was investigated by catching the spray particles in a hemispherical shell of gelatin and recovering them. This work is described in the First Quarterly Report.

Spray-particle velocities were roughly measured using spark shadowgraph pictures of the impact. This work is reported in the first Quarterly Report.

Attempts were made to measure spray-particle momentum with a ballistic pendulum. Difficulties involved in using the small target vacuum tank available made this impractical at the time and this project was abandoned. Spray-particle velocities were measured using particle detectors. The presence of small fast particles, with the large slow particles which make

up the bulk of the spray, made these results invalid as far as measuring energy distributions in the spray material. This project was abandoned. Velocity measurements could not be made accurately enough to allow a determination of the relative amounts of thermal energy and kinetic energy in spray material. It was only determined that the majority of the energy leaving the system as spray particles is in the form of kinetic energy.

Recrystallization and Strain Energy. The fraction of the energy associated with recrystallization and strained energy was determined by shooting a projectile into an enclosed cavity in a target block used as a calorimeter. Under these conditions all of the spray-particle energy is contained in the target and converted into heat and the difference between the energy appearing as heat and the initial kinetic energy of the projectile represents the energy going into recrystallization and strain energy. A slight correction must be made to account for the strain energy produced by the spray particle impacts which would not ordinarily appear in the target. This work is reported in the Third Quarterly Report.

A summary of the energy-partitioning work was presented in the Fourth Quarterly Report. This shows that the fraction of energy in each of the major categories changes with velocity. For this reason, it was determined that additional data should be obtained at velocities above 2 km/sec, which is well into the range of fluid-like impact for lead. In order to do this, a light-gas gun must be used, so considerable time was spent during the fifth quarter in preparing the light-gas gun for operation. Unfortunately, this could not be completed and no data shots were obtained. During the quarter, target calorimeters were prepared to obtain this data. It is expected that it can be obtained in a short additional time either

through use of the light-gas-gun facility at Utah Research and Development Company or using our own gun.

Although these data are only for lead, they represent the first exploratory work into the important area of energy partitioning and provide the first valid basis for the extrapolation of theory to new conditions. They provide an additional body of data for testing theory besides the large amount of information on hole size and shape.

Transient Target Temperatures and Shock Heating. A project to measure the transient temperatures throughout a target during the cratering process was begun. Its purpose was to provide a means for determining the place of deposition of energy. This provides a means of testing any theory which purports to give wave strength at various places within the target or other details of the transient phenomena involved. Preliminary work in this area is described in the Fourth Quarterly Report. During this report period, additional targets were prepared and data were taken. Consistent results were not obtained and results cannot be reported at this time. The principal difficulty experienced was that of being unable to obtain sufficient gain from the available amplifiers to record the output from an individual thermocouple. A high-gain, fast-response amplifier was obtained but could not be put into operation in time for results to be reported here. Recommendations for an extension of this work will be made in Section 5.

Some experiments were conducted to attempt to measure the target temperature in the flowing surface of a forming crater. A tiny thermocouple was imbedded in a target and arranged so that the eroding crater surface would contact the thermocouple wires and form the junction. Inconsistent

results were obtained in the few shots made. Indicated temperatures ranged from a few hundred degrees up to those expected behind a shock wave at the impact velocities used, or 1300 °K.

The preliminary results obtained as to the place of energy deposition in impact led to the suspicion that shock heating, which is the only means of heat generation in an invisid-flow theory of cratering, is inadequate to explain the highly localized heat deposition observed. To check this, approximate calculations of the expected shock heating were performed and were reported in the Fourth Quarterly Report. It was concluded from this that shock heating could not account for the observed temperature distributions in targets. It appears that another energy dissipating mechanism exists comparable in magnitude to the shock-heating mechanism. It was surmised that this has to do with the energy needed to break bonds and cause material to flow and the frictional energy involved in flow. This is an area in which much work has been done on the combined stress-strain and flow properties of materials such as rubber, asphalt, resins, etc. at relatively low velocities. Its applicability to high-velocity impact is limited because of the materials involved, the velocities used, and the lack of a comprehensive two-dimensional theory of flow to describe the results. No comparable work has been done for the conditions of interest in high-velocity impact.

A careful determination of surface material displacement was made for one case of impact in a lead target. This work was reported in the Third Quarterly Report. It again indicated the highly localized deposition of energy in impact. The information was used along with other information from energy partitioning in the formulation of a kinematic theory describing

cratering for the case investigated. This is discussed in Section 3.6 below.

Energy of Deformation. To explore the possibility of measuring the actual energy going into deformation in high-velocity impact, a new project was initiated during the last quarter. If a cylindrical projectile is shot against a similar cylindrical target which is stationary but free to move, the target and projectile are equally deformed and a measurement of impact velocity and the knock-on velocity of either the target or projectile allows the amount of energy going into internal energy to be calculated. The impact velocity must be low enough so that no mass is lost from the target or projectile. From the following equations, it is seen that a simple measurement of the ratio of impact-velocity to target-velocity allows the fraction of energy going into internal energy to be calculated.

For a cylinder of mass m impacting a similar cylinder, the momentum equation is

$$m v_1 = m u_1 + m u_2$$

v_1 = velocity of projectile before impact

u_1 = velocity of projectile after impact

u_2 = velocity of target after impact

The energy equation is

$$\frac{1}{2} m v_1^2 = \frac{1}{2} m u_1^2 + \frac{1}{2} m u_2^2 + f\left(\frac{1}{2} m v_1^2\right)$$

where f is the fraction of the original kinetic energy which appears as

internal energy of the target and projectile. Eliminating u and solving for f gives

$$f = \frac{2u_2}{v_1} - \frac{2u_2^2}{v_1^2}$$

By relating the observed deformation and the observed energy, an insight can be gained into the actual energy involved in deformation and in impact. The program was to shoot projectiles of various materials and various lengths at similar targets over velocities ranging from that where the impact is purely elastic up to velocities where material is lost from the target-projectile system.

To make the measurements of projectile velocity and target velocity and to produce a precisely aligned impact, the system shown schematically in Fig. 1 was developed.

During this report period, the system was tested, and the gun and gun-barrel velocity-measuring system were found to work successfully. Precisely controlled and aligned impacts could be obtained. The target and projectile could be recovered undamaged. It was found that velocities up to 1.5 km/sec could be used successfully with copper rods. Throughout the test period, the target velocity was not measured successfully. The tests were conducted in the open air and shock waves caused false timing signals, grid wires stretched before breaking and other difficulties prevented the obtaining of correct velocities. This work is believed to be of considerable importance since, as far as is known, it represents the first attempt to measure the energies involved in flow under the high-pressure conditions met in high velocity impact. This experimental work will be continued and an

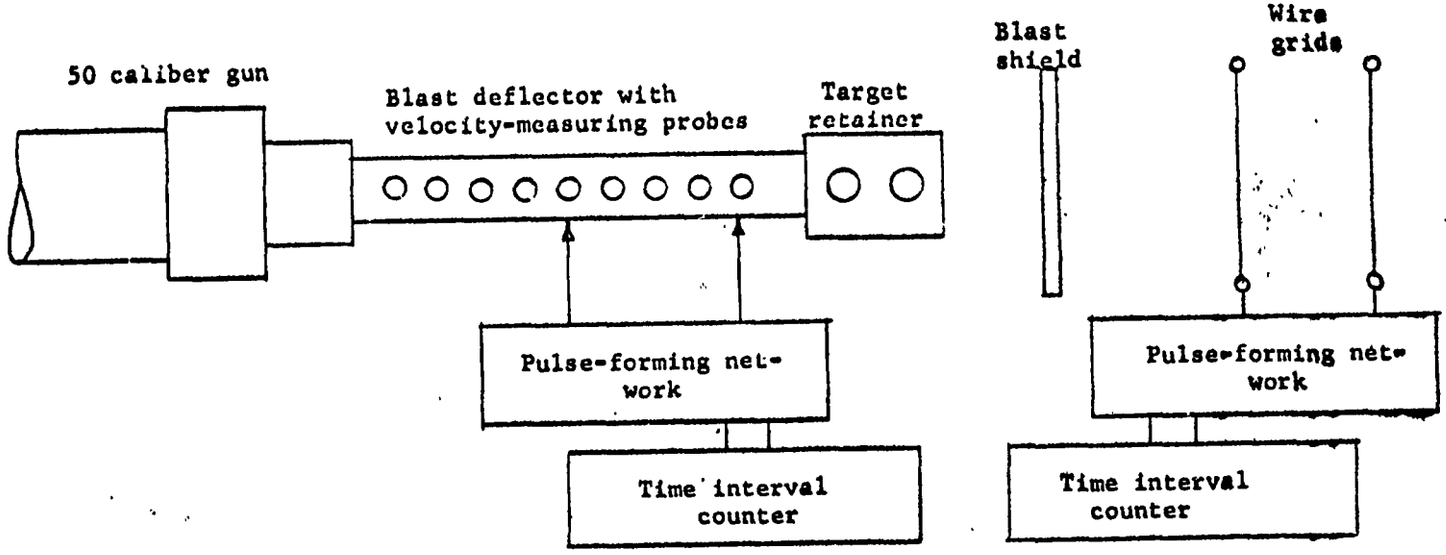

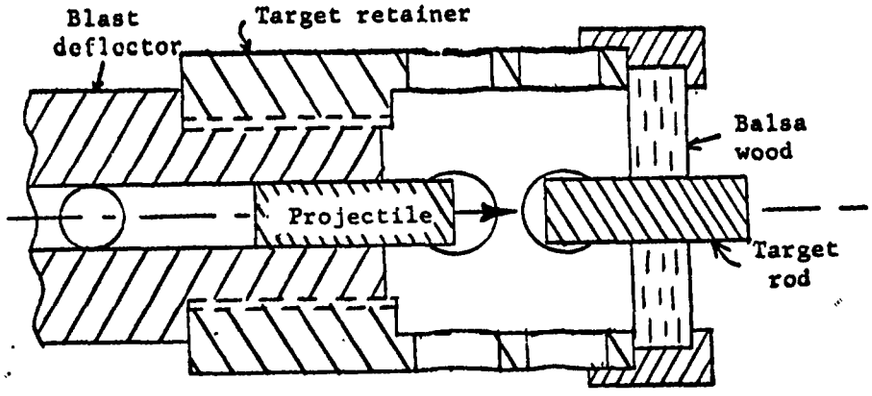

Fig. 1. Schematic diagram of system for measuring energy of deformation by measuring projectile velocity and target "Knock-on" velocity.

analysis of the data made if the time period of this contract is extended. This simple experiment could be extended for considerable additional useful information by using high-speed photography to observe the deformation as it occurrs and possibly by using calorimetry to measure the heat involved and to determine the fractions of internal energy going into heat and into strain energy.

3.2 Material Properties

The goal of this project is to be able to describe material properties under conditions met in high velocity impact by general mathematical expressions instead of by tables of numerical data. With simplified descriptions of material properties, more complex porcesses may be successfully investigated. In any investigation of flow phenomena, no progress can be made unless the material involved can be accurately described under all of the conditions met in the problem. Consequently, one of the major goals of the work under the present contract has been to obtain useful descriptions of material properties. This effort has been notably successful in that an "equation of state" has been discovered which is generally applicable in the compression of gases, liquids, and metals from low pressures up to the very high pressures involved in high velocity impact. The equation is of the form

$$\frac{u}{pv} = mu^k$$

where u is internal energy, p pressure, v volume, and m and k are constants. It was found that this equation describes the compression data of Bridgeman

and the Los Alamo shock-compression data for metals. It also describes the Bridgeman compression data for liquids. The theoretical basis for this equation has been developed. This work is reported in Technical Report UU-II referred to in Section 2.

After the publication of this report, it was discovered that the equation is not strictly valid for processes such as adiabatic expansions involving p and v separately. It appears to apply generally where the product pv is involved such as in shock-wave compressions. This general equation then serves as a complete equation of state for gases over certain limited regions and possibly other materials. At the present time, however, it can only be used as the equation of a particular process; in this case, the shock compression or the static compression of metals. The limits of its validity are unknown beyond the data available. A further work of greatest importance is a further analysis of this equation to understand its complete significance in order that similar equations can be developed for other processes. Its simplicity and utility spur the hope that similar results can be obtained for the other processes.

During the past quarter, the energy-storage transitions, denoted by changes in the value of k for a given material, were investigated more fully. The results of this work are reported in Appendix A attached to this report.

3.3 Wave Motion in Impact

The transport of energy in the impact region by means of wave motion is of fundamental importance in impact phenomena. A program of theoretical

and experimental investigation of wave motion for a variety of materials for various impact geometries was undertaken. The goal was to provide basic understanding necessary for the formulation of accurate theoretical models of the overall cratering and penetration process.

Analysis of Idealized Systems. One project carried out in this area has consisted of the theoretical and experimental investigation of simplified systems which could be analyzed. This work has been completed and reported in Technical Report UU-12 referred to in Section 2. The work consisted of the analysis of waves in linear materials for a wave propagating down a bar, along a cone, along an exponential plate, in a radial direction in a cylinder, and in spherical geometry. Wave front conditions were analyzed under the approximation that the wave could be described by one space variable and remained plane in the case of the bar, cone, and exponential plate. With these assumptions, it was found that the product of stress, area, and velocity at the wave front remained constant for constant-velocity or constant-pressure impact conditions. This allows a great simplification in the description of wave propagation. For the case of plane waves in nonlinear materials such as a gas, it was also found that the product of stress, area, and velocity was constant.

Shock-Wave Properties of Metals. A second project in this area, which as been previously unreported, consisted of the calculation of shock-wave conditions for the impact of two dissimilar materials using the equation of state derived under the material studies. This work will be reported here for completeness since it provides a useful body of data for anyone concerned with impact problems.

Figure 2 shows the system considered with the usual variables of wave

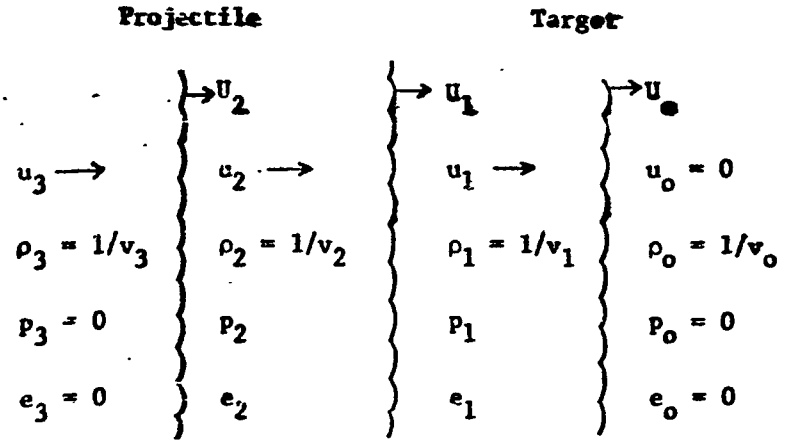

Fig. 2. Variables for plane impact of two materials. Laboratory frame of reference.

velocity U, material velocity u, density ρ, pressure p, internal energy e, and specific volume v. Note that u is used for internal energy in other sections of this report. The context makes the usage clear.

The shock relations for the target material (subscripts o, 1) are as follows:

Mass:

$$\rho_o U_o = \rho_1 (U_o - u_1)$$

$$\frac{\rho_1}{\rho_o} = \frac{U_o}{U_o - u_1}$$

$$U_o = \frac{\rho_1 U_1}{\rho_1 - \rho_o} \qquad (1)$$

define

$$\mu_1 = \frac{\rho_1 - \rho_o}{\rho_o} = \frac{v_o}{v_1} - 1 \qquad (2)$$

then

$$U_o = \frac{(\rho_1/\rho_o)\, u_1}{(\rho_1 - \rho_o)/\rho_o} = \frac{1}{\mu_1} \frac{\rho_1}{\rho_o}\, u_1 \qquad (3)$$

or

$$u_1 = \frac{\rho_1 - \rho_o}{\rho_1} U_o = \mu_1 \left(\frac{\rho_o}{\rho_1}\right) U_o$$

Force:

$$\rho_1 u_1 (u_1 - U_o) = -p_1 \qquad (4)$$

using Eq. 1

$$p_1 = \rho_o U_o u_1 \qquad (5)$$

Energy:

$$\rho_1 \left(\frac{1}{2} u_1^2 + e_1\right)(u_1 - U_o) = -p_1 u_1 \qquad (6)$$

using Eq. 1

$$p_1 u_1 = \rho_o U_o \left(\frac{1}{2} u_1^2 + e_1\right) \qquad (7)$$

using Eq. 5

$$\rho_o U_o v_1^2 = \rho_o U_o \left(\frac{1}{2} u_1^2 + e_1\right)$$

$$e_1 = \frac{1}{2} u_1^2 \tag{8}$$

The shock relations for the projectile material (subscripts 2, 3) are as follows:

Mass:

$$\rho_2 (u_2 - U_2) = \rho_3 (u_3 - U_2)$$

$$\frac{\rho_2}{\rho_3} = \frac{u_3 - U_2}{u_2 - U_2}$$

$$\rho_2 u_2 - \rho_2 U_2 = \rho_3 u_3 - \rho_3 U_2$$

$$(\rho_3 - \rho_2) U_2 = \rho_3 u_3 - \rho_2 u_2$$

$$U_2 = \frac{\rho_3}{\rho_3 - \rho_2} u_3 - \frac{\rho_2}{\rho_3 - \rho_2} u_2 \tag{9}$$

define

$$\mu_2 = \frac{\rho_2 - \rho_3}{\rho_3} = \frac{v_3}{v_2} - 1 \tag{10}$$

using Eq. 10 and Eq. 9 and the fact that $u_2 = u_1$

$$U_2 = \frac{u_2}{\mu_2}\frac{\rho_2}{\rho_3} - \frac{u_3}{\mu_2} = \frac{u_1}{\mu_2}\frac{\rho_2}{\rho_3} - \frac{u_3}{\mu_2} \tag{11}$$

Force:

$$\rho_3 u_3 (u_3 - U_2) - \rho_2 u_2 (u_2 - U_2) = p_2$$

using Eq. 9

$$\frac{\rho_3 u_3 (u_3 - U_2)}{\rho_3 (u_3 - U_2)} - \frac{\rho_2 u_2 (u_2 - U_2)}{\rho_2 (u_2 - U_2)} = \frac{p_2}{\rho_2 (u_2 - U_2)} = \frac{p_2}{\rho_3 (u_3 - U_2)} \tag{12}$$

$$u_3 - u_2 = \frac{p_2}{\rho_2 (u_2 - U_2)} = \frac{p_2}{\rho_3 (u_3 - U_2)} = u_3 - u_1 \tag{12}$$

Energy:

$$\rho_3 \left(\frac{1}{2} u_3^2\right)(u_3 - U_2) - \rho_2 \left(\frac{1}{2} u_2^2 + e_2\right)(u_2 - U_2) = p_2 u_2 \tag{13}$$

using Eq. 9

$$\frac{\rho_3 \frac{1}{2} u_3^2 (u_3 - U_2)}{\rho_3 (u_3 - U_2)} - \frac{\rho_2 \left(\frac{1}{2} u_2^2 + e_2\right)(u_2 - U_2)}{\rho_2 (u_2 - U_2)} = \frac{p_2 u_2}{\rho_2 (u_2 - U_2)} = \frac{p_2 u_2}{\rho_3 (u_3 - U_2)}$$

$$\frac{1}{2} u_3^2 - \left(\frac{1}{2} u_2^2 + e_2\right) = \frac{p_2 u_2}{\rho_2 (u_2 - U_2)} = \frac{p_2 u_2}{\rho_3 (u_3 - U_2)} \tag{14}$$

using Eq. 14 in Eq. 12.

$$\frac{1}{2} u_3^2 - \frac{1}{2} u_2^2 - e_2 = u_2(u_3 - u_2) = u_2 u_3 - u_2^2$$

$$e_2 = \frac{1}{2}\left(u_3^2 - 2u_2 u_3 + u_2^2\right) = \frac{1}{2}(u_3 - u_2)^2$$

$$= \frac{1}{2}(u_3 - u_1)^2 \qquad (15)$$

The Hugoniot equation may be written as follows

$$e_1 - e_o = \frac{p_1 - p_o}{2}(v_o - v_1) = \frac{(p_1 - p_o)}{2} v_1\left(\frac{v_o}{v_1} - 1\right)$$

If $e_o = p_o = 0$

$$e_1 = p_1 v_1 \frac{1}{2} \mu_1$$

Using this relation, the Bailey equation of compression $e/pv = me^k$ (see Section 3.2) may be written in the form

$$\frac{e_1}{p_1 v_1} = m_1 e_1^{k_1} = \frac{1}{2} \mu_1$$

Thus

$$\mu_1 = \frac{\rho_1 - \rho_o}{\rho_o} = \frac{v_o}{v_1} - 1 = M_1 e_1^{k_1}$$

$$\frac{\rho_1}{\rho_o} = M_1 e_1^{k_1} + 1 \tag{16}$$

$$\mu_2 = \frac{\rho_2 - \rho_3}{\rho_3} = \frac{v_3}{v_2} - 1 = M_2 e_2^{k_2}$$

$$\frac{\rho_2}{\rho_3} = M_2 e_2^{k_2} + 1 \tag{17}$$

These equations, which essentially describe the material in the compression process, can be used to solve the various shock relations in terms of one unknown. As will be seen, it is convenient to solve for the unknowns in terms of the material velocity.

For the target material we have the following equations:

Using Eqs. 16, 3, and 8

$$U_o = \frac{1}{\mu_1} \frac{\rho_1}{\rho_o} u_1 = \frac{\left(M_1 e_1^{k_1} + 1\right) u_1}{M_1 e_1^{k_1}} \tag{18}$$

$$U_o = \frac{\left[M_1\left(\frac{1}{2} u_1^2\right)^{k_1} + 1\right] u_1}{M_1\left(\frac{1}{2} u_1^2\right)^{k_1}} \tag{18a}$$

define

$$M_1\left(\frac{1}{2}\right) = L_1 \tag{19}$$

$$U_o = \left(1 + \frac{1}{L_1 u_1 2k_1}\right) u_1 \tag{20}$$

Using Eq. 20 in Eq. 5

$$p_1 = \rho_o u_1^2 \left(1 + \frac{1}{L_1 u_1 2k_1}\right) \tag{21}$$

Using Eq. 20 in Eq. 1

$$\rho_1 = \rho_o \frac{U_o}{U_o - u_1} = \rho_o \frac{1}{1 - \frac{u_1}{U_o}}$$

$$= \rho_o \frac{1}{1 - \frac{1}{1 + \frac{1}{L_1 u_1 2k_1}}} = \rho_o \frac{1 + \frac{1}{L_1 u_1 2k_1}}{1 + \frac{1}{L_1 u_1 2k_1} - 1}$$

$$= \rho_o \frac{1 + \frac{1}{L_1 u_1 2k_1}}{\frac{1}{L_1 u_1 2k_1}} = \left(L_1 u_1^{2k_1} + 1\right) \rho_o \tag{22}$$

The same procedure may be used for the projectile material. Using Eq. 17 in Eqs. 11 and 15,

$$U_2 = \frac{u_1}{\mu_2}\frac{\rho_2}{\rho_3} - \frac{u_3}{\mu_2} = \frac{u_1\left(M_2 e_2^{k_2} + 1\right)}{M_2 e_2^{k_2}} - \frac{u_3}{M_2 e_2^{k_2}} \tag{23}$$

$$U_2 = \frac{u_1\left\{M_2\left(\frac{1}{2}\right)^{k_2}\left[\left(u_3 - u_1\right)^2\right]^{k_2} + 1\right\} - u_3}{M_2\left(\frac{1}{2}\right)^{k_2}\left[\left(u_3 - u_1\right)^2\right]^{k_2}} \tag{23a}$$

define

$$M_2\left(\frac{1}{2}\right)^{k_2} = L_2 \tag{24}$$

$$U_2 = \frac{u_1\left\{L_2\left[\left(u_3 - u_1\right)^2\right]^{k_2} + 1\right\} - u_3}{L_2\left[\left(u_3 - u_1\right)^2\right]^{k_2}}$$

$$U_2 = u_1\left[1 - \frac{u_3 - u_1}{u_1 L_2\left[\left(u_3 - u_1\right)^2\right]^{k_2}}\right] \tag{25}$$

Using Eq. 17 in Eq. 12

$$p_2 = \rho_3(u_3 - U_2)(u_3 - u_1) = \rho_3(u_3 - u_1)\left(u_3 - \frac{u_1}{\mu_2}\frac{\rho_2}{\rho_3} + \frac{u_3}{\mu_2}\right)$$

$$= \rho_3(u_3 - u_1)\left[\frac{u_3(\mu_2 + 1)}{\mu_2} - \frac{u_1(\rho_2/\rho_3)}{\mu_2}\right] \qquad (26)$$

from Eq. 26

$$p_2 = \rho_3(u_3 - u_1)\left[u_3\left(1 + \frac{1}{\mu_2}\right) - u_1\frac{(\mu_2 + 1)}{\mu_2}\right]$$

$$= \rho_3(u_3 - u_1)\left[u_3 + \frac{u_3}{\mu_2} - u_1 - \frac{u_1}{\mu_2}\right]$$

$$= \rho_3(u_3 - u_1)\left[(u_3 - u_1) + \frac{(u_3 - u_1)}{\mu_2}\right]$$

$$= \rho_3(u_3 - u_1)\left[(u_3 - u_1) + \frac{(u_3 - u_1)}{M_2 e_2}k_2\right]$$

$$p_2 = \rho_3(u_3 - u_1)\left[(u_3 - u_1) + \frac{(u_3 - u_1)}{L_2(u_3 - u_1)}2k_2\right]$$

$$p_2 = \rho_3 (u_3 - u_1)^2 + \frac{\rho_3}{L_2} \frac{(u_3 - u_1)^2}{(u_3 - u_1)^{2k_2}}$$

$$= \rho_3 (u_3 - u_1)^2 \left[1 + \frac{1}{L_2 (u_3 - u_1)^{2k_2}} \right] \tag{27}$$

Using Eq. 25 in Eq. 9 we find

$$\rho_2 = \rho_3 \left[L_2 \left[(u_3 - u_1)^2 \right]^{k_2} + 1 \right] \tag{28}$$

It is seen that the equations for energy, pressure, and density in target and projectile are symmetrical in u_1 and $u_3 - u_1$. (Compare Eqs. 8 and 15; 21 and 27; 22 and 28.) Because of this, a single plot of any of these properties versus material velocity may be used for a given material considered as target or projectile.

If Eqs. 21 and 27 could be solved simultaneously, all unknowns could be determined in terms of the impact velocity u_3. This can be done graphically from a plot of p vs. u_1 or $u_3 - u_1$ for the target and projectile materials. A projectile pressure, p, is chosen and the value of $u_3 - u_1$

found. The same p is used and the target u_1 is found. From this, u_3 can be found. The process is repeated until the correct impact velocity u_3 is found. If target and projectile are of the same material, the equations are simplified since $u_1 = u_3/2$, and a graphical solution is not necessary.

Plots of pressure vs. $u_3 - u_1$ or u_1 are given in Figs. 3 to 8 for Pb, Fe, W, Mg, Al, and Cu. The values of M, k, and L used are indicated in Table I.

Because of the work being done in the laboratory on impact into lead, plots of shock velocity and material velocity in the target were prepared for the impact of these materials into lead. These are shown in Figs. 9 to 14.

Considerable work was done on the development of analytical solutions for reflected and other distributed waves. Progress was made and the approximate methods of describing such waves were developed. This work is

Table I

Values of M, k, and L for Eqs. 16, 17, 19, and 24. Use of these values gives good agreement with Los Alamos data. Comparable values can be derived from data in Technical Report UU-11 (See Section 2). c.g.s. values are used.

	Pb	Fe	W	Mg	Al	Cu
M	4.62×10^{-5}	3.78×10^{-5}	6.51×10^{-6}	7.46×10^{-6}	5.00×10^{-6}	6.47×10^{-6}
k	0.403	0.389	0.469	0.458	0.468	0.469
L	3.49×10^{-5}	2.885×10^{-5}	4.71×10^{-6}	5.43×10^{-6}	3.62×10^{-6}	4.67×10^{-6}

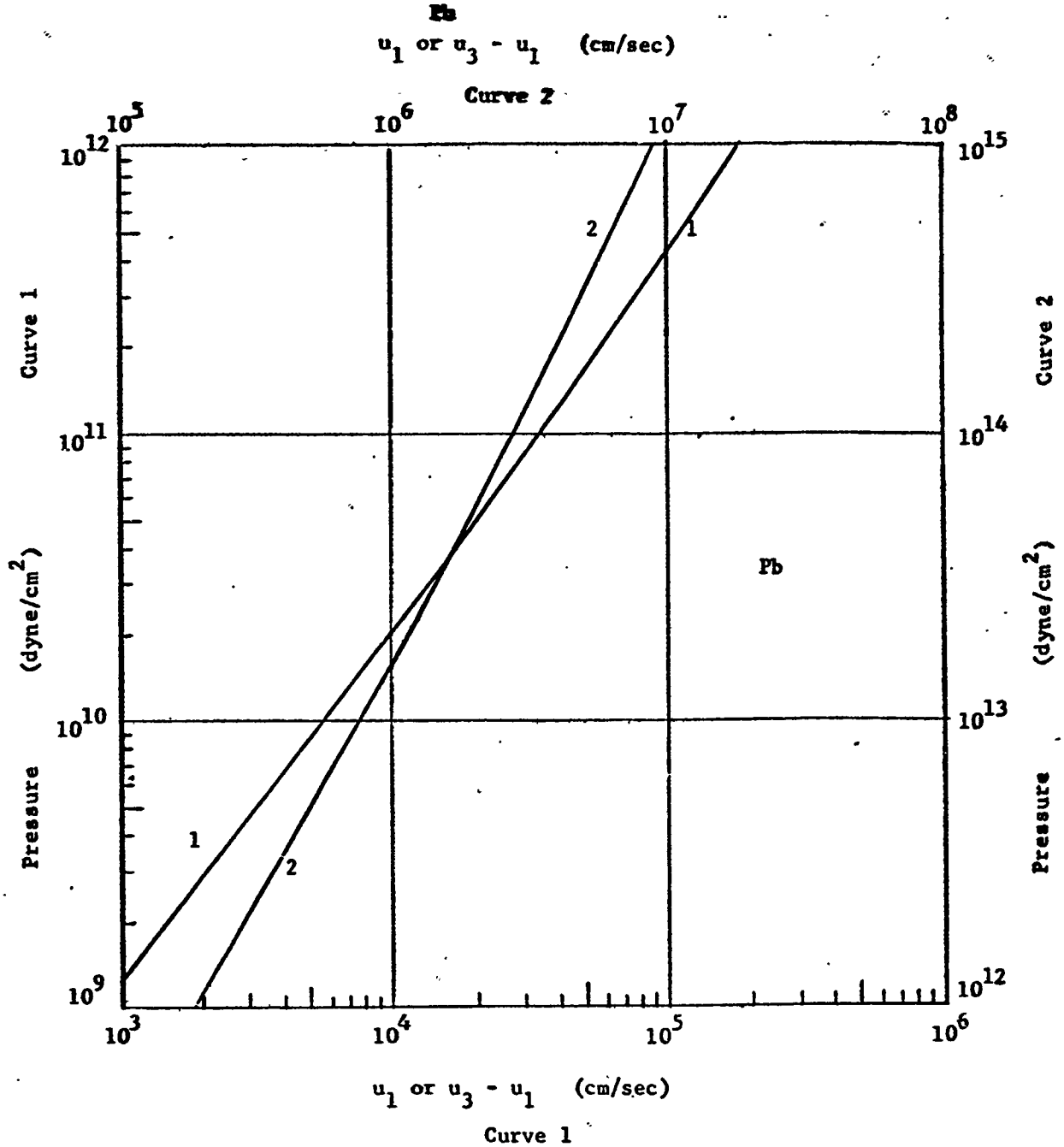

Fig. 3. Pressure behind a plane wave as a function of material velocity.

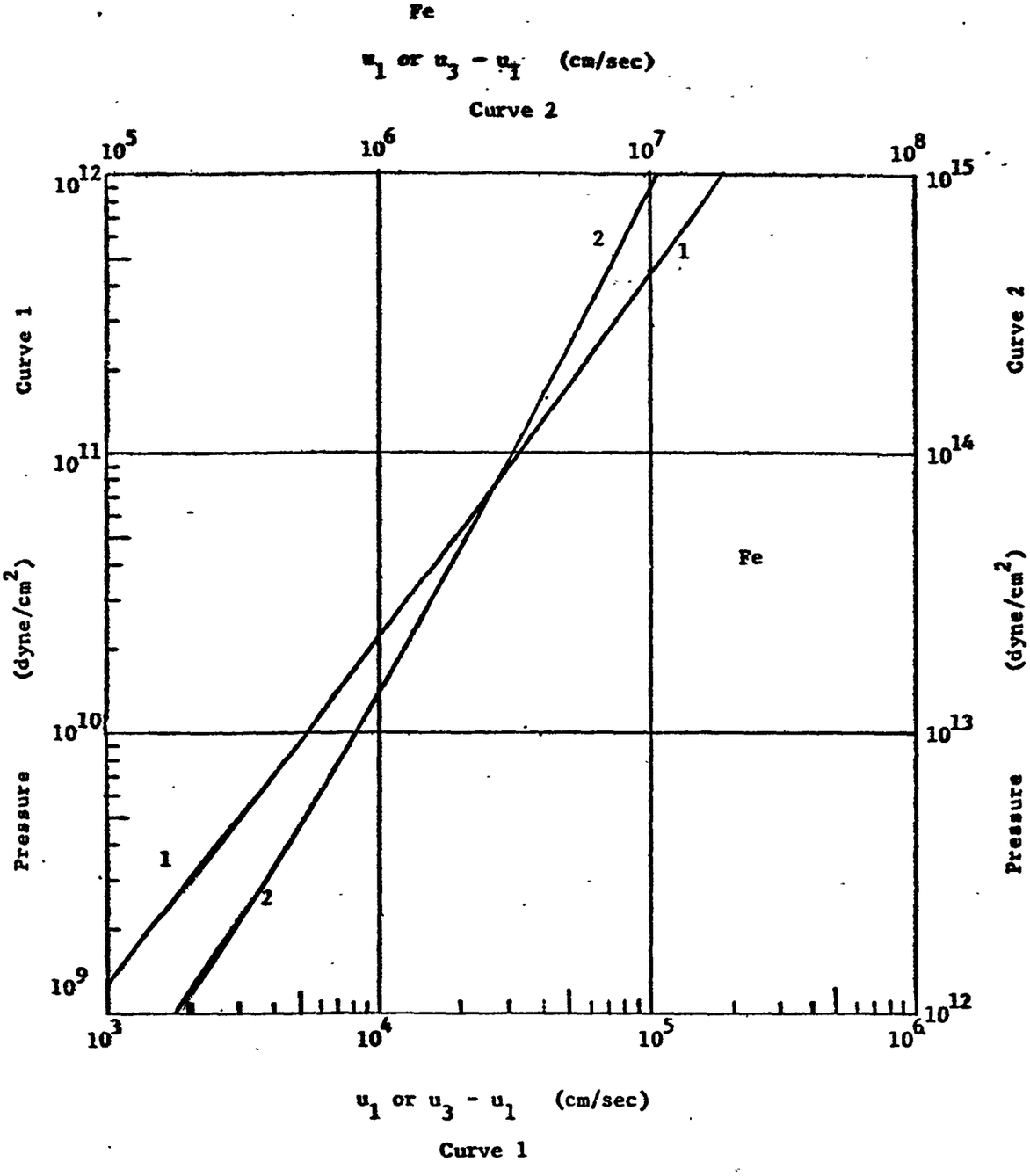

Fig. 4. Pressure behind a plane wave as a function of material velocity.

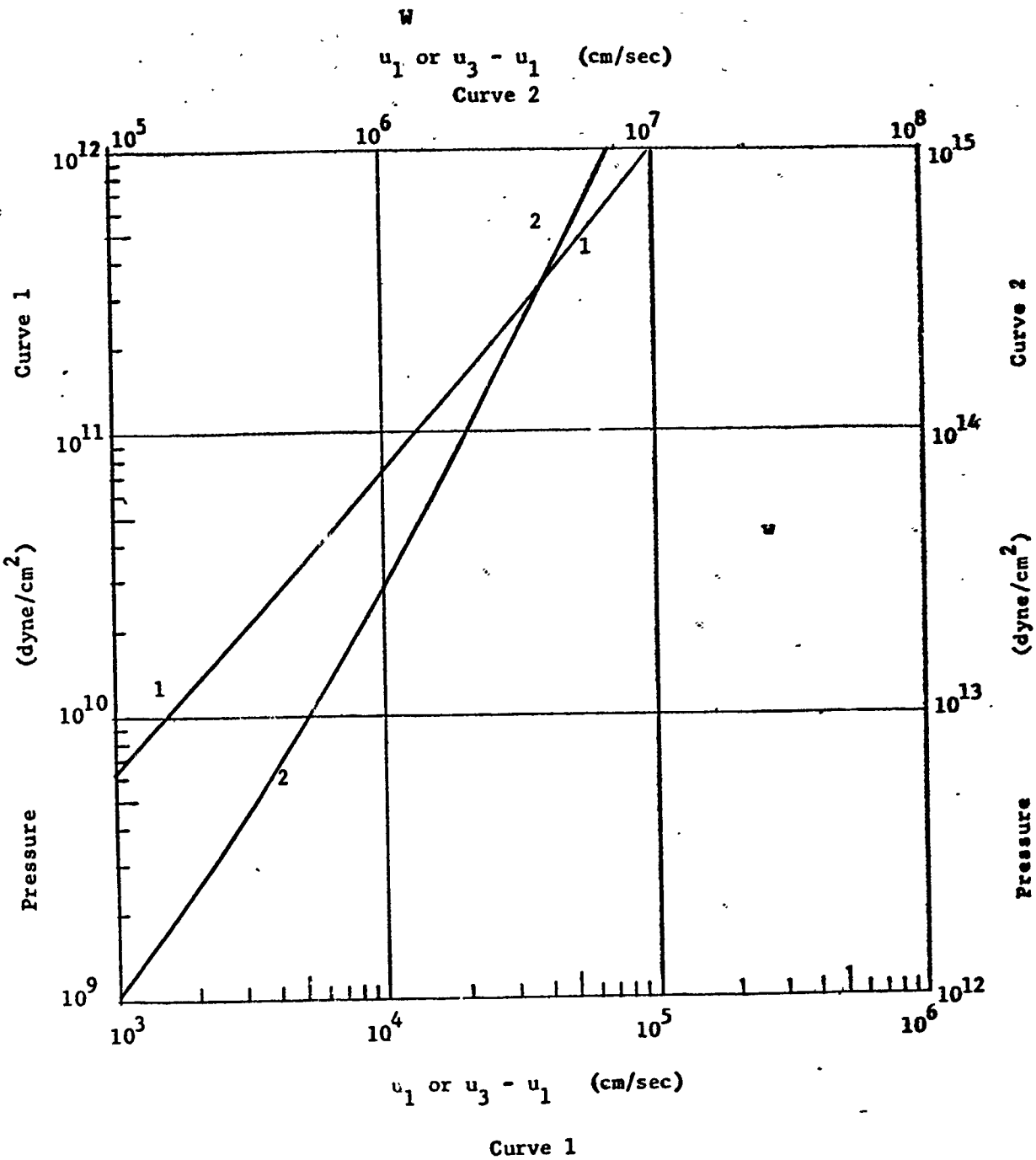

Fig. 5. Pressure behind a plane wave as a function of material velocity.

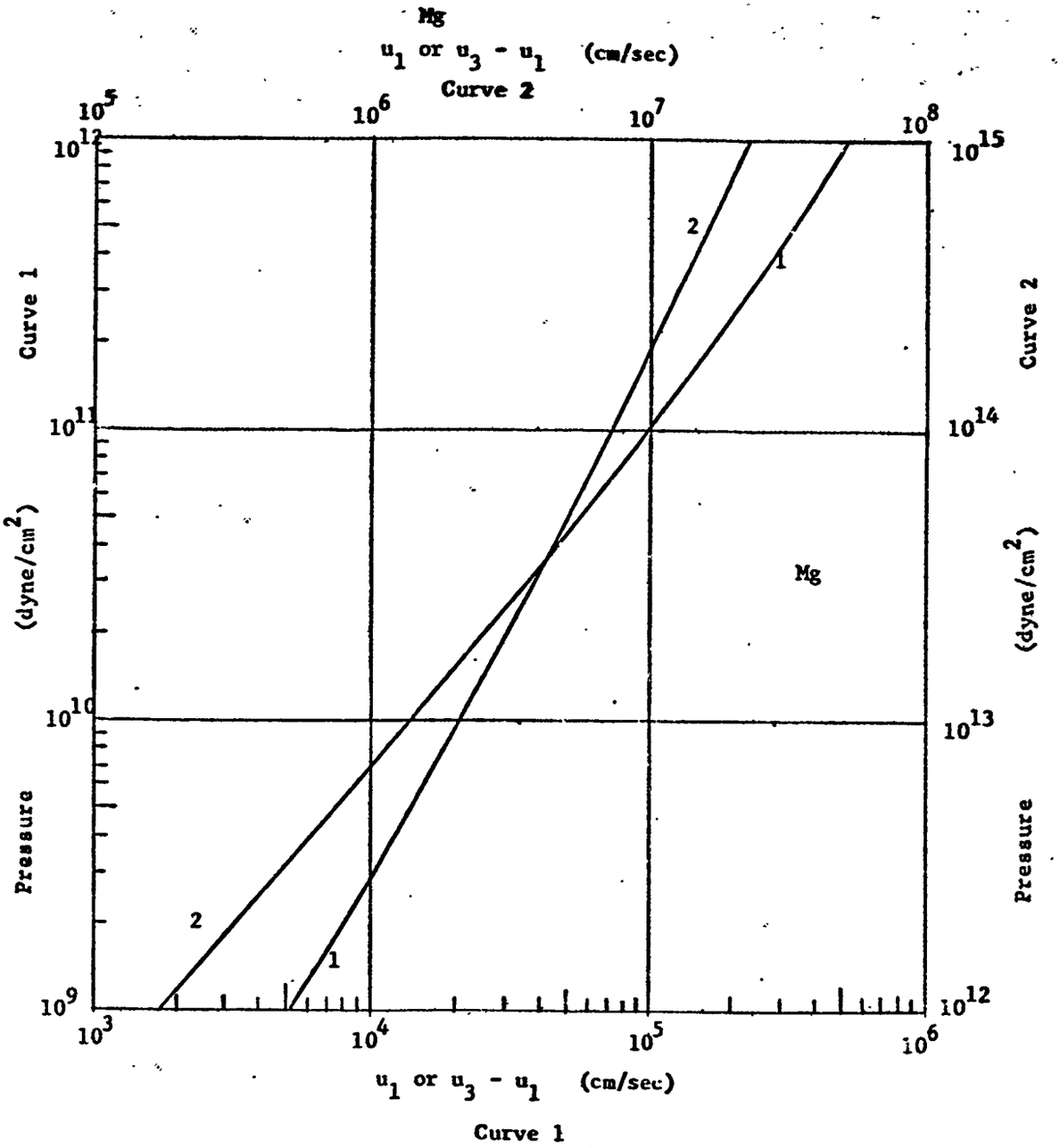

Fig. 6. Pressure behind a plane wave as a function of material velocity.

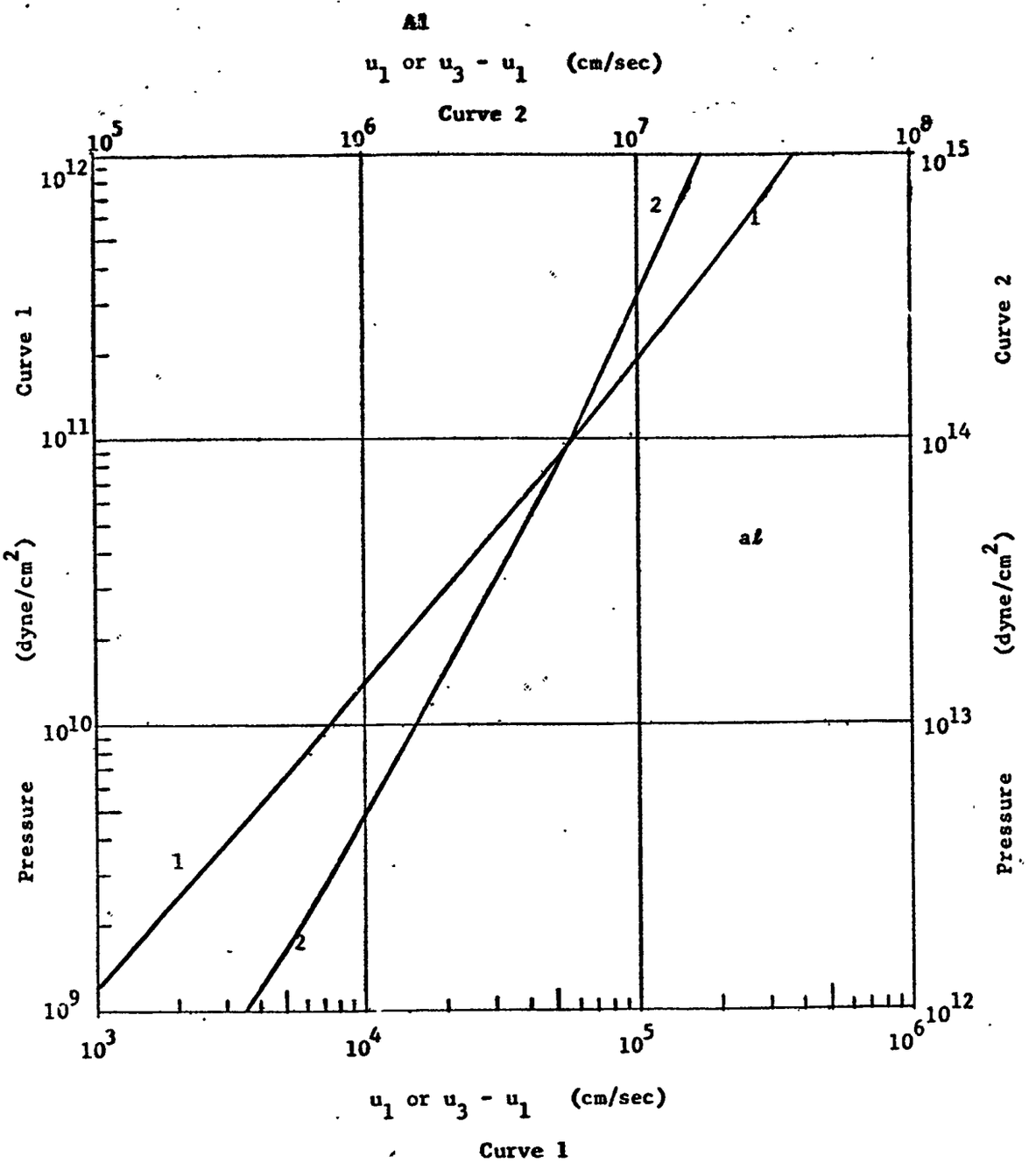

Fig. 7. Pressure behind a plane wave as a function of material velocity.

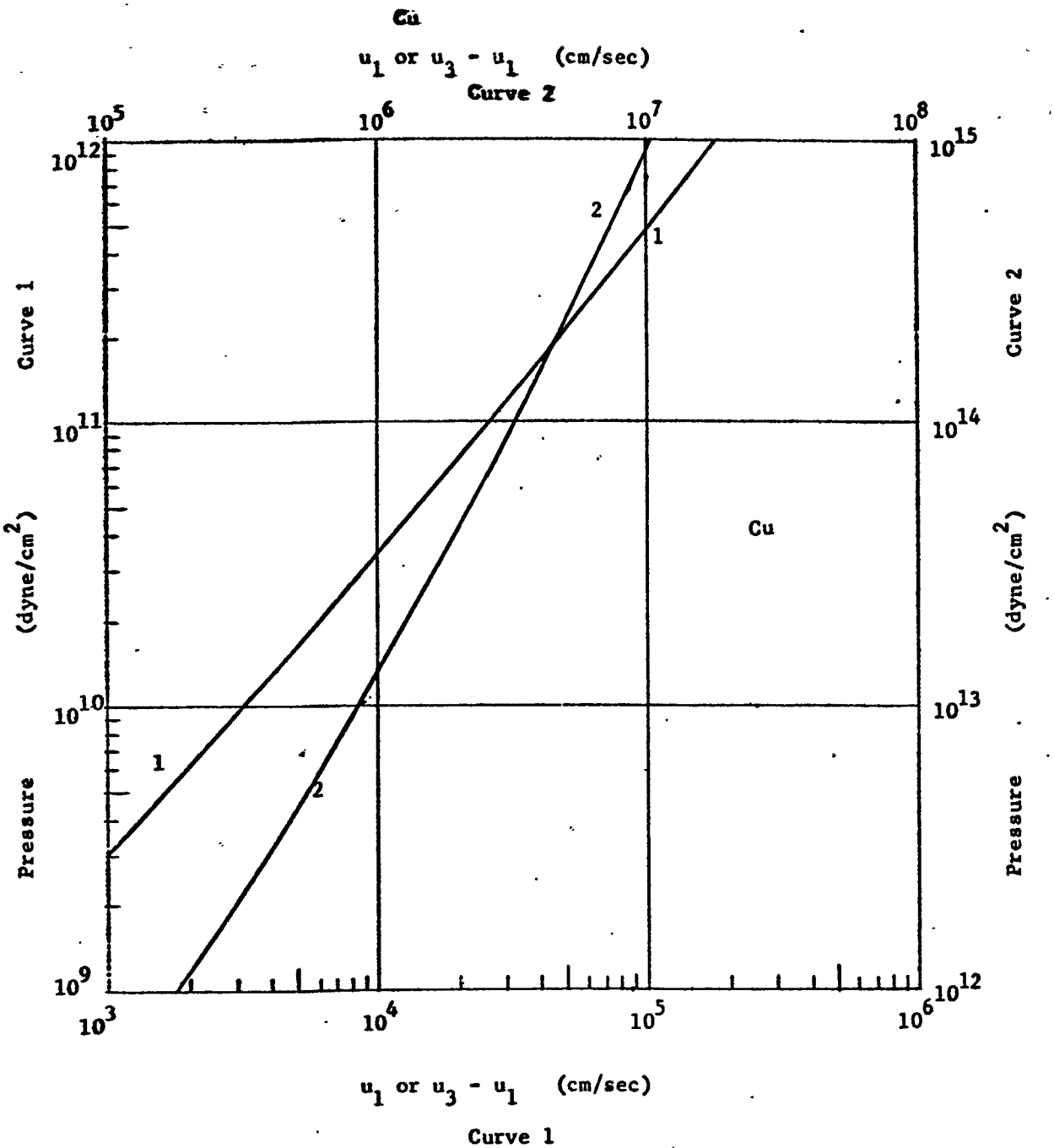

Fig. 8. Pressure behind a plane wave as a function of material velocity.

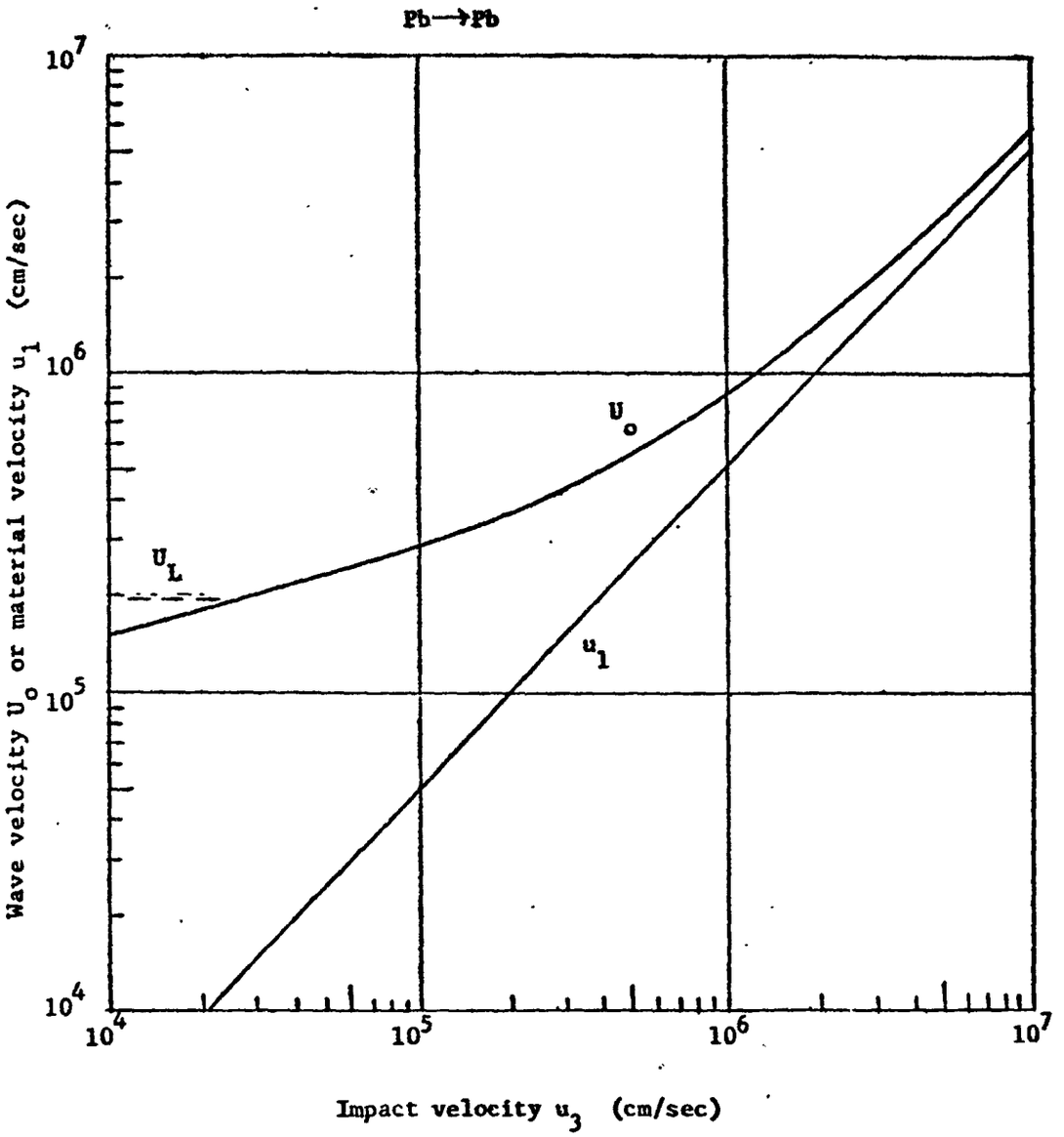

Fig 9. Wave and material velocity as a function of impact velocity for plane impact in a lead target. The longitudinal dilitational elastic wave velocity is shown as U_L.

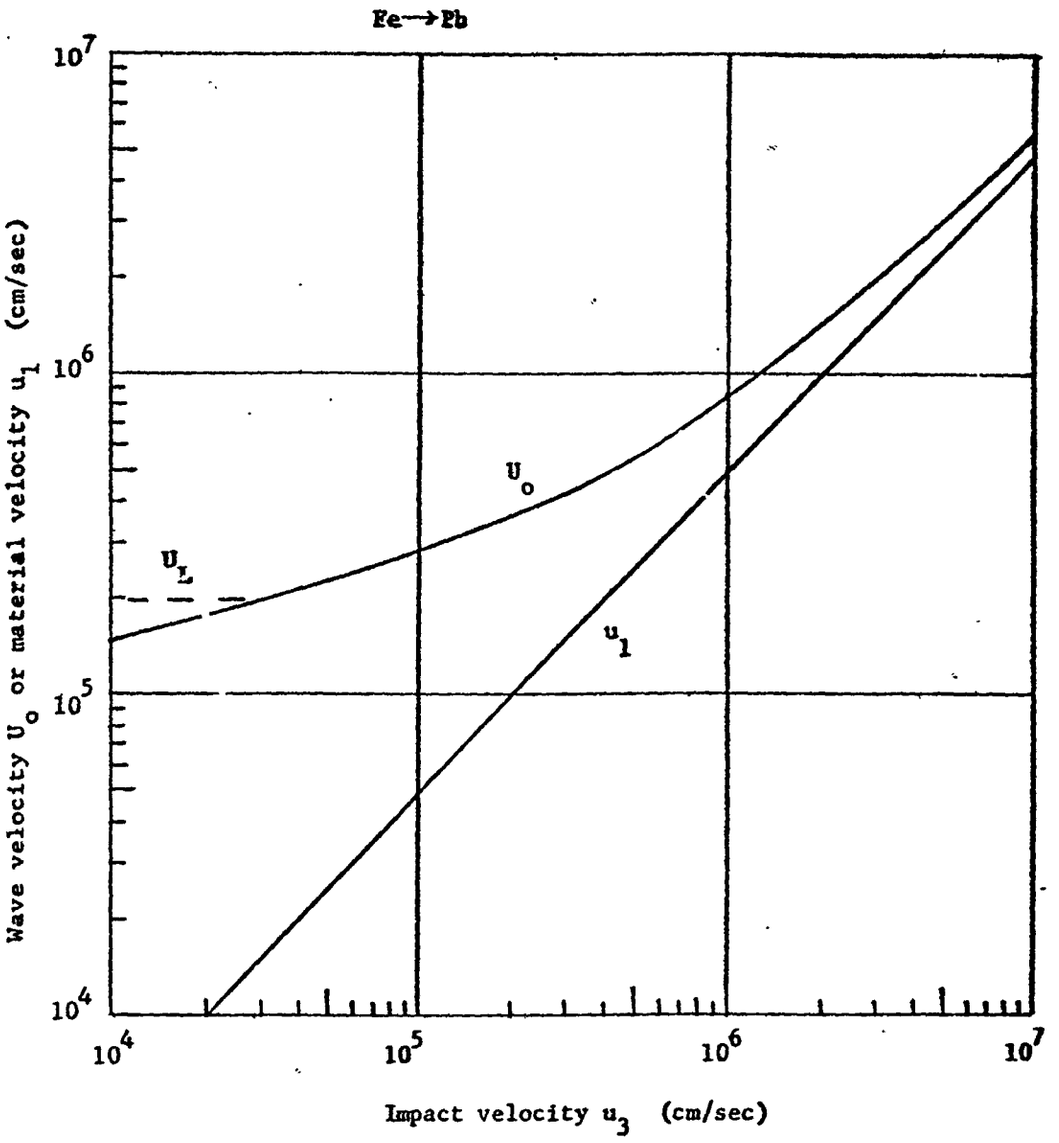

Fig. 10. Wave and material velocity as a function of impact velocity for plane impact in a lead target. The longitudinal dilitational elastic wave velocity is shown as U_L.

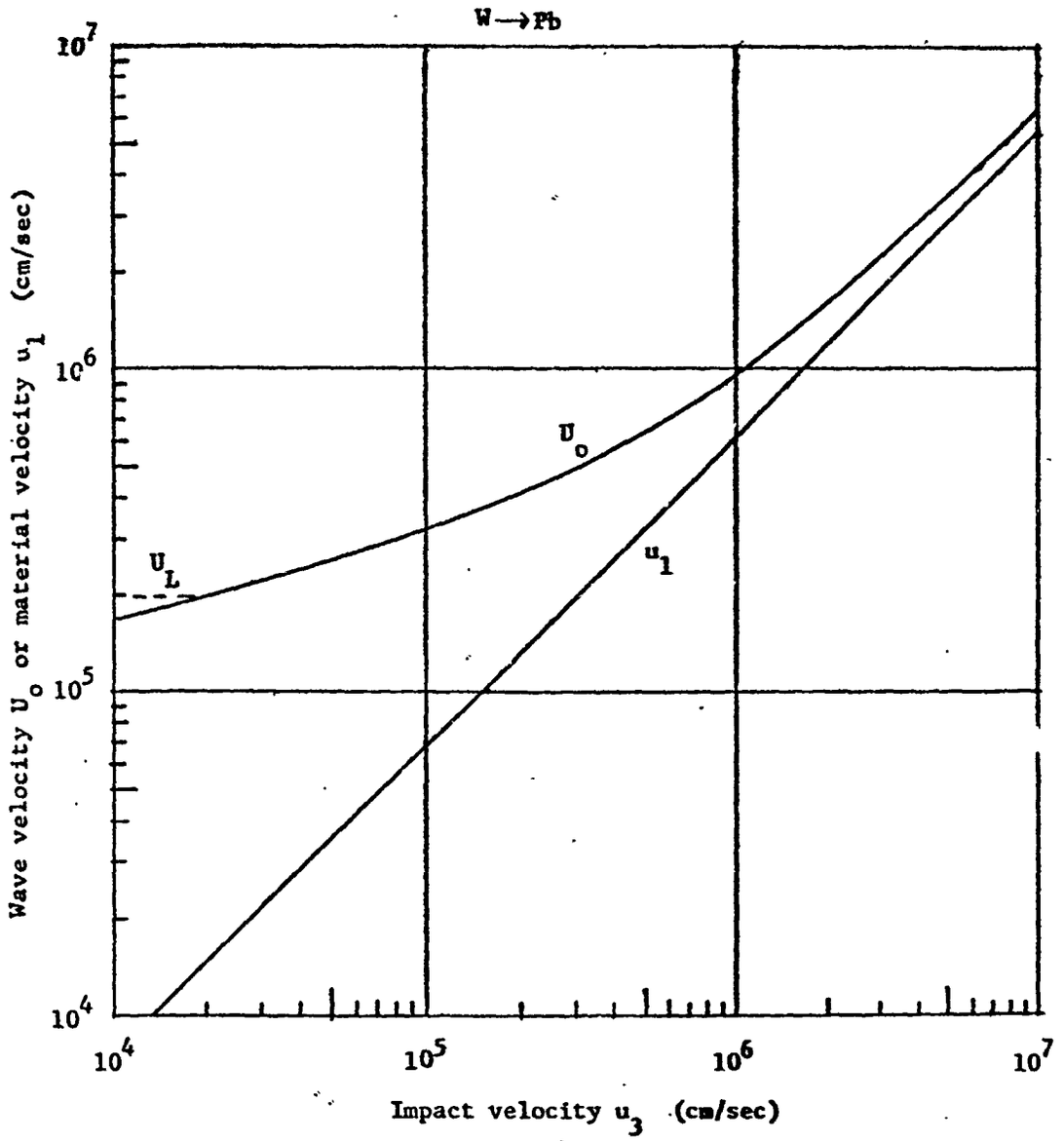

Fig. 11. Wave and material velocity as a function of impact velocity for plane impact in a lead target. The longitudinal dilitational elastic wave velocity is shown as U_L.

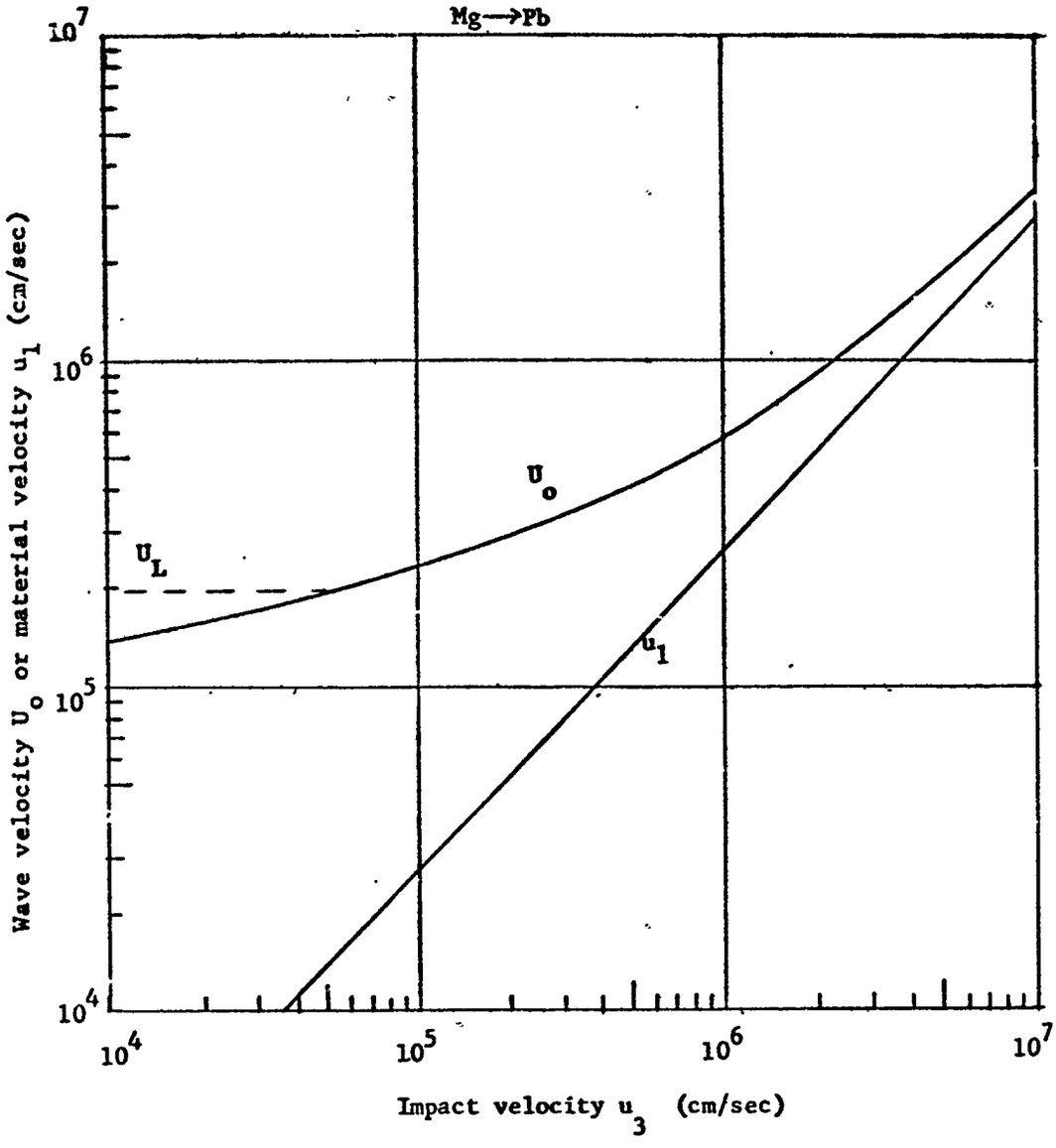

Fig. 12. Wave and material velocity as a function of impact velocity for plane impact in a lead target. The longitudinal dilitational elastic wave velocity is shown as U_L.

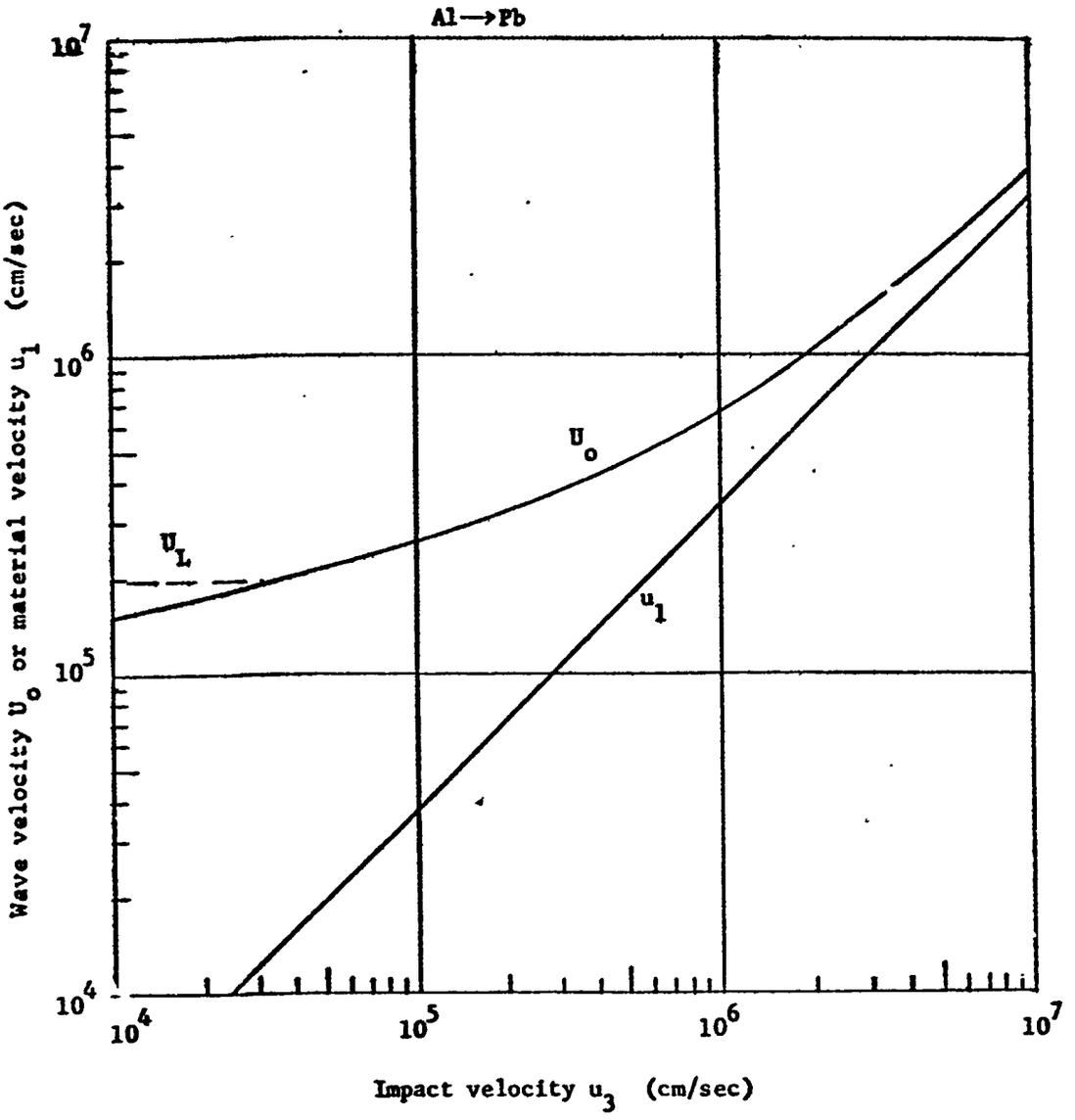

Fig. 13. Wave and material velocity as a function of impact velocity for plane impact in a lead target. The longitudinal dilitational elastic wave velocity is shown as U_L.

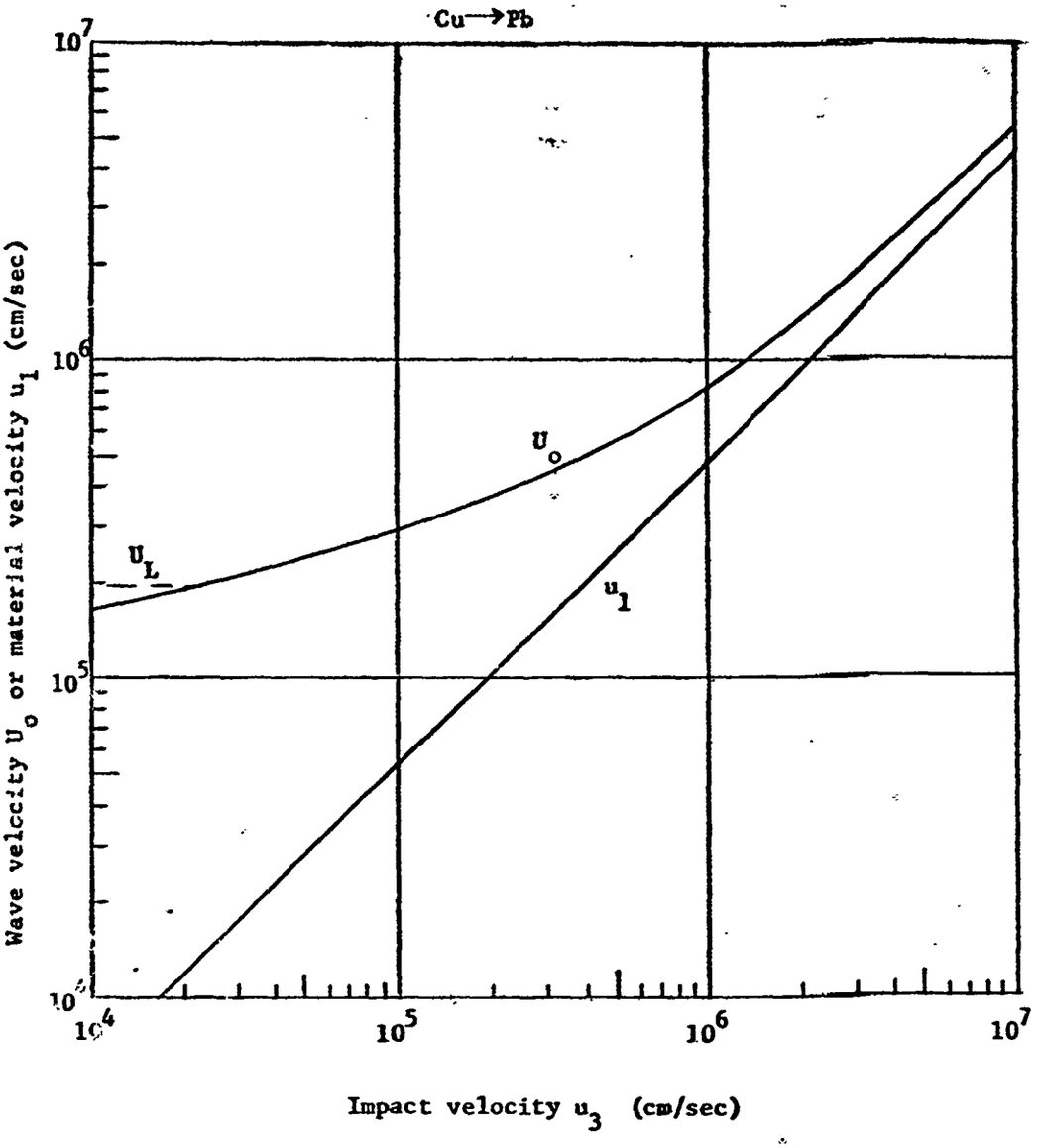

Fig. 14. Wave and material velocity as a function of impact velocity for plane impact in a lead target. The longitudinal dilitational elastic wave velocity is shown as U_L.

of fundamental importance in discussing thin-target impact. Unfortunately the limits of validity of the work were not ascertained and the work has remained uncompleted. This is an area of considerable importance for further research since useful engineering calculations depend on the development of simplified theory and approximate methods of describing the physical processes occurring.

Impact Scaling Laws. A third project in this area, also previously unreported, has been a check on various scaling laws which have been suggested. In the Fifth Hypervelocity Impact Symposium, R. L. Bjork proposed a scaling law relating the penetration produced in a given target material by different projectile materials to the density of the projectile materials and the material velocity produced in the target. The law took the form

$$\frac{(P/D)_{A\rightarrow B}}{(P/D)_{B\rightarrow B}} = \frac{2u_1}{u_3}\left(\frac{\rho_3}{\rho_o}\right)^{1/3}$$

where $(P/D)_{A\rightarrow B}$ is the ratio of penetration to projectile diameter for projectile material A into target material B, and $(P/D)_{B\rightarrow B}$ is the same for target and projectile of the same material. Velocities and densities are the same as used above in Fig. 2.

To make this check, the quantity $\left(2\ u_1/u_3\right)\left(\rho_3/\rho_o\right)^{1/3}$ was computed for the six materials used previously and the results plotted vs. impact velocity in Fig. 15. These results are in general agreement with Bjork's. Experimental data are also shown for these materials impacting into lead.

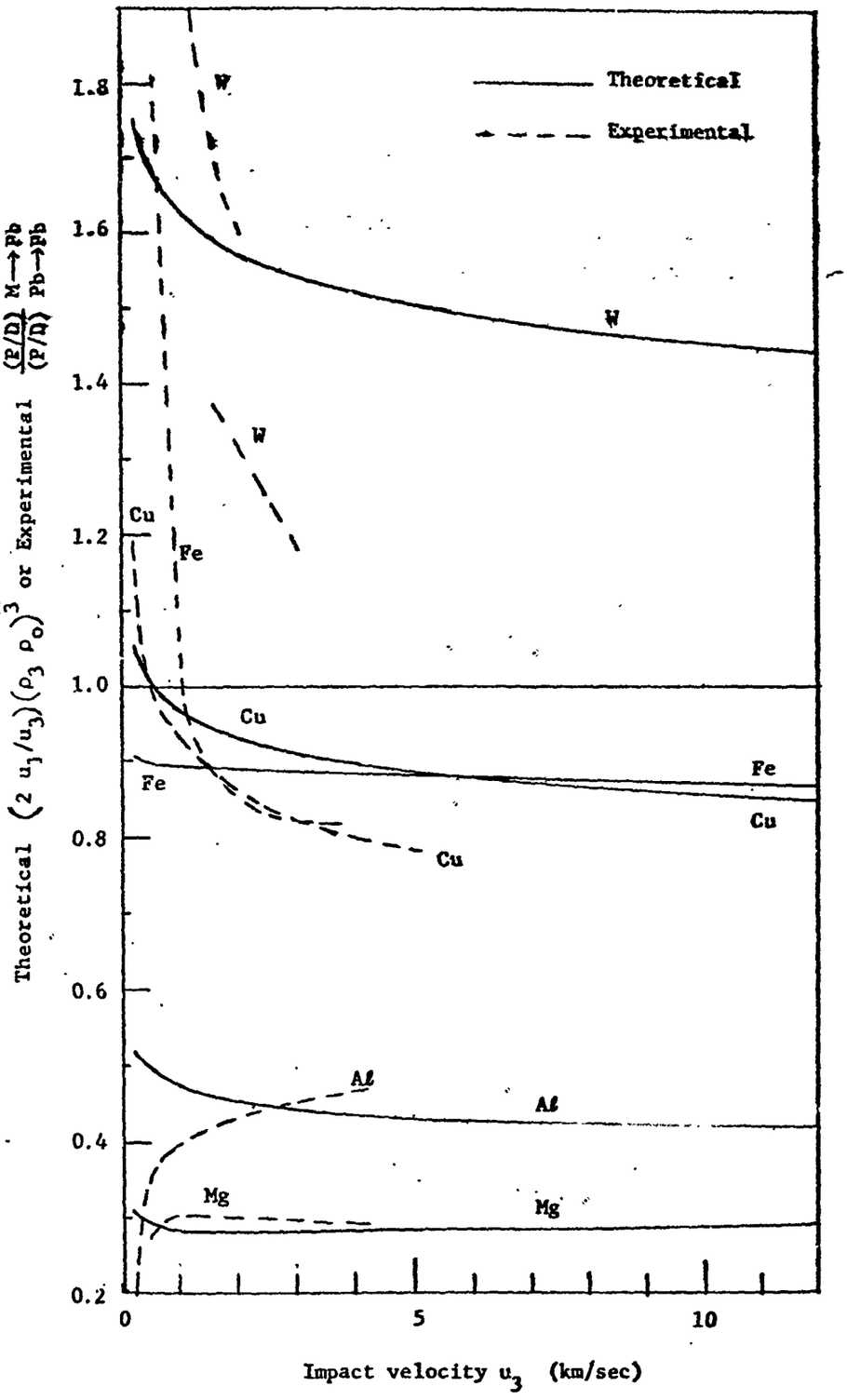

Fig. 15. Comparison of Bjork's impact scaling law with experimental penetration ratios for various metal projectile lead.

It is seen that agreement between experiment and theory is good for impact velocities around 2 km/sec where the best data are available, although the different slopes of the experimental and theoretical curves make the law suspect. Projectile strength can account for the wide disagreement at low velocities.

An attempt was made to compare the scaling predicted by Bailey in Technical Report UU-11, (See Section 2), which relates crater formation to the "transmitted energy," $p_1 u_1$ x area. It was found that the inverse square variation of transmitted energy does not predict the velocity dependence of cratering actually observed for given materials and the ratio of different materials to lead is not good.

3.4 Transient Measurements in Impact

This project is concerned with developing techniques and instrumentation for observing transient phenomena occurring during impact.

Subsurface Measurements. A major project in this area has consisted of an investigation into the use of piezo-electric crystals buried in the target to measure sub-surface pressure transients. This project was essentially completed and a report prepared, Technical Report UU-13 referred to in Section 2. It was found that small barium titanate pressure transducers buried in the target allowed the measurement of transient pressure waves. The method gives information about wave propagation and stress levels in elastic and plastic waves. The method holds great potential for obtaining results by using various other materials as transducers.

Surface-Flow Measurements. A second project in this area has consisted

of using surface photography and shadowgraph photography to obtain information about transient flow. For this work, various light sources have been developed using relatively standard techniques. Barium-titanate-capacitor spark-gap sources, transmission-line spark-gap sources, and an underwater high-pressure arc source have been developed. During the past quarter, a Kerr cell shutter was developed for use with these sources. One project involved the investigation of surface motion, particularly the propagation of waves, by observing the reflection of bright light sources in a highly-polished surface during impact. The problem was analyzed, light sources were developed, arrangements were made to borrow a rotating mirror streak camera for the photography. This project was abandoned when it was learned that the contract would not be renewed. No consistent data have been obtained using surface photography although several isolated pictures have been taken. This is an area worthy of considerable further research, since visualization of the processes occurring is essential before adequate theoretical models can be developed.

3.5 Spray-Particle Generation

This project is concerned with understanding the factors which determine the spray particle field generated on both sides of a thin target during high-velocity impact.

Impact Flash. During the first quarter of the contract, some time was spent finishing a project begun under Contract AF 04(647)-942. This project was concerned with observations of the generation of the tiny fast spray particles which appear immediately at impact. These particles are

primarily responsible for the impact flash for impact in air. They are relatively unimportant in considering the overall mass loss or energy loss in impact. They are important in various types of impact detectors and as a laboratory tool in meteor-physics studies. A report on these particles and on their relation to meteor physics is given in Technical Report UU-10 referred to in Section 2. An abstract is given in the First Quarterly Report.

Thin-Target Penetration. A second project has involved shadowgraph studies of thin-target penetration. Preliminary results have been obtained for lead targets and show the generation of spray material and the propagation of deformation. Various velocities have been measured, pressure decay calculated, and the general phenomena observed. A preliminary report on this work is included as Appendix B attached to this report. Further work on spray-particle mass and energy distributions was planned based on the techniques developed in the energy-partitioning studies. These could not be carried out because of lack of manpower.

3.6 Impact Theory

This project is considered to be the summation of all the others and has consisted of observing the impact process in selected systems and formulating theoretical models to describe it. Work in this area has ranged from a formulation of simple correlations between observed impact parameters and observed crater parameters to attempts to formulate simplified dynamical models of the overall process based on the laws of fluid flow and material properties. An example of a correlation law is given in

Technical Report UU-11 where the "transmitted energy" (pressure times velocity) is correlated with hole size. This correlation law is valid over a very limited range but fails at higher velocities. Evidence from previous work* and from the decay of pressure in thin targets indicates that pressure decays faster than would be concluded by assuming constant transmitted energy.

A kinematic description of the cratering process in lead was developed in connection with partitioning measurements and presented in the Third Quarterly Report. It is believed that such a model could be generalized to other materials although this is impossible at the present time because the necessary detailed data on energy division and on the cratering process are not available for any other material. The main utility of this work is probably in serving as a guide for the development of a further dynamical model which must give the results obtained in this instance. Considerable effort has been spent in attempts to develop suitable dynamical models of cratering. This work has not yet proved generally successful, although the results fit the limited data available for lead impact. This incomplete work can not be reported yet. It is felt that, at present, any efforts in this line are at best uncertain and are probably doomed to failure because the order of magnitude of the importance of the various processes occuring is not known. This is illustrated in the discussion of the failure of the hydrodynamic models to explain the observed

---

* Technical Report UU-9, AFBSD-TDR-62-185, Contract AF 04(647)-942, Penetration and Cratering by Palmer, et. al., High Velocity Laboratory, University of Utah, Salt Lake City, Utah, 30 June 1962.

energy partitioning. The attempt to measure the energy involved in deformation illustrates a first try at remedying the situation and providing the basic data necessary before a simplified theory can be reliably derived. Any further work in impact theory must rely on data not now available which indicates the relative importance of the various processes. Otherwise the theory becomes merely a correlation with existing data which is suspect outside the region of validity of the data.

4. DISCUSSION OF PROJECTS AND CONCLUSIONS

The various projects discussed above have provided considerable new information of a fundamental nature. The energy partitioning study has shown that energy partitioning changes with velocity and thus impact correlations cannot be made beyond the range of the data. It provides the basic data for the formulation of impact theory. The need for such data for other materials than lead and for a wide range of velocities is clearly indicated. New simple techniques have been developed and proven valid for measuring recrystallization and locked-in strain energy and spray particle energy. Techniques for the measurement of subsurface transient temperature distributions have shown promise and can probably be further developed.

The work on material properties has resulted in the formulation of general equations describing the impact properties of materials over energy ranges of at least four orders of magnitude. The complete range of applicability of this equation has not been investigated, although the limited investigations and comparisons with static compressional data for liquids and metals, shock wave compressional data for metals, and general data for gases indicate great value and utility.

Equations describing the initiation of flow and the flow properties of materials under the conditions met in impact are necessary before a successful theory can be developed. The formulation of such equations is not now in sight. The basic understanding of the processes is not available and techniques for making such measurements have not been developed. A preliminary experimental investigation into this area was begun and holds promise, although it was not possible to obtain significant data during this contract time.

The investigation of wave motion in idealized cases has shown the utility of simplified concepts to described wave propagation. Whether or not these simplified ideas on "transmitted energy" can be extended to the case of two-dimensional flow is unknown. It is believed that similar simplified approximations can be found for more complicated flows. Their great utility indicates the need for pursuing such an investigation.

The development of techniques for making transient measurements of the phenomena occurring in impact has proceeded and promises to be a most important tool in further investigations of impact.

The use throughout this research of the approach of observing the details of the impact process and attempting to describe and understand them is certainly the only possible approach under the present state of the art where neither experimental nor theoretical data exist on materials and their behavior. The utility of the approach is shown by the one test case where energy partitioning measurements have shown the hydrodynamical model of impact to be in error. The test is not certain because of the different materials considered in the theory and in the experimental

investigation reported here, yet the general aspects of the work certainly cast doubt on the validity of the former theory. This could not be done by earlier data on hole size. This work is worthy of further research.

The overall goal of the project, that of developing general theory applicable to a wide variety of materials and impact conditions, was not met. The gathering of essential background information required more time than was expected and the magnitude of the problem was probably underestimated. It is felt that the work as carried out was justified and that few changes could have been made considering the time and level-of-effort involved. The work provides a basis in new experimental techniques and a source of ideas and criticism for any further work in the field. Further progress will not be made without considerable additional information on material properties and on the details of the fundamental properties operating in the flow of material under the conditions generated in high velocity impact.

5. RECOMMENDATIONS

A proposal has been submitted to the Air Force Ballistic Systems Division and Aerospace Corporation requesting that this contract be extended for a three-month period to meet the immediate goals of further analysis of the data collected on this project, the possible formulation of theory, and the collection of some additional data. The data desired are in the energy partitioning study for velocities up to 5 km/sec, and in the study of the energy involved in deformation by the rod-to-rod impact process.

For long-range goals, it is recommended that the fundamental investigations begun and carried out in this work be extended and continued. It is recommended that fundamental studies of material flow under the high pressure conditions and under the high stress-rate conditions met in high velocity impact be made. The details of the expansion process involved in high velocity impact can be investigated by impact techniques. It is recommended that work in this area be supported in the future. It is recommended that wave propagation under the actual conditions met in high velocity impact be further investigated. It is recommended that investigations of techniques for better measurements of the transient conditions involved in impact be made. It is expected that these recommended fundamental studies will provide a necessary body of information for the formulation of theoretical models of the impact process and will lead to a solution of engineering problems.

Because of the complexity of the overall problem, and the lack of information available now and which can be expected in the near future, it is recommended that accelerator development to be supported in order that experimental data can be obtained to test any theory and to provide a check on engineering design at velocities from missile velocities to meteor velocities.

APPENDIX A

Energy-Storage Transitions in Materials

Neil P. Bailey

CONTENTS

1. INTRODUCTION

In Technical Report UU-11, equations of state describing the stored internal energy u as a function of only the pv product were developed for metals and some liquids. That the energy depends only upon the pv product was checked by Bridgman static test data and by Los Alamos impact data. The form of equation established is

$$\frac{u}{pv} = mu^k \qquad (1)$$

where k is the fraction of any internal energy increment du that goes to excite new modes of energy storage.

One very interesting thing appeared in Figs. 5 and 6 of Report UU-11. For both water and C_8H_{16} liquid, the factor k experienced an abrupt decrease. This means an abrupt decrease in the excitation of new modes of energy storage. The fact that a change in the electric conductivity of water is observed in this same range indicates that this transition involves the electrons. This thought suggests the possibility that a careful investigation might reveal the same trend in metals and other solids.

2. COMPRESSION TRANSITIONS

To resolve this point, a very careful analysis of water, sodium, borax glass, lead, and beryllium has been made. By choosing very

compressible and noncompressible metals as well as nonmetals, the investigation has been kept quite general. Tables 1, 2, 3, 4, and 5, together with Fig. 1, show the analysis of Bridgman data by the methods of Articles 5 and 6 of Report UU-11.

Table 1

Water at 80 Degrees F.

$$p_o v_o = \frac{14.7 \times 144}{1 \times 62.4} = 34.0 \text{ ft. lb. per lb.}$$

p/p_o	v/v_o	$\log_{10} v_o/v$	$pv/p_o v_o$
199.7	.99116	.003858	198.0
299.6	.98688	.005736	296.0
399.5	.98270	.007578	393.0
499.4	.97872	.009343	489.0
599.2	.97483	.011071	584.0
699.1	.97094	.012806	679.0
799.0	.96725	.014461	773.0
898.8	.96366	.016079	865.0
999.0	.96006	.017702	960.0
1098.5	.95666	.019944	1051.0
1198.4	.95335	.020746	1141.0
1298.3	.95005	.022254	1233.0
1398.2	.94684	.023723	1323.0
500	.97900	.009922	489.5
1000	.96083	.017356	960.8
2000	.93011	.031468	1860.0
3000	.90551	.043106	2716.5
4000	.88431	.053391	3537.2
5000	.86643	.062265	4332.2
6500	.84370	.073818	5640.0
8000	.82444	.083842	6595.5

Table 2

Sodium

$$p_o v_o = \frac{14.7 \times 144}{.971 \times 62.4} = 34.94 \text{ ft. lb. per lb.}$$

p/p_o	v/v_o	$\log_{10} v_o/v$	$pv/p_o v_o$
2,500	.9666	.015023	2,417
5,000	.9376	.027982	4,688
10,000	.8885	.051343	8,885
15,000	.8489	.071144	12,934
20,000	.8164	.088097	16,328
25,000	.7890	.102923	19,725
30,000	.7700	.113509	23.100
40,000	.7370	.132533	29,480
50,000	.7080	.149967	35,400
60,000	.6830	.165579	38,580
70,000	.6610	.179799	46,270
80,000	.6410	.193142	51,280
90,000	.6230	.205520	56,070
100,000	.6060	.217527	60,600

Table 3

Borax Glass

$$p_o v_o = \frac{14.7 \times 144}{2.23 \times 62.4} = 15.21 \text{ ft. lb per lb.}$$

p/p_o	v/v_o	$\log_{10} v_o/v$	$pv/p_o v_o$
5,000	.9655	.015245	4,828
10,000	.9369	.022831	9,369
15,000	.9143	.038911	13,715
20,000	.8946	.048371	17,892
25,000	.8770	.057004	21,925
30,000	.8660	.062482	25,980
40,000	.8450	.073143	33,800
50,000	.8250	.083546	41,250
60,000	.8080	.092589	48,480
70,000	.7920	.101275	55,440
80,000	.7780	.109020	62,240
90,000	.7650	.116339	68,850
100,000	.7530	.123205	75,300

Table 4

Lead

$$p_o v_o = \frac{14.7 \times 144}{11.34 \times 62.4} = 3.0 \text{ ft. lb. per lb.}$$

p/p_o	v/v_o	$\log_{10} v_o/v$	$pv/p_o v_o$
19,350	.9590	.018180	18,580
29,000	.9443	.026270	27,350
38,700	.9253	.033720	35,800
48,400	.9108	.040580	44,100
58,000	.8976	.046920	52,050
67,600	.8855	.052810	60,000
77,250	.8745	.058240	67,500
87,000	.8644	.063290	75,200
96,600	.8551	.067980	82.600

Table 5

Beryllium

$$p_o v_o = \frac{14.7 \times 144}{1.845 \times 62.4} = 18.4 \text{ ft. lb. per lb.}$$

p/p_o	v/v_o	$\log_{10} v_o/v$	$pv/p_o v_o$
2,417	.9976	.001040	2,410
4,836	.9953	.002050	4,810
9,671	.9906	.004100	9,570
14,504	.9861	.006080	14,310
19,342	.9819	.007930	19,000
24,168	.9781	.009620	23,660
29,014	.9744	.011260	28,260
33,849	.9706	.012960	32,840
38,648	.9671	.014530	37,400

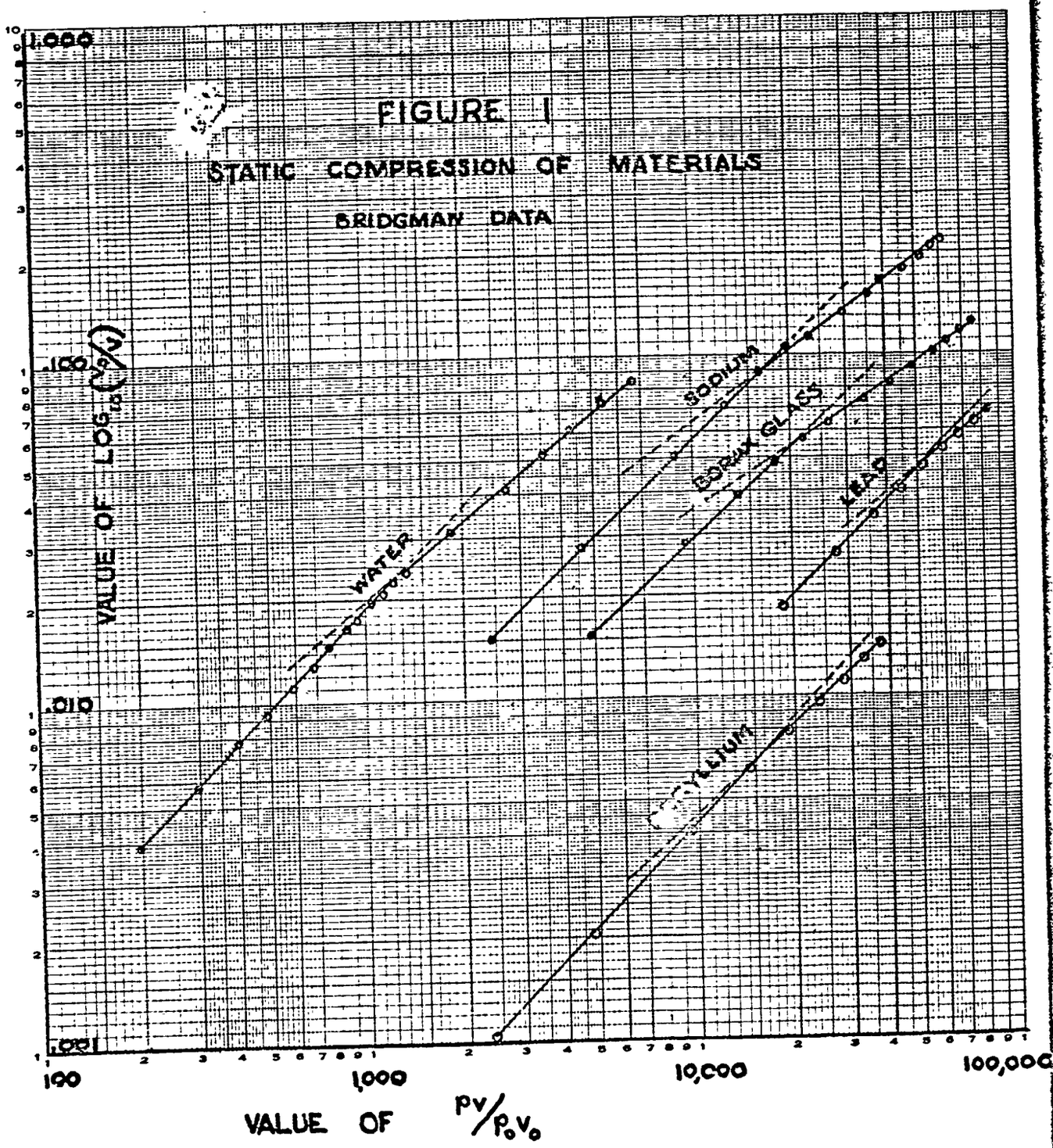
FIGURE 1
STATIC COMPRESSION OF MATERIALS
BRIDGMAN DATA
1.000
.100
.010
.001
VALUE OF $\log_{10}(P_0/V)$
WATER
SODIUM
BORUM GLASS
LEAD
BERYLLIUM
100
1,000
10,000
100,000
VALUE OF PV/P_0V_0

Figure 1 makes it clear that all the materials shown -- liquid, solid, and metal -- do, indeed, have transitions at increased pressure. The change in the slope k is more marked in very compressible materials such as sodium than it is in a closely packed structure like beryllium. These transitions were not detected during the preparation of Report UU-11 because many slide-rule calculations were used. Following the procedures of UU-11, Table 6 gives the values of k and m in

$$\frac{u}{pv} = mu^k \qquad (1)$$

Table 6

Equations of State

Materia	Before Transition		After Transition		$p_o v_o$
	k	1/m	k	1/m	
Water	.494	1235	.446	912	34.00
Sodium	.482	1964	.398	885	34.94
Borax Glass	.477	1762	.387	859	15.21
Lead	.482	1467	.444	1068	3.00
Beryllium	.495	6025	.472	5117	18.40

Figure 2 shows the corresponding u/pv vs. u lines and Fig. 3 shows a larger scale plot for lead and beryllium along with the corresponding Los Alamos impact test points.

Figure 3 indicates that for beryllium the Los Alamos or impact points are on the transition line, implying that the transition occurs during impact. However, for lead the first points are near the line

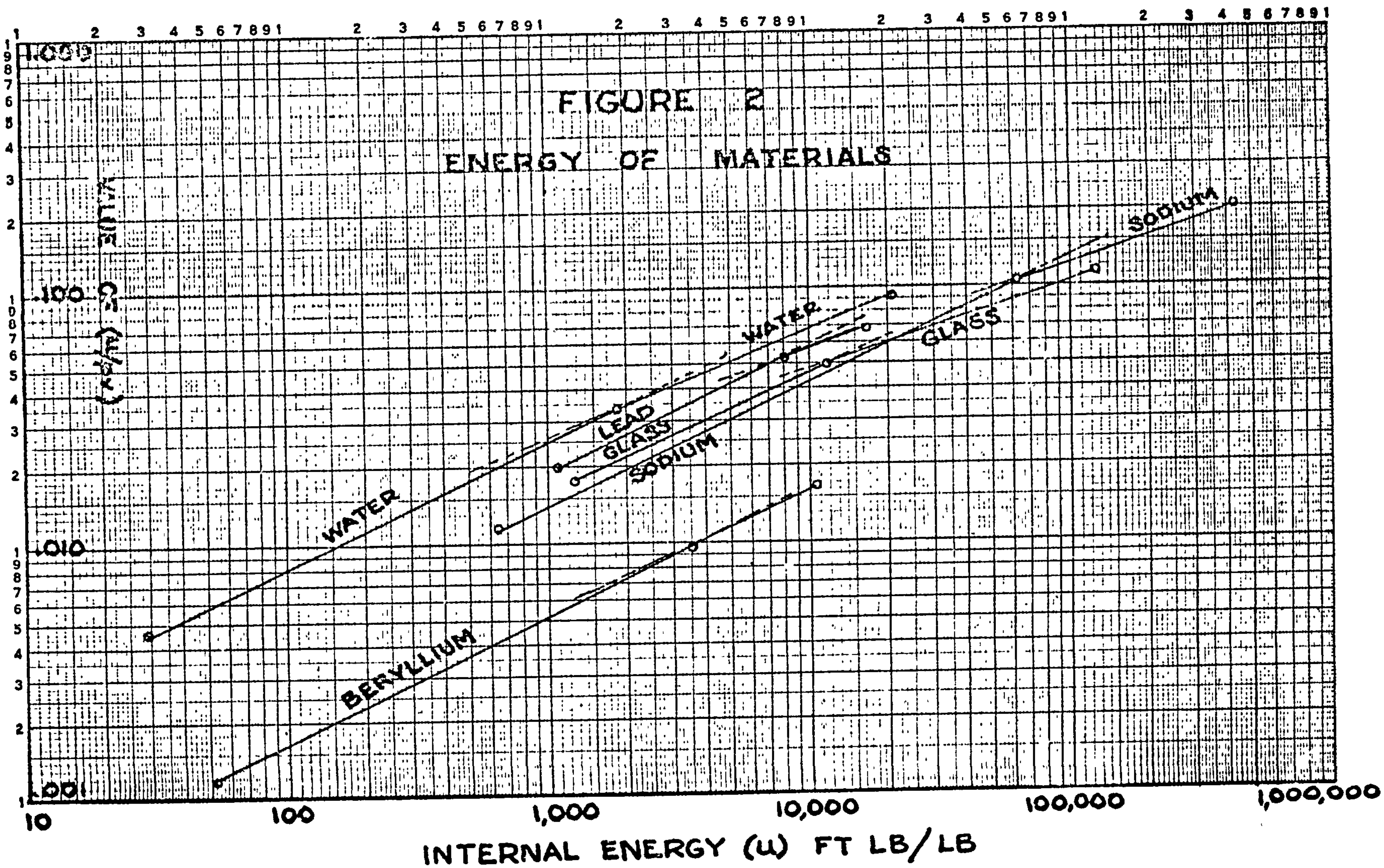
FIGURE 2
ENERGY OF MATERIALS
VALUE OF (u/ρ x)
1.000
.100
.010
.001
10
100
1,000
10,000
100,000
1,000,000
INTERNAL ENERGY (u) FT LB/LB
WATER
LEAD
GLASS
SODIUM
BERYLLIUM

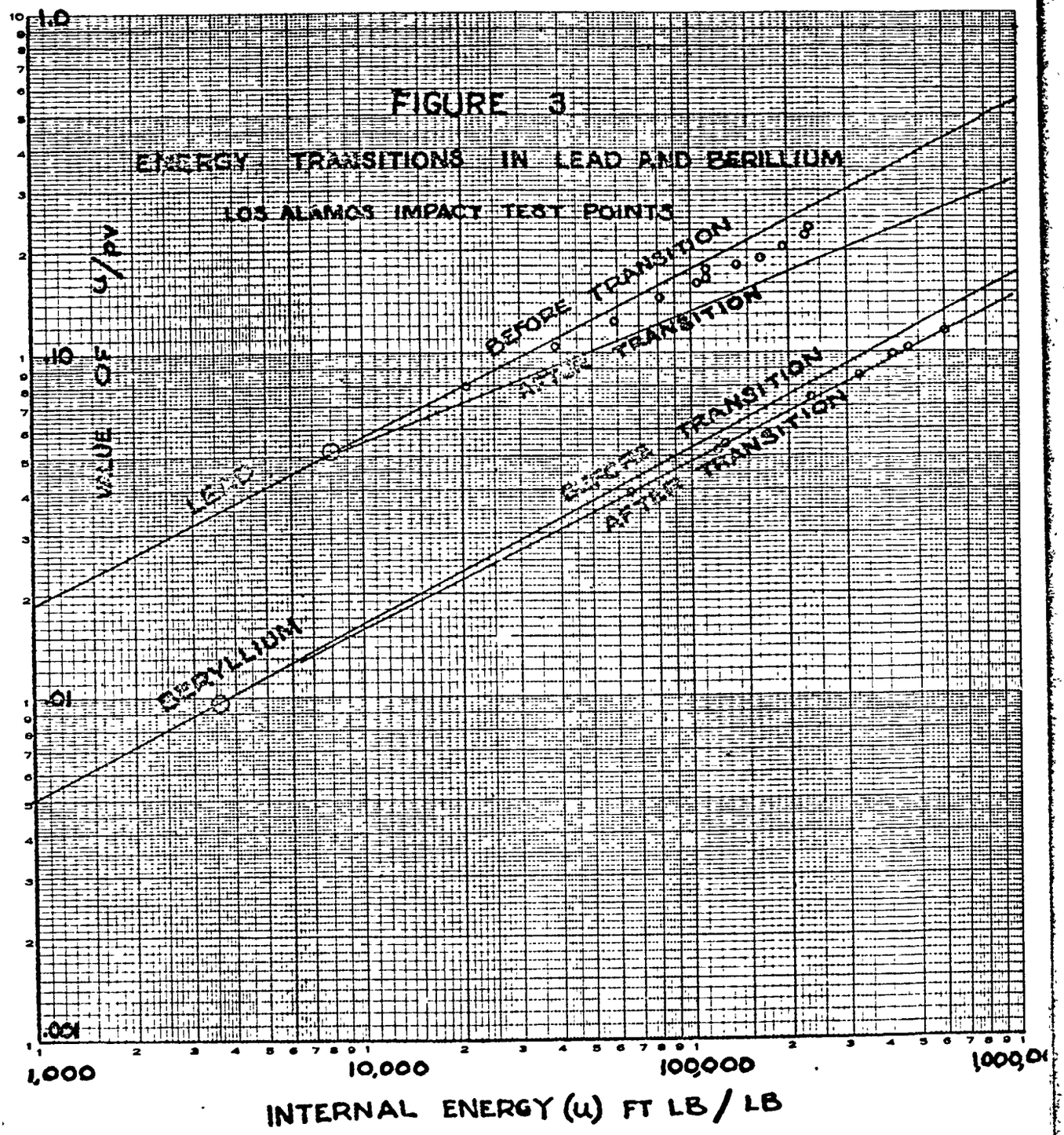
FIGURE 3
ENERGY TRANSITIONS IN LEAD AND BERILLIUM
LOS ALAMOS IMPACT TEST POINTS
1.0
.10
.01
.001
VALUE C_v J/R
LEAD
BEFORE TRANSITION
AFTER TRANSITION
BERYLLIUM
BEFORE TRANSITION
AFTER TRANSITION
1,000
10,000
100,000
1,000,0
INTERNAL ENERGY (u) FT LB / LB

before transition and at no time does it appear that the full transition occurs during impact. These two sets of results cannot be taken as conclusive but they do raise a point of doubt. It is not clear that a material with a static test transition will exhibit the same transition when tested under impact conditions. More information is needed.

3. EFFECT OF TRANSITIONS ON IMPACT PRESSURES

An idea of the magnitude of the effect of energy transitions on impact pressures may be illustrated for the case of lead. Lead is chosen because it has only a minor transition as shown by Fig. 1. Other materials experience more profound transitions.

Using the approach of Article 8, Report UU-11, the case of any material impacting any other material may be analyzed. For any energy level u, and pv product, each material reaches a pressure ratio given by,

$$\left(\frac{p}{p_o}\right)^2 - \frac{p}{p_o}\left[\frac{pv}{p_o v_o} + \frac{2u}{p_c v_o} - 1\right] - \frac{pv}{p_o v_o} = 0 \qquad (2)$$

The same approach for a plate a moving at velocity V_a striking a plate b moving at V_b gives

$$V_a - V_b = \text{relative velocity} = \sqrt{2g}\left[\sqrt{u_a} + \sqrt{u_b}\right] \qquad (3)$$

Each material is described by the State equation (Eq. 1) with such values of k and m as given in Table 6.

In this way, Fig. 4 was calculated, and it shows the effect of energy transition on the impact pressure of lead striking lead. Figure 3 suggests that the result could be any place between the two curves of Fig. 4.

4. IMPACT HEATING

The job of separating the part of the shock-produced internal energy that can be classes as softening, thermal, or lattice vibrational energy from that which is stored in lattice distortion or molecular forces is not a simple one. This part of the internal energy which softens and creates fluidity is equally significant in the space problem of missile penetration and cratering and in the modern processes of explosive forming or forging of metals.

Such material flow or escape is affected by three factors. It requires that the material be softened during impact, that pressures sufficient to overcome flow restraints exist, and that these conditions are sustained long enough for flow to occur. When cylinders impact endwise, their impacting ends are "upset" or "mushroomed" and their free ends are little changed. The pressure, the softening energy, and the degree of lateral restraint are all constant along the length of the cylinders. This means that the only difference is the time duration through which these conditions are sustained. The impacting ends of the cylinders are under high pressure during the full wave traversing time and the free ends are stressed only momentarily.

FIGURE 4.

EFFECT OF ENERGY TRANSITION ON PLANE IMPACT PRESSURE OF LEAD STRIKING LEAD

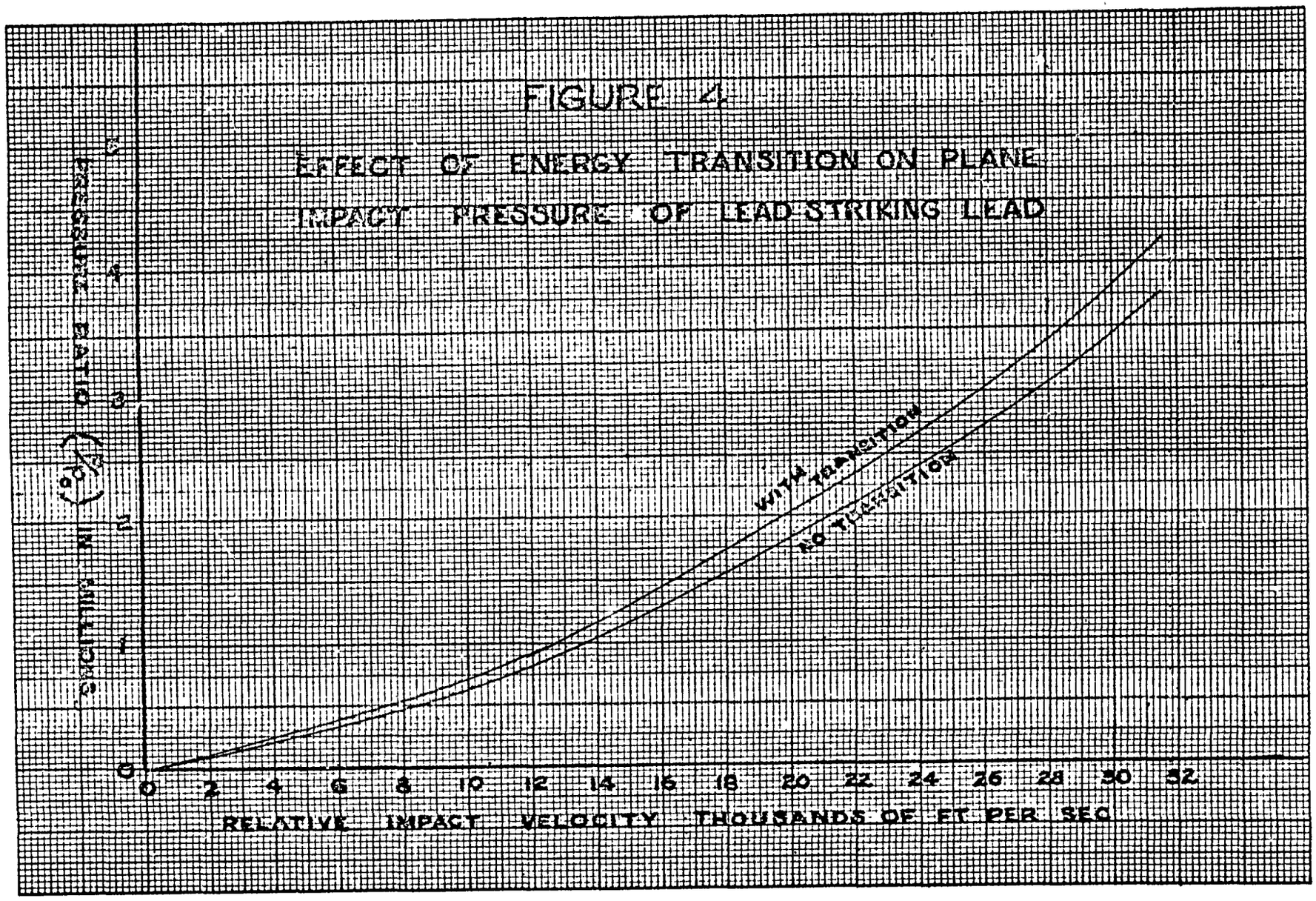

In Report UU-11, "Stored Energy of Compressed Metals From Shock and Static Tests," the basis was established for certain conclusions concerning the energy of metals. It was postulated that at high pressures all of the internal energy u delivered mechanically is uniquely measured by the pv product. The internal energy u represents that stored in Newtonian force fields and that individually possessed kinetically by the molecules. This was verified by analyzing shock test data. It was shown that

$$\frac{u}{pv} = mu^k \qquad (1)$$

where m is a constant for any metal and k is the constant fraction of each internal energy increment that goes to excite new modes of energy storage.

In Report UU-11, it was further shown that if the constant-temperature static compression of metals is described by the path equation

$$du = - pdv \qquad (4)$$

and if Eq. 1 is assumed to apply, the m and k so determined from static tests are the same as the values determined from dynamic or shock tests. This makes it appear that Eq. 4 does not mean the same thing in the compression of metals and liquids as it does in the compression of gases. In gases, field forces between molecules are negligible and all pressure

manifestations are the consequence of the thermal energy of the individual molecules. Consequently, during a reversible adiabatic process described by Eq. 4, there is a rise in temperature of the gas.

In contrast, pressure effects in solids and liquids are primarily the consequence of Newtonian forces between molecules and only secondarily the result of the kinetic energy of individual molecules. All of this strongly suggests that Eq. 4 describes a compression of a metal when the internal forces between molecules are in equilibrium with the externally applied pressure and in such a situation, no energy goes to kinetic energy of individual molecules or thermal energy. During a shock compression such forces are not in balance and some energy does go to excite the thermal energy of molecules.

Because all effects in a gas are kinetic, the same equation of state will describe the medium whether the energy is added mechanically or thermally. It is quite evident that this is not the case for metals because thermal energy unaided cannot store energy in the mechanical force fields. Unlike a gas, the volume of metal does not increase indefinitely at zero pressure. This means that thermal energy possessed by atmospheric pressure p_o metal is not measurable by the pv change alone. It can be related to the specific volume through the specific heat c of the metal and its bulk or volume coefficient of thermal expansion a.

$$u - u_o = c(T - T_o) \qquad (5)$$

and

$$v = v_o \left[1 + a(T - T_o)\right] \tag{6}$$

giving

$$u - u_o = \frac{c}{a}\left(\frac{v}{v_o} - 1\right) \tag{7}$$

At the present time, values of c and a are known at atmospheric pressure but not at elevated pressures.

In summary, then, the present state of the art is something like this. At pressures above say 2000 atmospheres, the energy of metals is described by Eq. 1. In this pressure range, any process where the energy is all stored in Newtonian forces is described by Eq. 4. At atmospheric pressure when all of this force energy has been released the residual thermal energy is described by Eq. 7.

This leaves undescribed the energy of metals in the normal strength of materials or elastic range. This is really no serious handicap in studying shock phenomena since the actions involved span this range.

APPENDIX B

Penetration Studies by Photographic Techniques

by

R. V. Bunnag and E. P. Palmer

TABLE OF CONTENTS

I. INTRODUCTION

Extensive research in cratering, penetration, and the theory of stress-wave propagation has been carried out in an attempt to develop a successful mathematical theory of high-velocity impact[1]. So far, no general theory has been developed. To develop this theory, an intensive study of the processes occurring in the impacted body is needed in order to find basic information on which processes are significant to the system. Work reported here was done to obtain this basic information for high-velocity perforation of thin targets.

Humes, Hopko and Kinard[2] have investigated the perforation of single aluminum targets used as "Meteor Bumpers." They show a series of spark shadowgraphs in which exit spray particles can be studied. Also Kineke[3] has observed spray formation in lead and crater formation in wax in a sequence of flash radiograph pictures. Palmer[4] has reported on spray-particle energies for impact in lead targets. Others[5,6,7,8] have studied overall perforation effects without observing the details of any processes occurring.

In this experiment, a series of spark shadowgraphs was taken to show details of perforation produced by the impact of steel balls on lead plates. The use of spark shadowgraph pictures gives information on surface flow, wave motion, impact flash, and spray-particle generation.

II. THEORETICAL CONSIDERATIONS

2.1 Spray Particles

A kinematic model of crater formation in lead has been developed by Palmer[9] and used to relate the amount of spray material generated to the kinetic energy of the impacting projectile. As yet, no dynamic theory is available to relate forces and material motions. Before such a theory can be developed, additional experimental information must be obtained on the time and place of spray-particle generation This must be related to the general flow and wave motion occurring. An examination of detailed shadowgraph pictures can be expected to give some information on these subjects.

It is noticed that the process of spray formation in perforation is exactly the same as in cratering at the beginning. A later times the different flow and wave motion in the two cases can be expected to cause differences in spray-particle generation.

2.2 Stress Waves

In high velocity impact, many kinds of stress waves are generated, especially in the three-dimensional case. Because of complexity, a multi-dimensional waves analysis has not been made. Some interesting information can be obtained utilizing one dimensional concepts and the fundamental relations of compressible fluid dynamics.[10]

$$\rho_o U = \rho(U - u) \quad \text{conservation of mass} \tag{2.21}$$

$$p - p_o = \rho_o Uu \quad \text{conservation of momentum} \tag{2.22}$$

$$pu = \rho_o U(e - e_o + u^2/2) \quad \text{conservation of energy} \tag{2.23}$$

U is wave velocity, u is material velocity, p is pressure, ρ_o is density, and e is internal energy.

Equations 2.21 and 2.22 may be used to eliminate u and U from Eq. 2.23. The result is frequently called the Rankine-Hugoniot relation

$$e - e_o = \frac{1}{2}(v_o - v)(p + p_o); \quad v = \frac{1}{\rho} \tag{2.24}$$

This equation with the equation of state

$$e = f(p,v) \tag{2.25}$$

of a certain material would provide a relation between p and v which is called the "Hugoniot p-v relation." The relation has been determined for specific metals by impact results.[10] With the relation of Eqs. 2.21 and 2.22, the relation of U and u, or p and u can be found. Hence,

$$p = \frac{\rho_o u^2}{1 - \rho_o/e_1} = \rho_o Uu \tag{2.26}$$

Figure 1 shows the relation of p and u for lead.

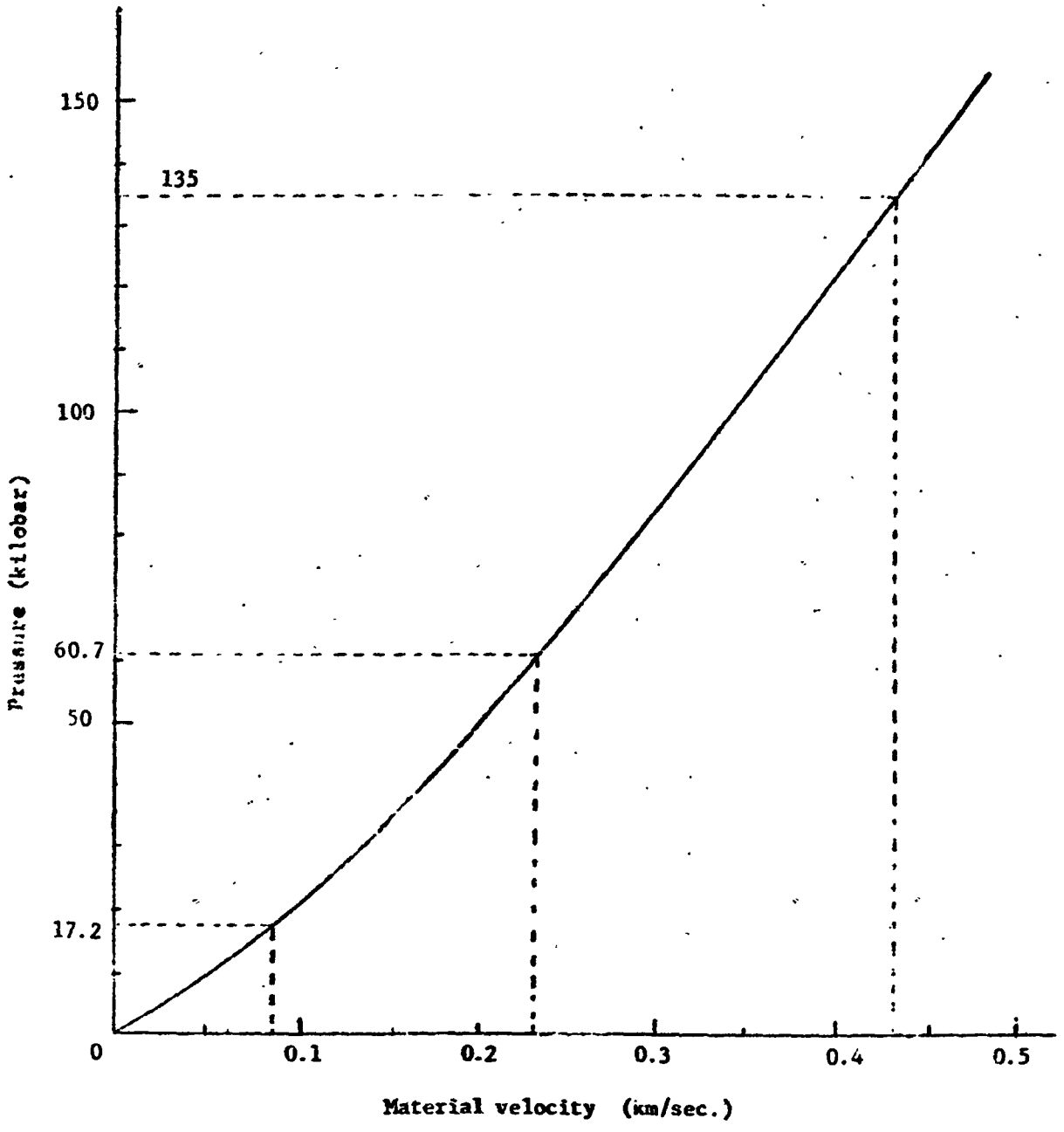

Fig. 1. Pressure vs.. material velocity for a plane shock wave propagating in lead.

The relation between material velocity u and free-surface velocity u_{fs} when a plane shock wave arrives at a free surface is given approximately by [11, 12]

$$u_{fs} = 2u \tag{2.27}$$

III. EXPERIMENTAL PROCEDURE AND EQUIPMENT

Figure 2 shows the experimental setup used in the tests. The purpose of the equipment is to take pictures of the impact process in sequence at known delay times after impact in order that surface flows, spray, enlargement of hole diameter, and stress waves can be investigated.

The sequence of pictures is made by taking one picture at a particular delay time after impact for each impact and repeating the process with different delays until the desired sequence is obtained. The assumption is made that each impact is the same. The major limitation of the method is that individual spray particles appear in only one picture and their history cannot be followed. The major experimental difficulty is that projectile velocity may vary slightly from shot to shot.

3.1 Firing Range

Gun and Projectiles. 7/32-inch diameter chrome-steel ball bearings were used as projectiles. They were accelerated in a smooth-bore, 22-calibre gun using 32 grains of Hercules 2400 Rifle Powder in 220-swift cases. The pellet velocity obtained was about 1.5 km/sec.

Vacuum Tank and Accessories. All shots were made inside the vacuum tank shown in Fig. 2 at a pressure ranging from 0.015 to 0.028 mm Hg. At this pressure, impact flash was reduced and did not interfere with the photography. Large spray particles are not significantly decelerated at this pressure, and projectiles do not lose velocity between gun and target. A Stokes model 212 Microvac pump is used with the system and pressure is measured with a Kinney McCloud Gage.

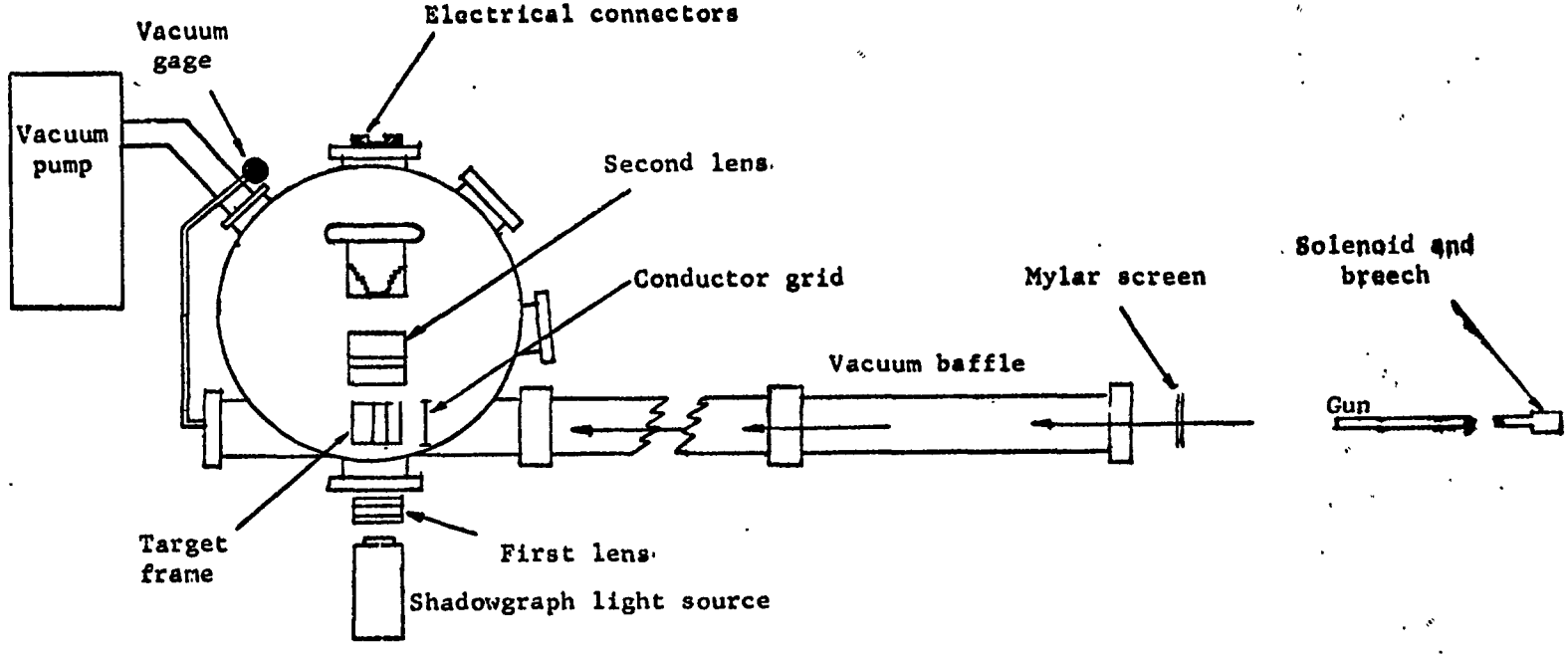

Fig. 2. Vacuum range and arrangement of photographic system.

Targets. Lead plates 2 inches wide, 4 inches long, and with thicknesses of 0.425 ± 0.01, 0.266 ± 0.004, and 0.132 ± 0.0005 inch were used for impact targets. The 0.132 and 0.266-inch targets were cut from lead plates but the 0.425 inch plates were milled from lead block.

3.2 Optical System

Since the intensity of a spark light source is barely adequate for high speed impact photography, the impact flash must be eliminated. A field-lens technique was chosen to do this. The usual single-lens system gives a good picture but it is very small; therefore, a modified parallel-ray optical system was employed as shown in Fig. 3. This system not only gives a larger picture but also eliminates the converging effect which makes the magnification difficult to determine. The system gives a clearly focused picture for any particle between the two lenses. If the camera lens is at the focal point of the second lens, and the light source is at the focus of the first lens, only the parallel light between the lenses enters the camera through a small diaphram opening and the diverging light from the impact flash is greatly reduced. A lens opening of f/22 was used.

Magnification of the system was determined by photographing two pins set 2 inches apart at the target. The image size on the film was 1.625 inches giving a magnification of 0.8125.

The major difficulty in making measurements of small surface displacements comes from the effect of the target not being exactly parallel with the light rays. The edge of the target then forms the apparent surface image. Every effort was made to position the target parallel with the

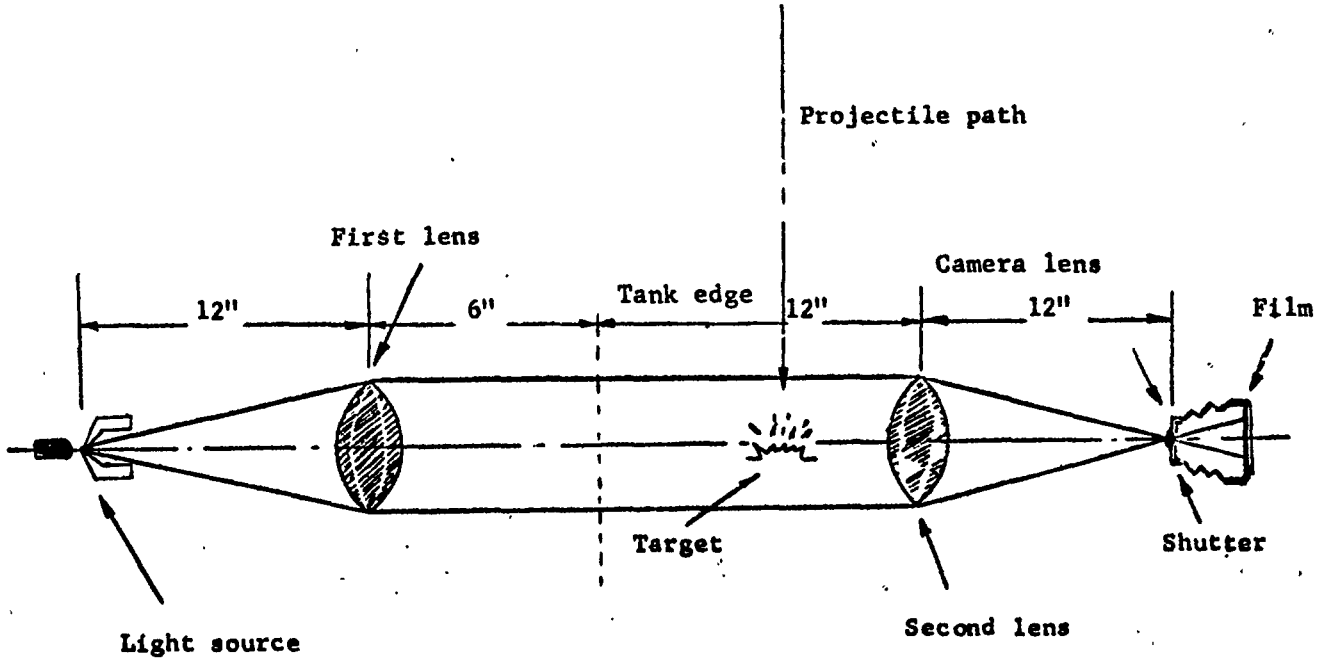

Fig. 3. Diagram of optical system.

light rays.

Lenses. Two aircraft-camera lenses were adapted for use in the system. They are Fairchild camera lenses with 12 inch focal length, and a 4 inch inner diameter. The lenses were shielded from spray with cover boxes with 1/8 inch-thick glass windows.

Light Source. A coaxial barium titanate capacitor was used for the storage capacitor of the light source. This spark light was available from previous work.[13] As used originally, it had an intensity of about 0.172×10^5 candle per sq. cm at 15 kilovolts capacitor potential. The pulse duration was about 2 micro sec. In this experiment it was found that 8 kilovolts potential was sufficient to give enough intensity for the camera. This probably reduced the light-pulse duration to less than one microsecond and the intensity to about 4×10^4 candle per square cm. The light source is shown in Fig. 4.

Cameras. Two Polaroid Land cameras were used, one for oscilloscope sweep recording and the other for photographing the impact process. Polascope type 410 film with a speed of ASA 10,000 was employed for impact photography, but for sweep recording, an ordinary Type 47 ASA 3000 film was used. A blue gelatin filter was used before the lens for impact photography in order to reduce the light-pulse duration.

The impact-camera shutter was electrically synchronized with the gun firing circuit. The oscilloscope camera was manually operated.

3.3 Timing and Control Circuits

A schematic diagram of the timing and control circuits used is shown in Fig. 5. Projectile velocity is measured using an aluminized

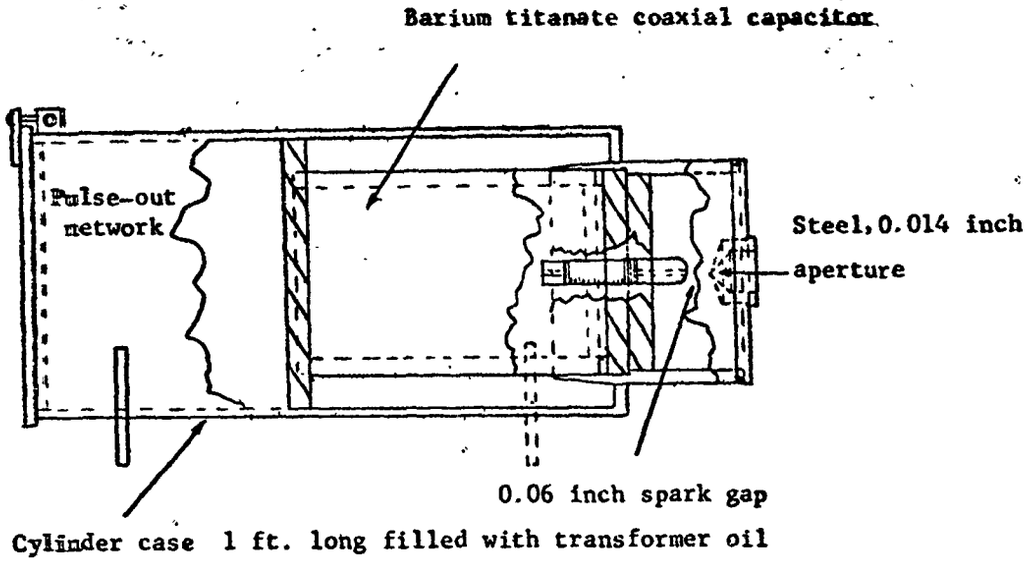

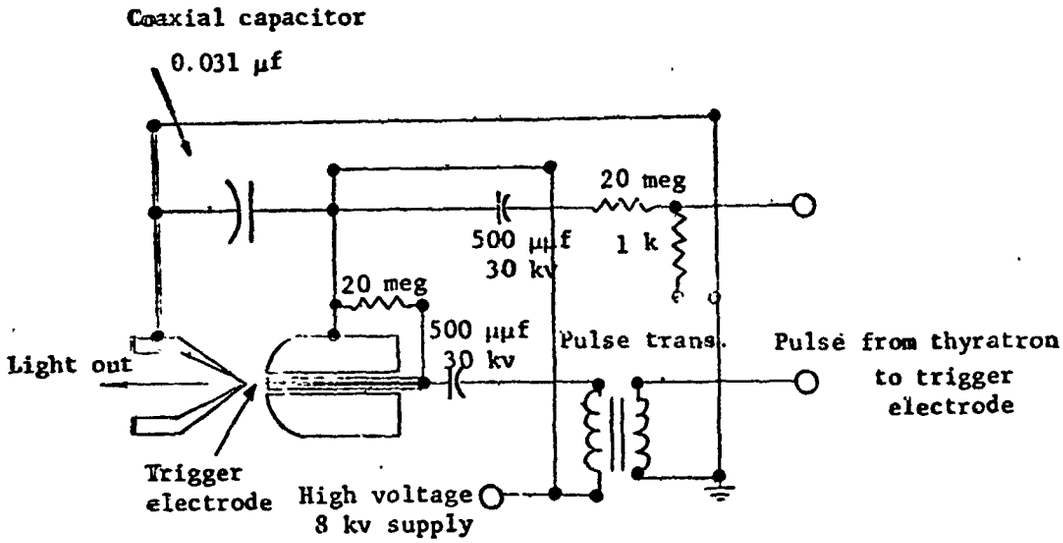

Fig. 4. Spark-gap light source.

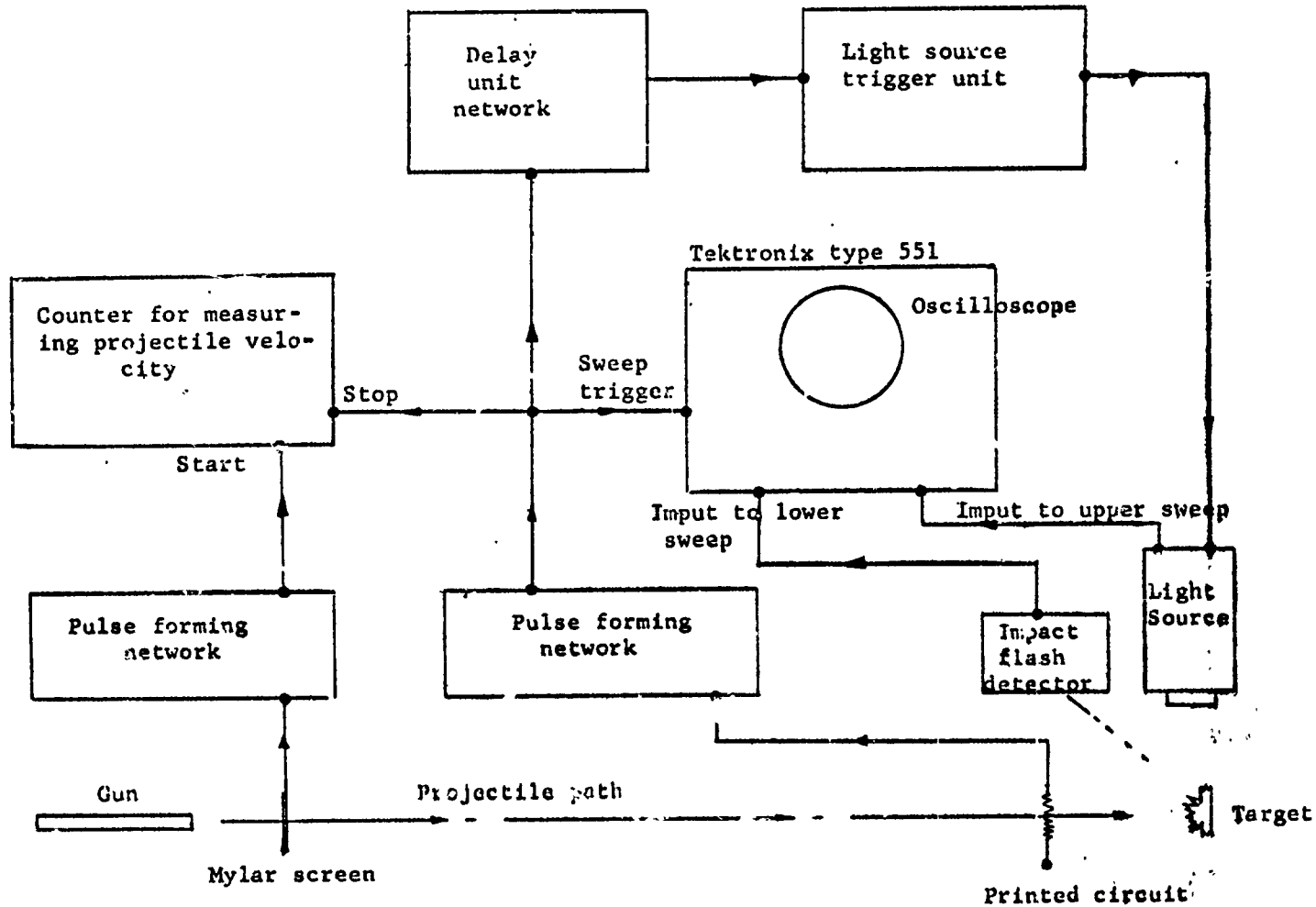

Fig. 5. System block diagram.

Mylar screen and a printed-circuit grid to start and stop a time-interval counter. The light flash is controlled by a pulse from the grid through a delay circuit. The time of impact is determined by observing the impact flash, and the time of the light flash is determined by a pulse sent from the light source. A description of the individual units follows.

Time-Interval Counter and Pulse-Forming Networks. For velocity measurement, a Berkeley universal Eput and Timer model 7360 is used. A starting pulse is obtained from a capacitor-type pulse-forming network employing an aluminized-Mylar screen as a "make" switch. The circuit is shown in Fig. 6. The output pulse is about 90 volts positive. The counter is stopped by a pulse caused by breaking a conducting grid painted on paper. The two switches are set 26.5 ft. apart. The circuit of the second pulse-forming network is shown in Fig. 7. The output pulse is about 80 volts positive.

Delay Unit and Light-Source Trigger Unit. The trigger pulse from the second pulse forming network is fed to a delay unit to control the time of flash of the light source. The circuit diagram and pulse waveforms of the unit are shown in Fig. 8. The output pulse is about 200 volts. Delay can be controlled from 3 to 330 μ sec. Pulse width is 5 μ sec and rise time is 1 μ sec.

The pulse from the delay unit goes to a light-source trigger unit using a thyratron pulse-forming circuit and a pulse transformer. The circuit diagram is shown in Fig. 9. The trigger unit is a modified Navy radar modulator unit. The output from the trigger unit is a 10 kilovolt, 1 μ sec duration pulse. When this pulse is applied to the trigger electrode of the spark gap, the gap breaks down and discharges the

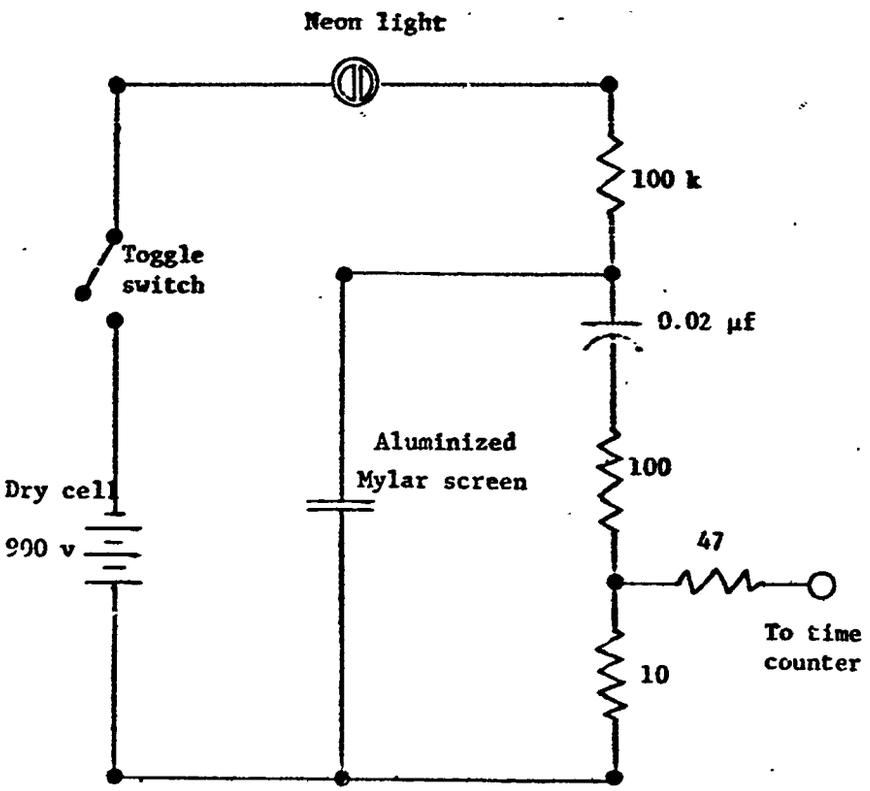

Fig. 6. Make-type pulse-forming circuit with aluminized Mylar screen.

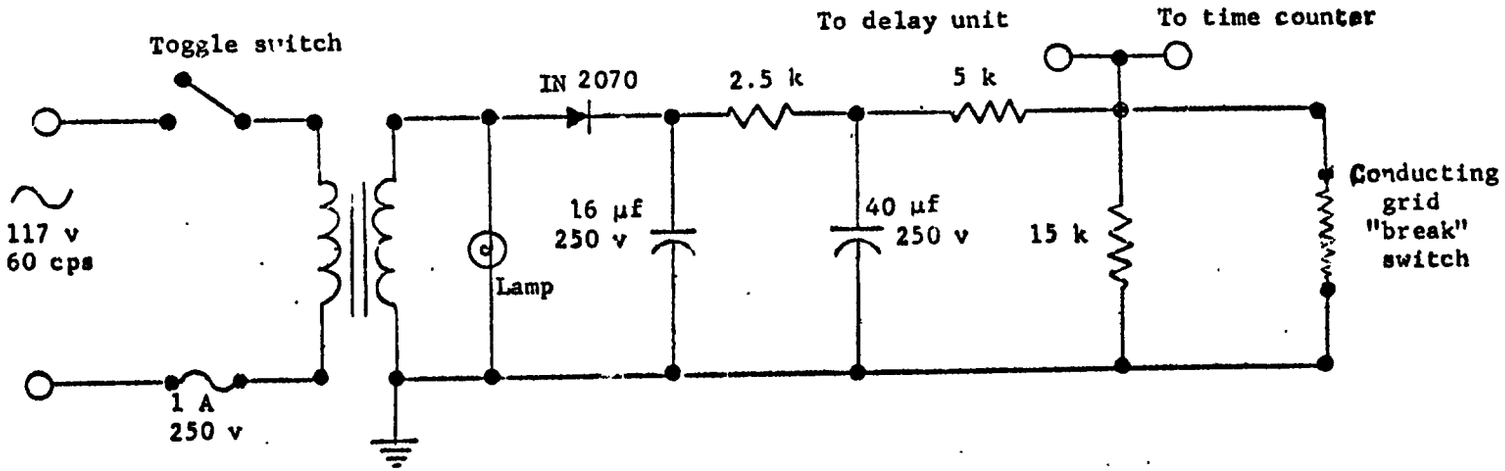

Fig. 7. Break-type pulse-forming network with conductor grid.

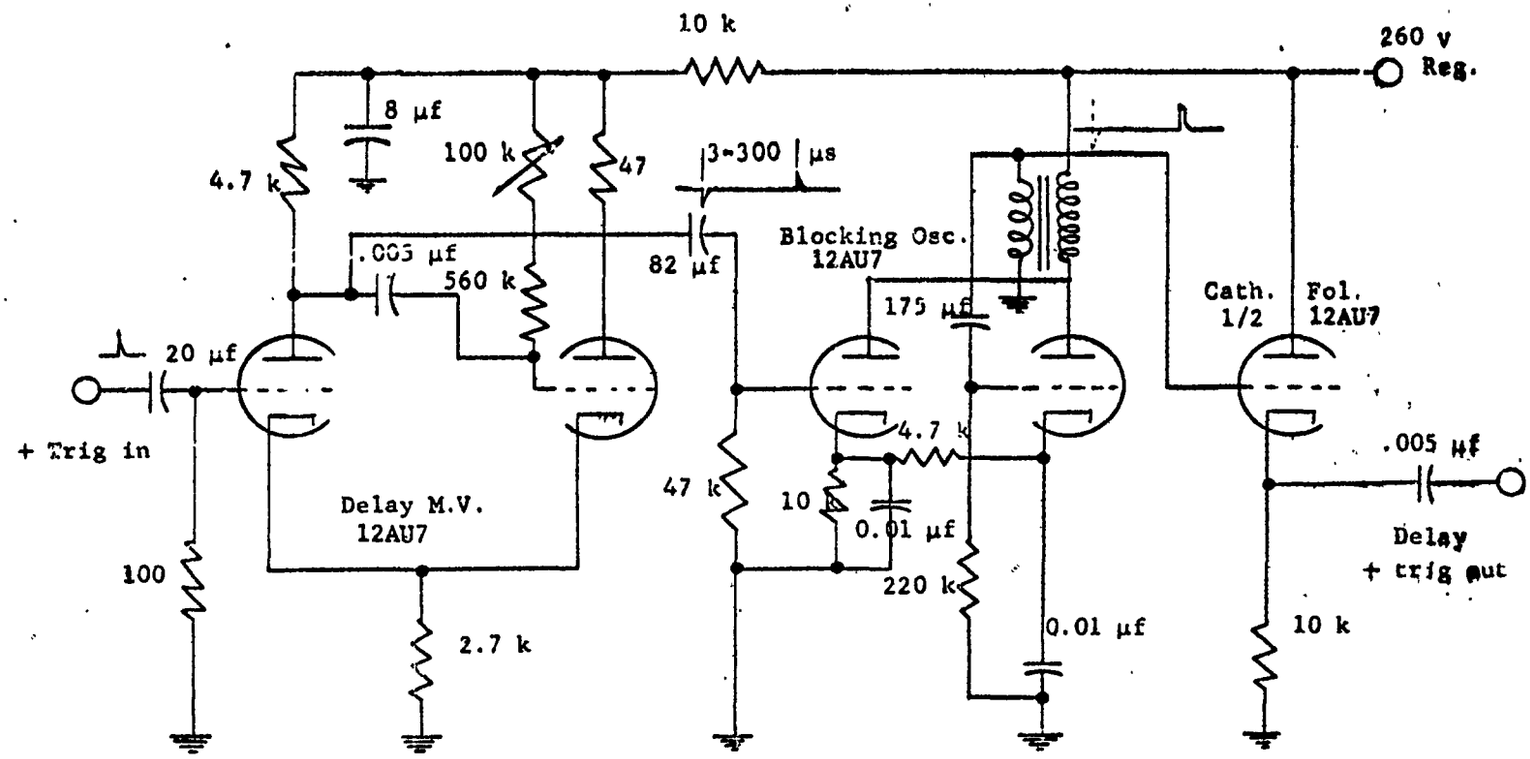

Fig. 8. Pulse delay circuit.

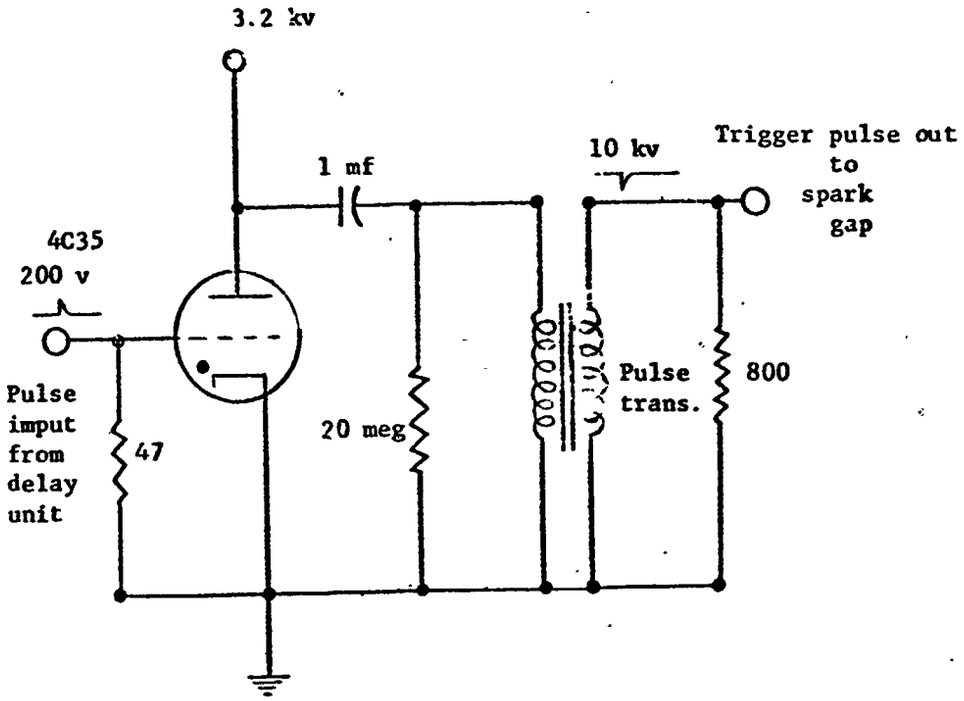

Fig. 9. Thyratron switching circuit.

storage capacitor producing the light flash.

Phototube Circuit. The time of impact is determined by observing the impact flash with the phototube circuit shown in Fig. 10. The time of the light flash is determined by a pulse from the flash unit. The circuit connection is shown in Fig. 4.

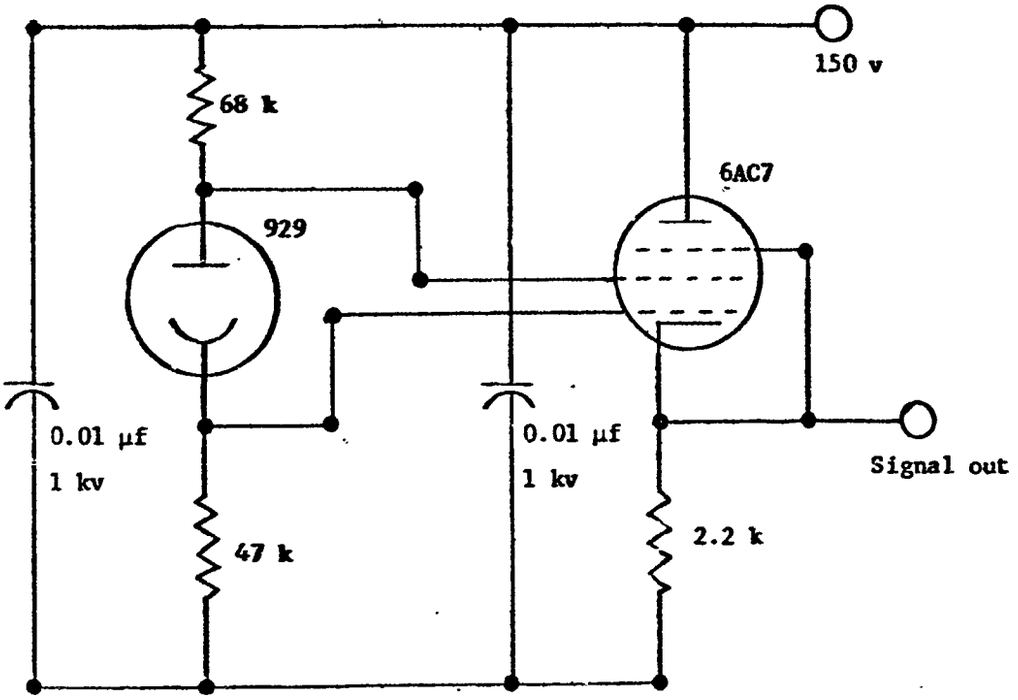

Fig. 10. Circuit diagram of phototube light detector.

IV. EXPERIMENTAL RESULTS

Typical impact oscillograms are shown in Fig. 11; the upper trace is the response from a 929 phototube. The lower trace is from the light source. The time difference between the pulses on the two traces is the approximate time after impact of the photograph. This is considered more accurate than a manual delay-setting reading.

Three series of impact shadowgraphs are shown in sequence in Figs. 12 to 15. Data of the experiments are in Appendix A. The experimental results are discussed under the headings, "Impact Flash," "Spray Particles," "Surface Flow," and "Penetration."

4.1 The Impact Flash

From the oscillograms it is seen that most impact flashes have a duration of about ten microseconds. A peak voltage of about 12 volts is observed at 200 micron pressure. The phototube load resistor is about 47 k ohm and the tube is placed 25 cm from flash point. The characteristic of the phototube is such that it will give about 50 μa plate current[9] for a luminous flux of 1 lumen. From this, the luminous flux received is calculated to be 5 lumen. With a phototube cathode area of 3.28 cm^2, the solid angle intercepted is 5.25×10^{-3} steradian. The candle power of the source is then about 950 candle power. Assuming an area for the impact flash of 1 cm^2, the brightness is about 950 candles per cm^2. This brightness does not have much effect on the photographs because of the optical system used and the use of the blue gelatin filter. Some impact flash can be noticed.

Sweep speed 50 μ sec/cm

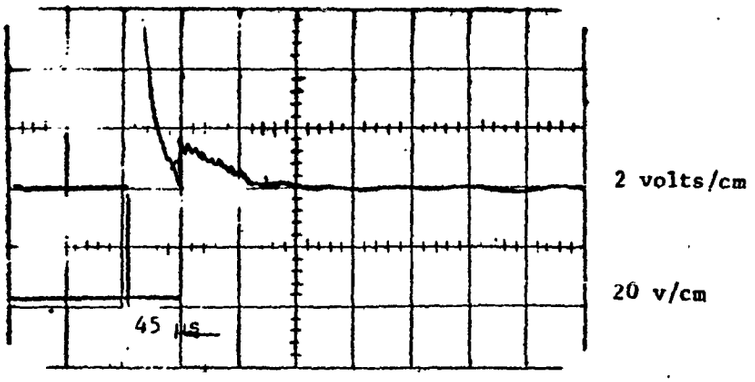

a. About 45 μ sec after impact.

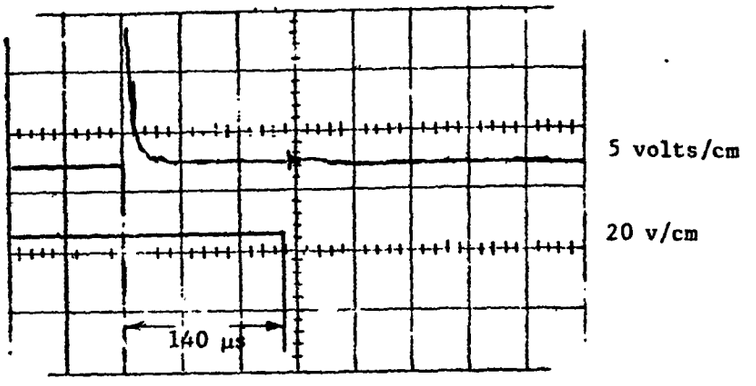

b. About 140 μ sec after impact.

Fig. 11. Typical impact oscillogram. The upper trace on the response from impact flash, the lower traces are pulses from light source.

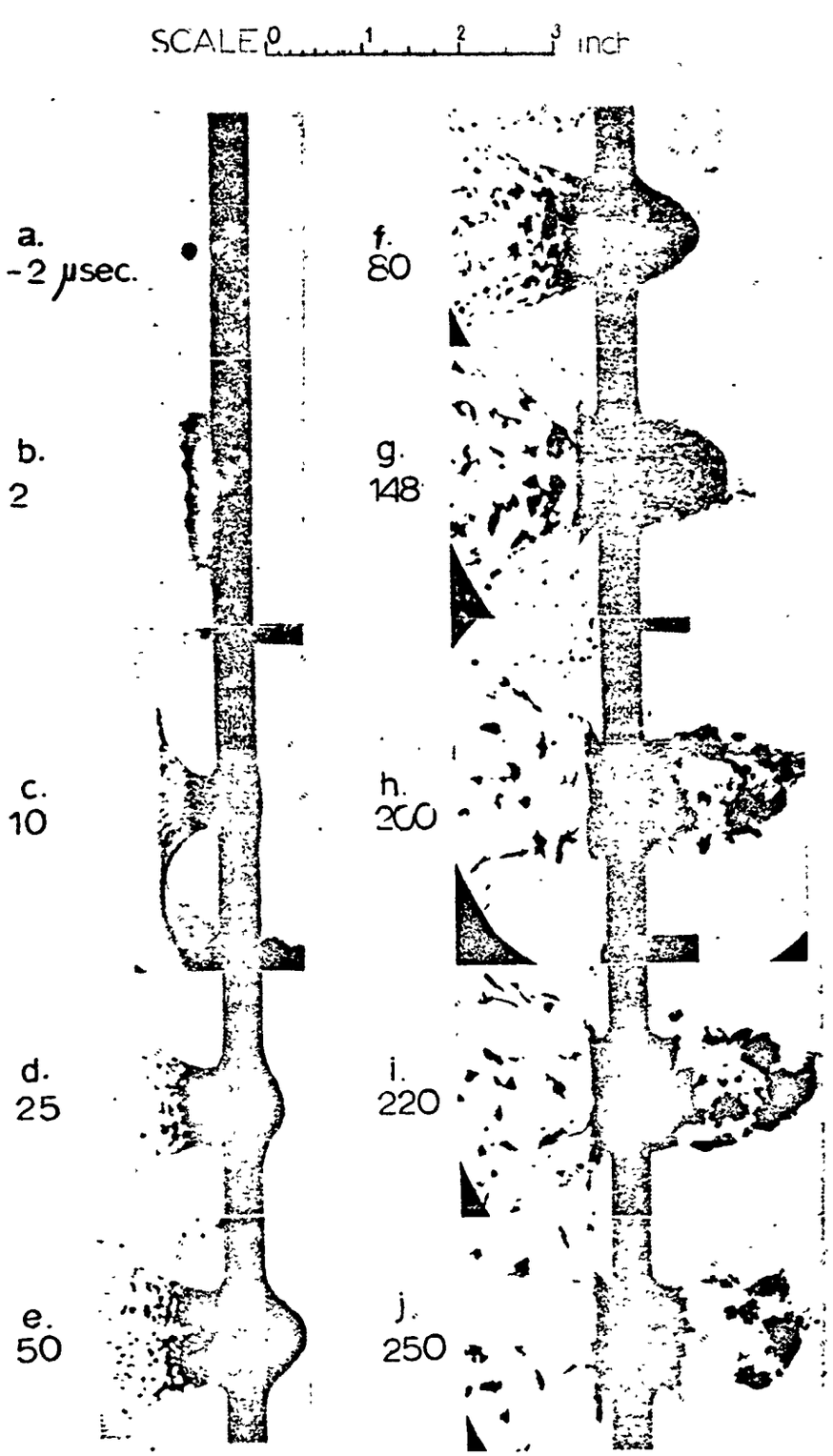

Fig. 12. Perforation of 0.426 inch target.

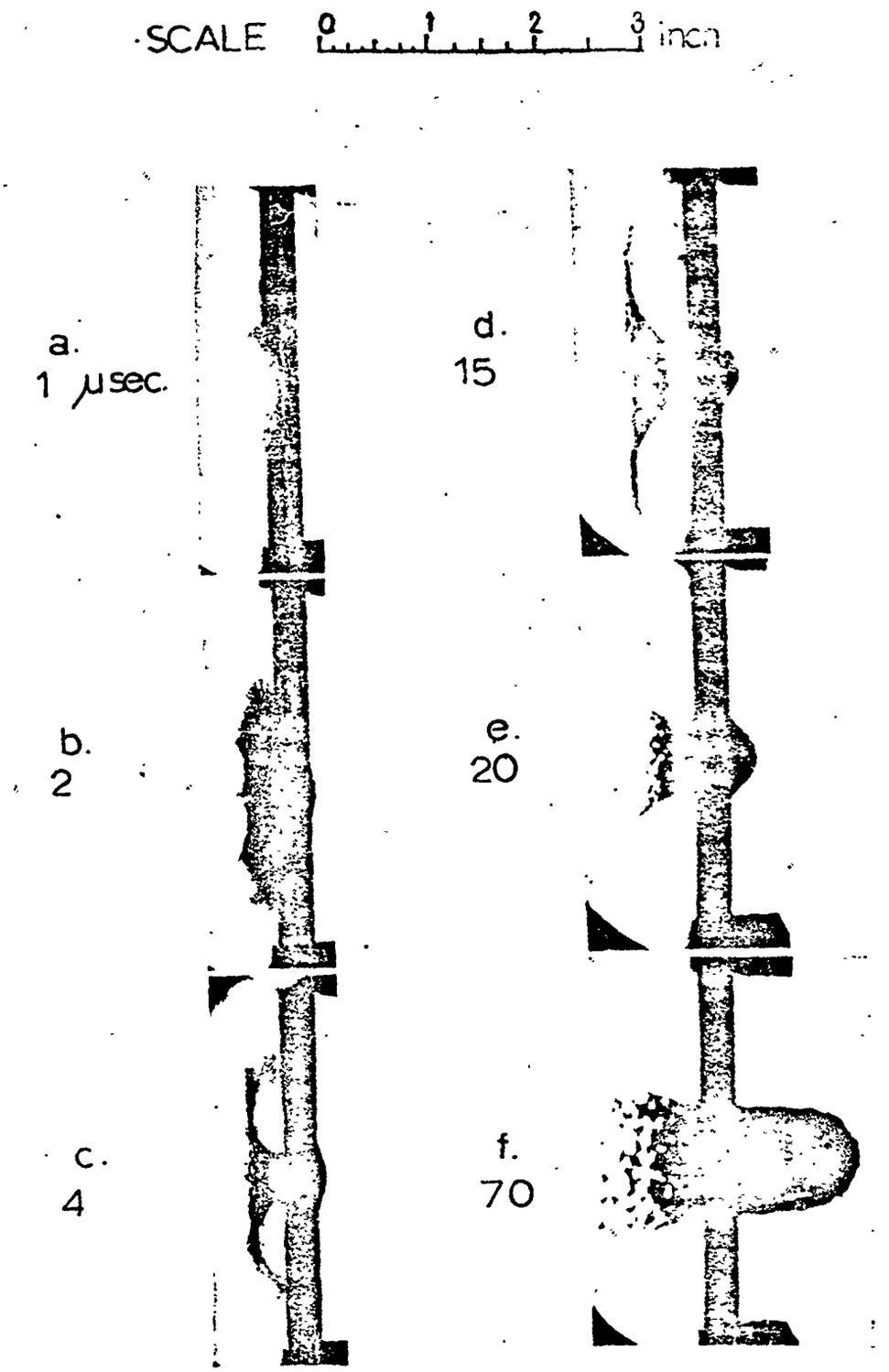

Fig. 13. Perforation of 0.266 inch target.

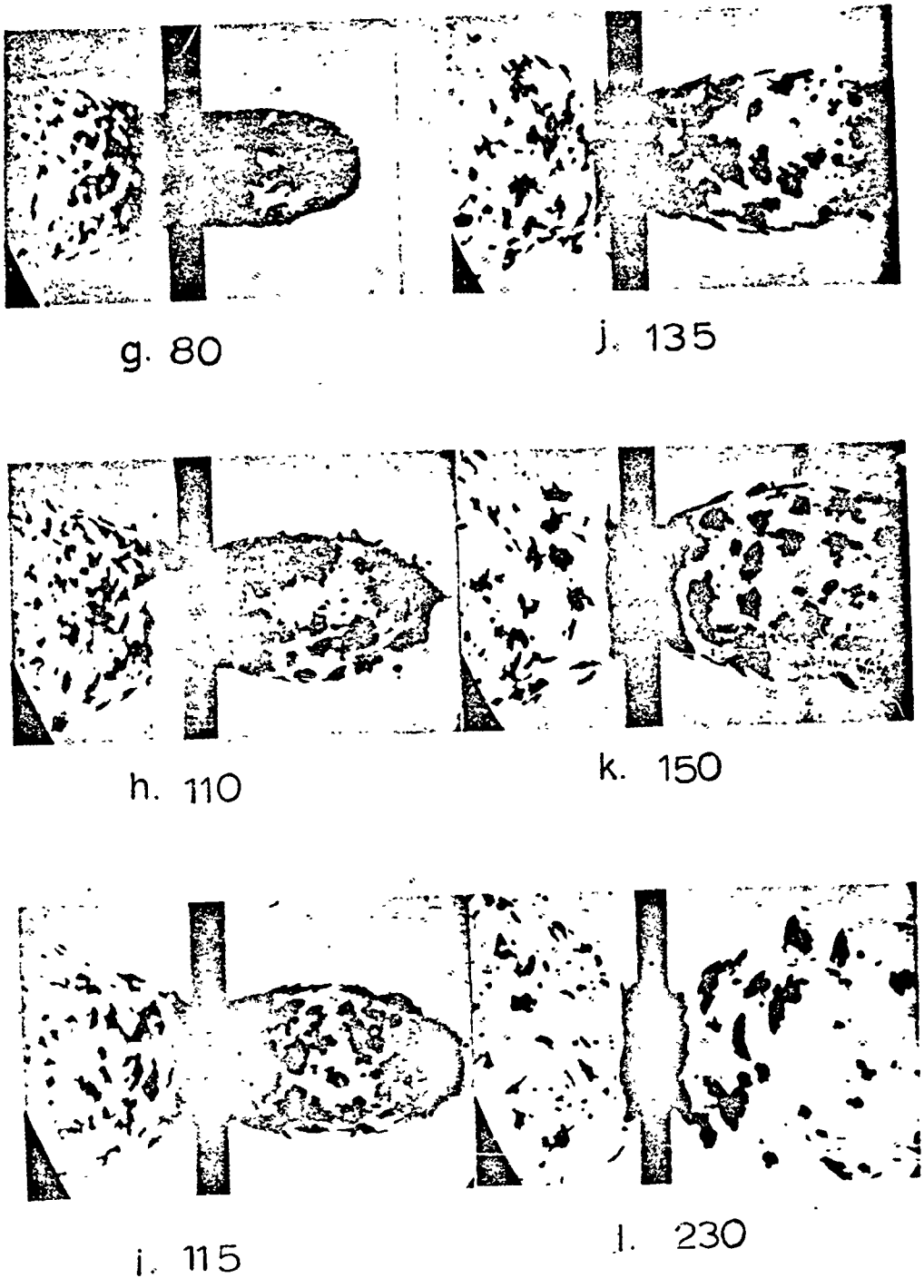

Fig. 14. Perforation of 0.266 inch target. (continued)

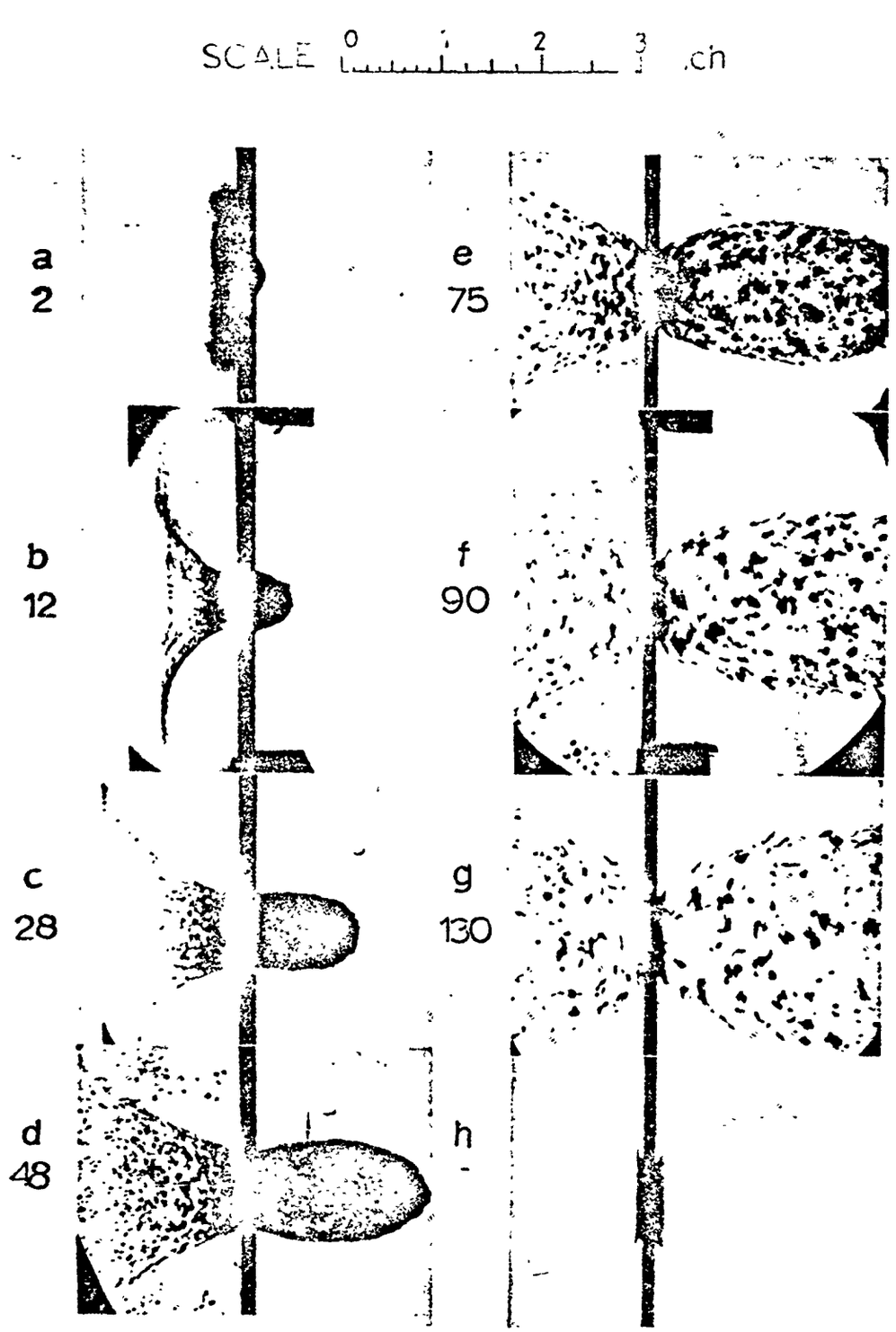

Fig. 15. Perforation of 0.132 inch target.

From the oscillograms and the known velocity of a pellet, it is possible to calculate the time the impact flash occurs after the pellet touches the target surface. The result is in the order of 1 to 2 micro seconds, which is in the range of error of the interpretation of oscillograms. Consequently it is reasonable to assume that the flash occurs at the time of impact. The time difference between the two pulses from the oscillograms is taken as the delay time after impact thoughout this work.

4.2 Spray Particles

Since the pellet perforates through the target, there are spray particles both at the front and back of the target. The results are as follows.

Front-Surface Spray Velocity. From Figs. 12 through 15, the distances of spray travel are measured, and with the corresponding time intervals from the oscillograms, the velocities are computed. Results are shown in Table I for various exit angles measured from the target face.

TABLE I

Spray Particle Velocities (km/sec)

Target	Time interval	1°	5°	15°	30°	45°
0.425 inch	0 - 2	11.6	10.8	10.1	7.66	4.69
	0 - 10	4.69	4.07	3.76	3.13	2.19
	2 - 10	3.13	2.8	2.68	2.15	1.57
0.266 inch	0 - 2	12.1	11.5	11.1	7	3.9
	0 - 4	6.5	6.2	7.8	4.3	3.1
	0 - 15	3.64	3.12	2.71	2.08	1.36
	4 - 15	2.55	1.99	1.7	1.41	0.56
0.132 inch	0 - 2	10.1	9.4	7.8	4.68	2.34
	0 - 12	4.82	4.17	3.9	3.38	2.3
	2 - 12	3.75	3.2	3.14	3.1	2.32

The velocity is found to vary with exit angle measured from the target face. The variation with target thickness is slight. The leading edge of the cloud of spray material is measured in all cases.

It is seen that the velocity decreases with time for a given exit angle. This indicates that the initial material coming off is very fine and is decelerated rapidly. The fastest material appears to be a cloud of smoke in the pictures. The larger particles which appear in the later photographs have lower initial velocities and their deceleration is negligible. The measured velocities are not exact because of the lack of precise knowledge of the time and place of origin of the material composing the cloud.

The velocities reported here are higher than those reported previously[4] for cratering in thick lead targets. In this earlier work, only large particles were observed over times of 10 to 115 μ sec. The major part of the energy and mass carried away with this spray material was associated with the large particles.

Back-Surface Spray Velocity. From Figs. 12 through 15, the back-surface spray can be observed. It is seen that the exit spray comes out at angles between 50 and 90 degrees with less variation of velocity with angle than the front spray. The instantaneous position of the front of the bulge is plotted Fig. 16. The slope of the lines gives the velocities indicated. The scatter in the data and the small amount of data prevent the observation of any changes in velocity which might be caused by material strength as the particles break free.

Target Mass Loss. The total mass of material lost as spray was found by weighing each target before and after the shot. The data are

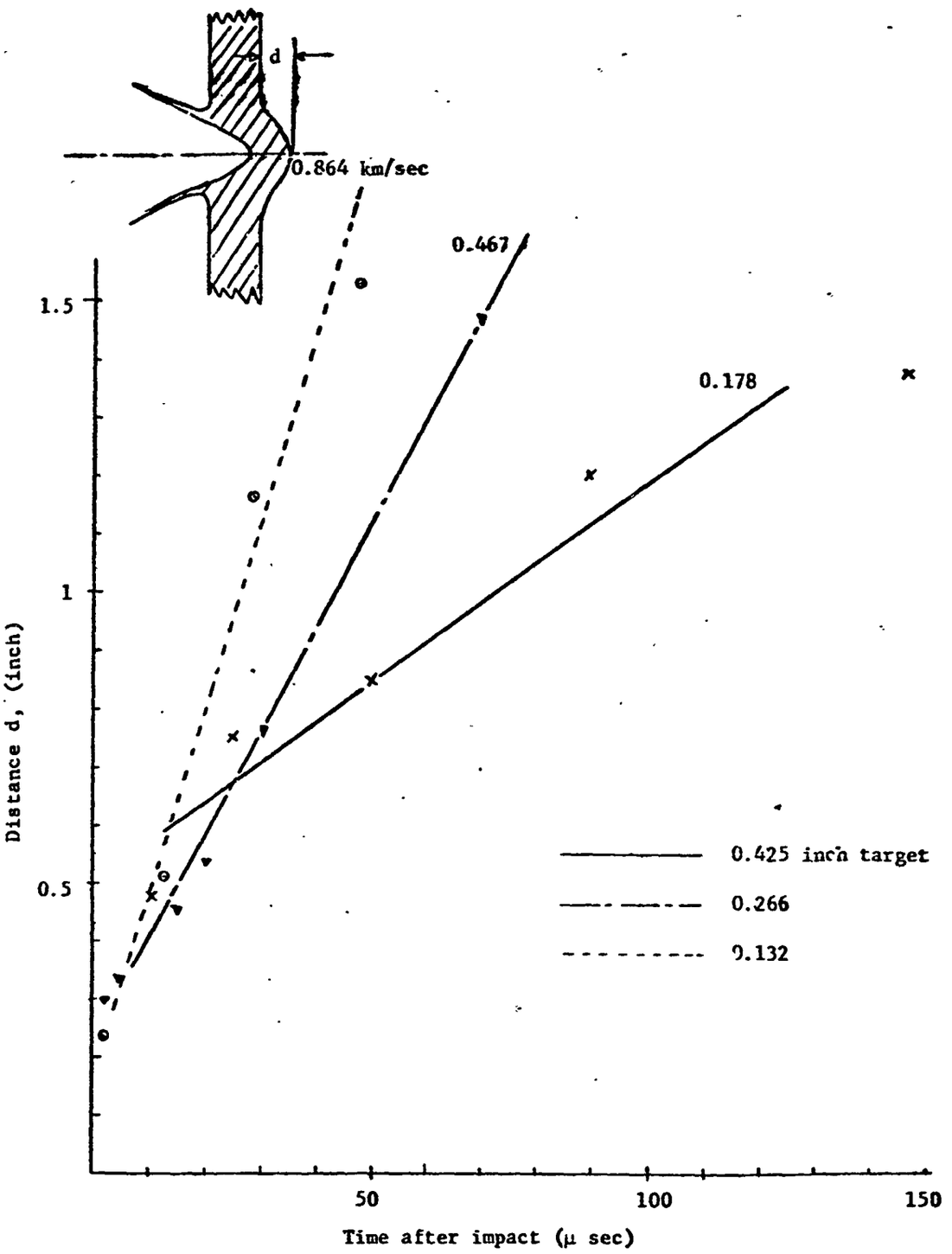

Fig. 16. Motion of the back free surface of the target.

in Appendix A. Average results are shown in Fig. 17. It is seen that spall mass increases with increasing target thickness, then reaches a peak and finally decreases. The value for a semi-infinite target is shown.[14]

4.3 Shock-Wave Pressure

If the back spray velocity is considered to be the free-surface velocity, the material velocity can be found from Eq. 2.27, $u_{fs} = 2u$. Knowing the material velocity, the pressure can be found from the data in Fig. 1. Shock velocity also can be calculated using Eq. 2.26.

The results for the pressure at three different depths, corresponding with the three target thicknesses used, are plotted in Fig. 18. The curve represents the pressure decay in a target in impact. For comparison, for a steel pellet penetrating into water,[15] the pressure wave decays inversely proportionally to the distance of travel, r. In this case shown here, the decay is more rapid than 1/r. This result agrees with the work of Moreno[16] who found that the pressure decay for impact in aluminum is faster than 1/r.

4.4 Surface Flow

In Figs. 12 to 15 the movement of material surfaces can be observed. These pictures can be used to determine the flow of the back surface in the direction of projectile travel as discussed in Sections 4.2 and 4.3. The radial expansion of the hole can be observed on both the front and back surfaces and the position of the inner surface of the hole can be estimated from the angle of ejection of the spray material. The relation of spray direction to hole diameter can be estimated from radiographs of

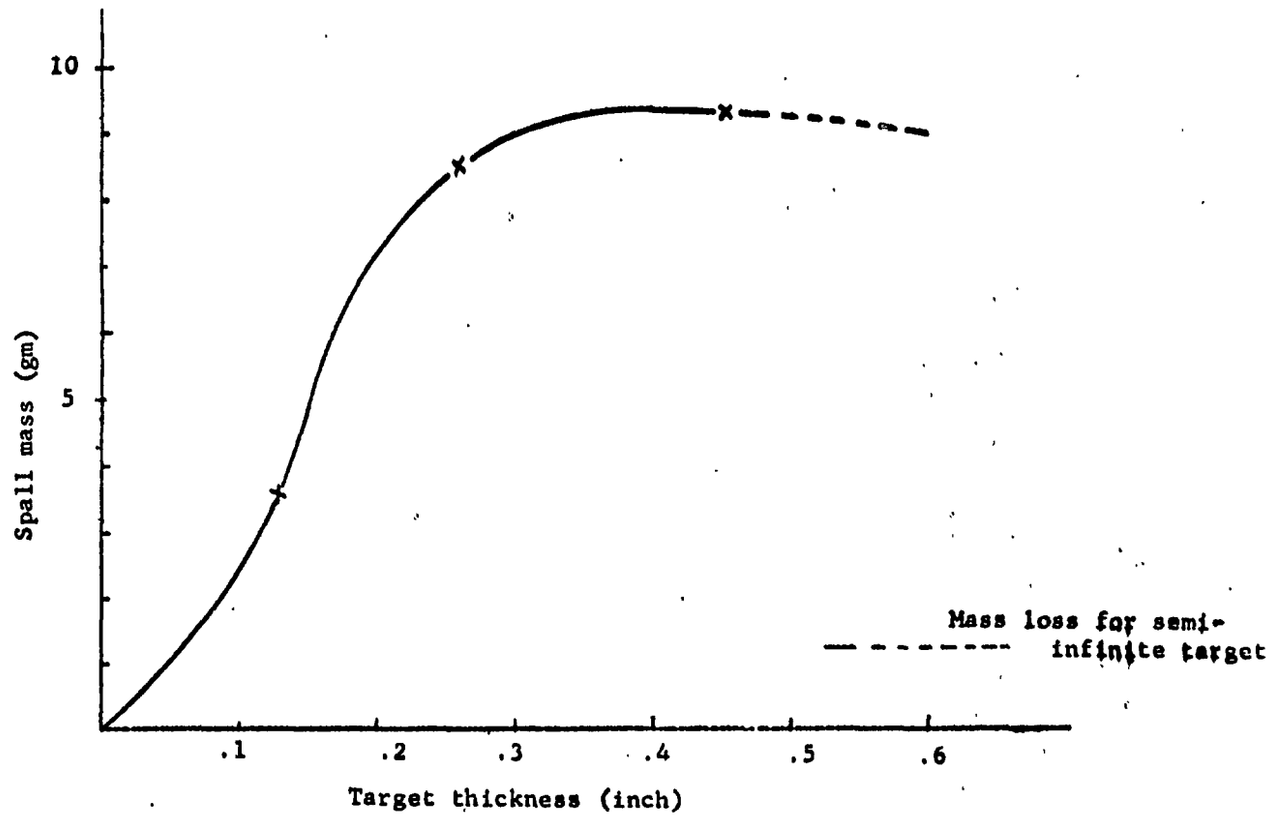

Fig. 17. Total mass loss vs. target thickness.

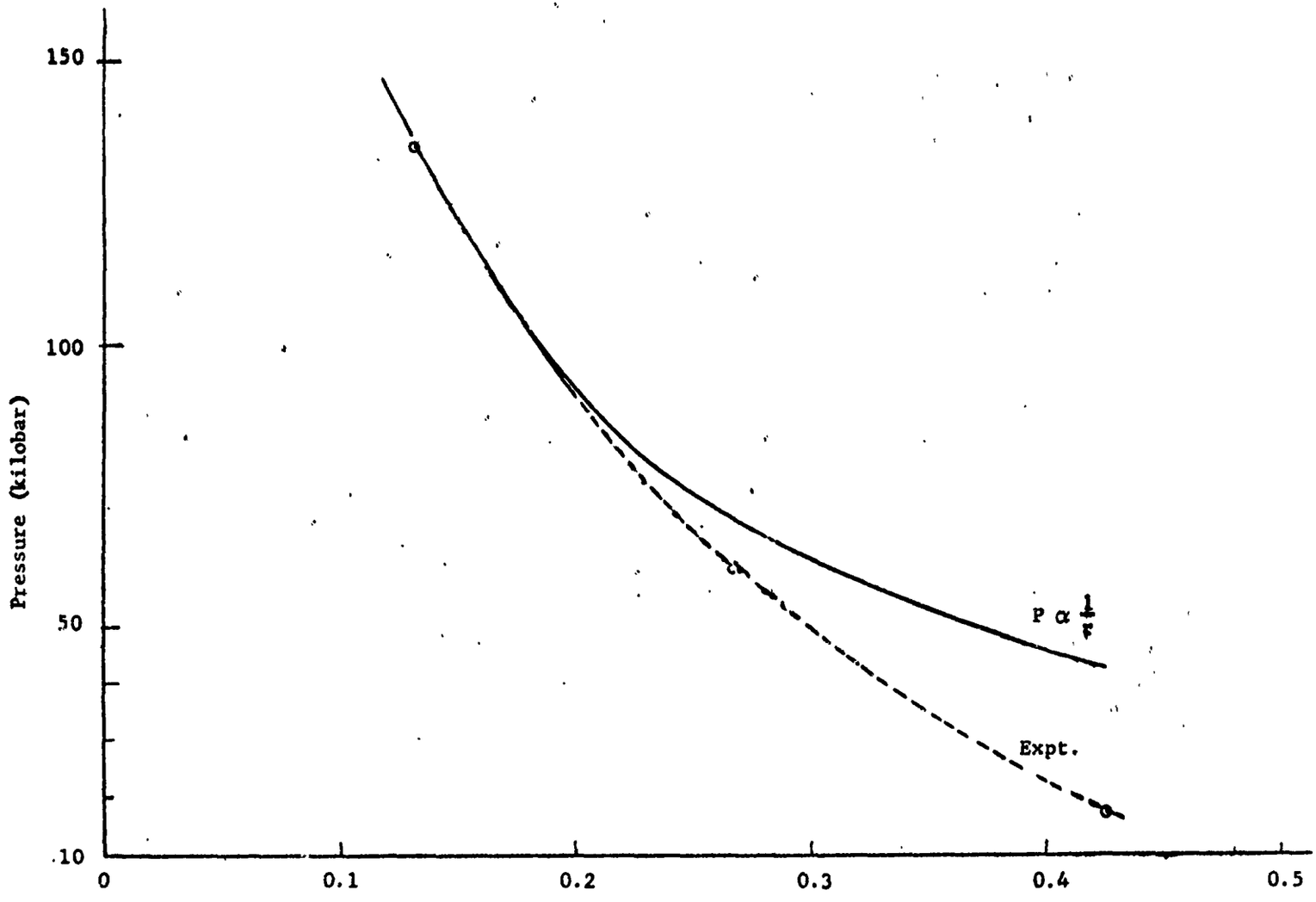

Fig. 18. Shock wave pressure.

cratering in other materials[3] although no data are available for lead). These measurements of the time history of hole enlargement are shown in Figs. 19 to 21. An empirical equation as follows was found to fit the data shown in Figs. 19 and 20.

$$r = mte^{\left(1 - \frac{t}{n}\right)} \tag{4.41}$$

where

r = instantaneous radius of deformed surface

t = time after impact

m,n = constants

The two arbitrary constants m and n are determined by their boundary conditions. For example at $t_1 = n_1$, $r_1 = m_1 t_1$. Thus

$$m_1 = \frac{r_1}{t_1}$$

The velocity of surface movement if obtained by differentating Eq. 4.41 with respect to time. Hence if V is an instantaneous velocity, then

$$V = me^{\left(1 - \frac{t}{n}\right)}\left(1 - \frac{t}{n}\right) \tag{4.42}$$

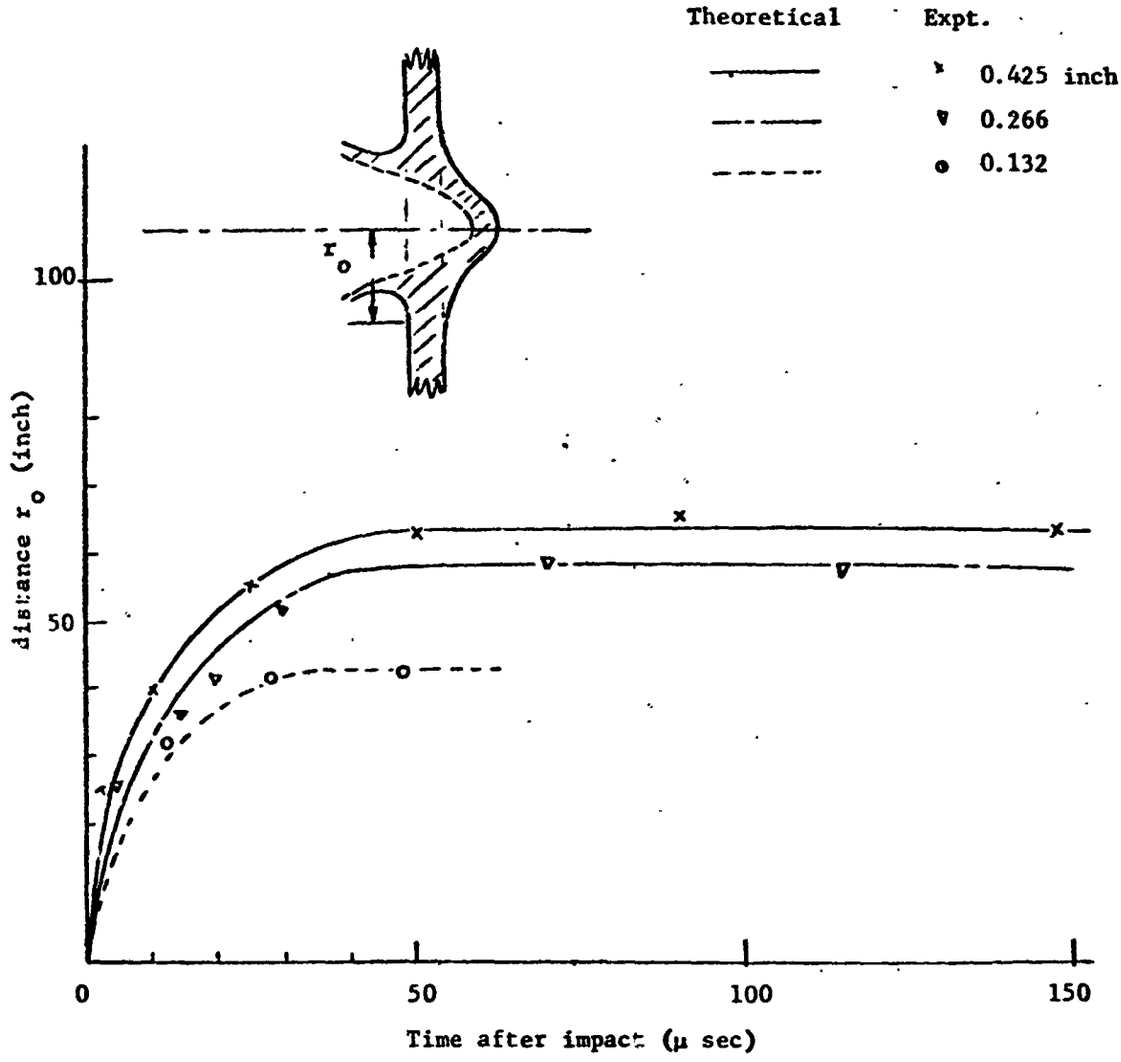

Fig. 19. Expansion of maximum outer lip radius, r_o.

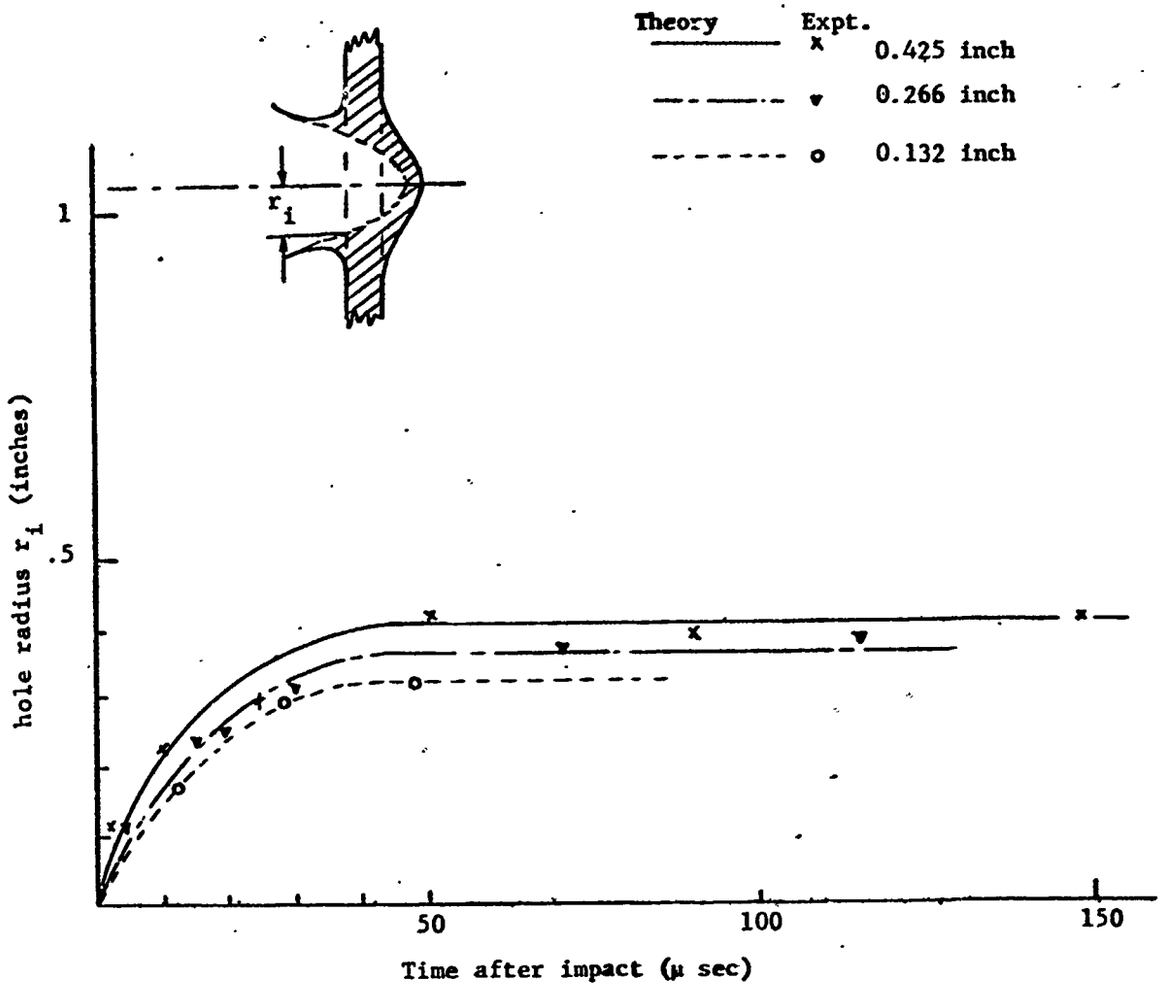

Fig. 20. Opening of perforation.

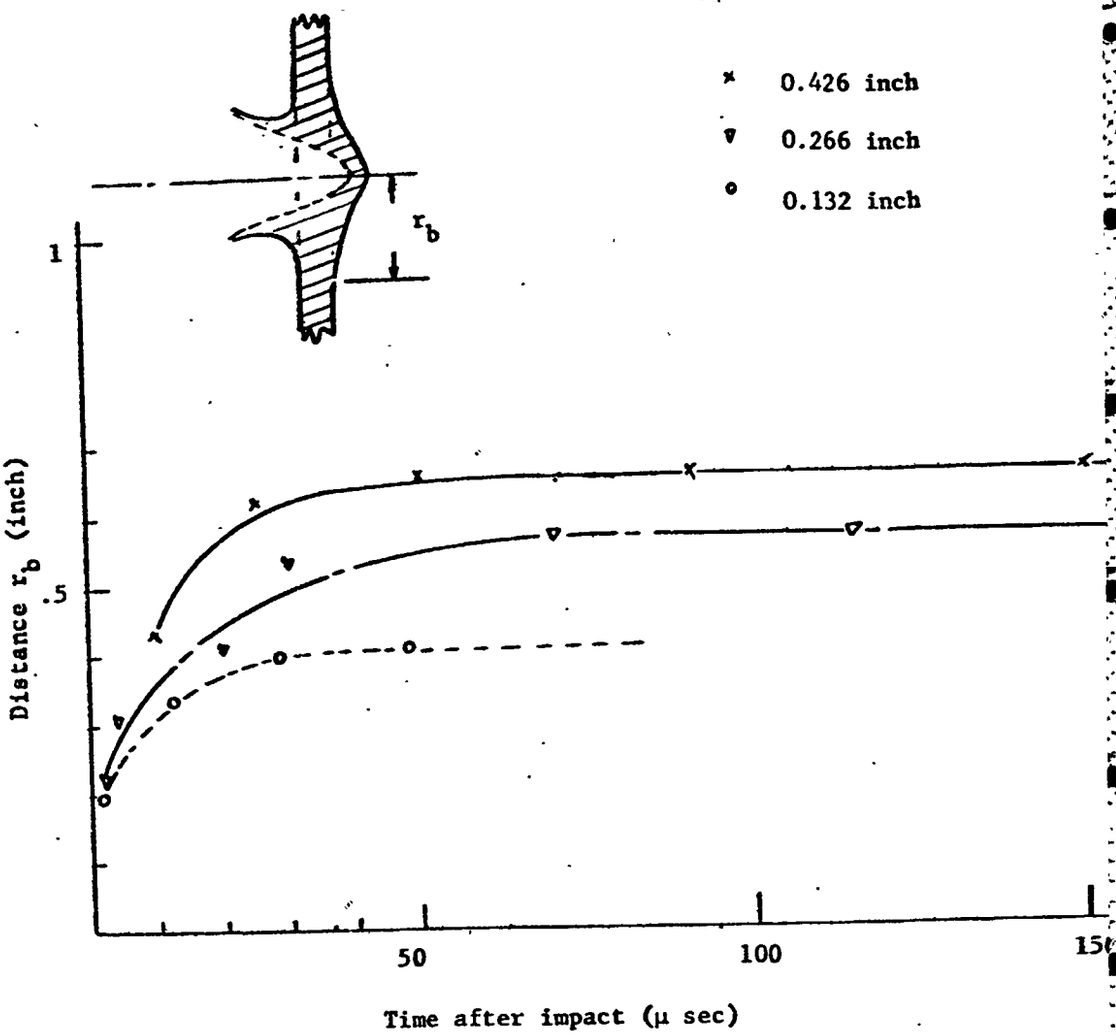

Fig. 21. Back-surface lip motion.

At t = 0, the initial velocity is

$$V_i = me$$

$$= 2.718\ m \qquad (4.43)$$

The curves in Figs. 19 and 20 represent theoretical plots from the empirical formulas. The need of the empirical formula is to provide smooth curves from which to obtain velocities, since numerical differentiation is inaccurate.

No simple equation was found to represent the data of Fig. 21 because of the variation in target thickness. The curves are fitted by eye and velocities obtained by graphical differentiation.

Values of m and n for various target thicknesses are shown below:

TABLE 2

Thickness inches	0.425		0.266		0.132	
	m inch/sec	n μ sec	m	n	m	n
Outer lip radius r_o	0.0132	48	0.0143	40	0.014	30
Hole radius r_i	0.00802	50	0.00805	46	0.0076	42

From Eq. 4.43, it is seen that initial velocities are a function of m. They should be the same for a particular impact velocity. Table 3 confirms this. The average intial velocities are found to be 0.958 km/sec for the

outer lip radius and 0.545 km/sec for the hole radius.

The radial velocities of the three disturbances represented by r_o, r_f, and r_b are shown in Figs. 22 to 24 for the three target thicknesses. These may be considered as distortion waves or plastic waves. These velocities may be compared with the elastic longitudinal bar-wave velocity of 1.2 km/sec and the longitudinal dilatational velocity of 2.1 km/sec.

4.5 Subsurface Waves

A plausible picture of the propagation of the shock wave, its decay into a sound wave, and the propagation of the plastic flow waves is shown in Figs. 25 to 27 for the three targets. The pictures are drawn from the photographs and the velocity data of the previous sections. The shock wave is shown as a dotted line and the beginning of the plastic flow as a dashed line.

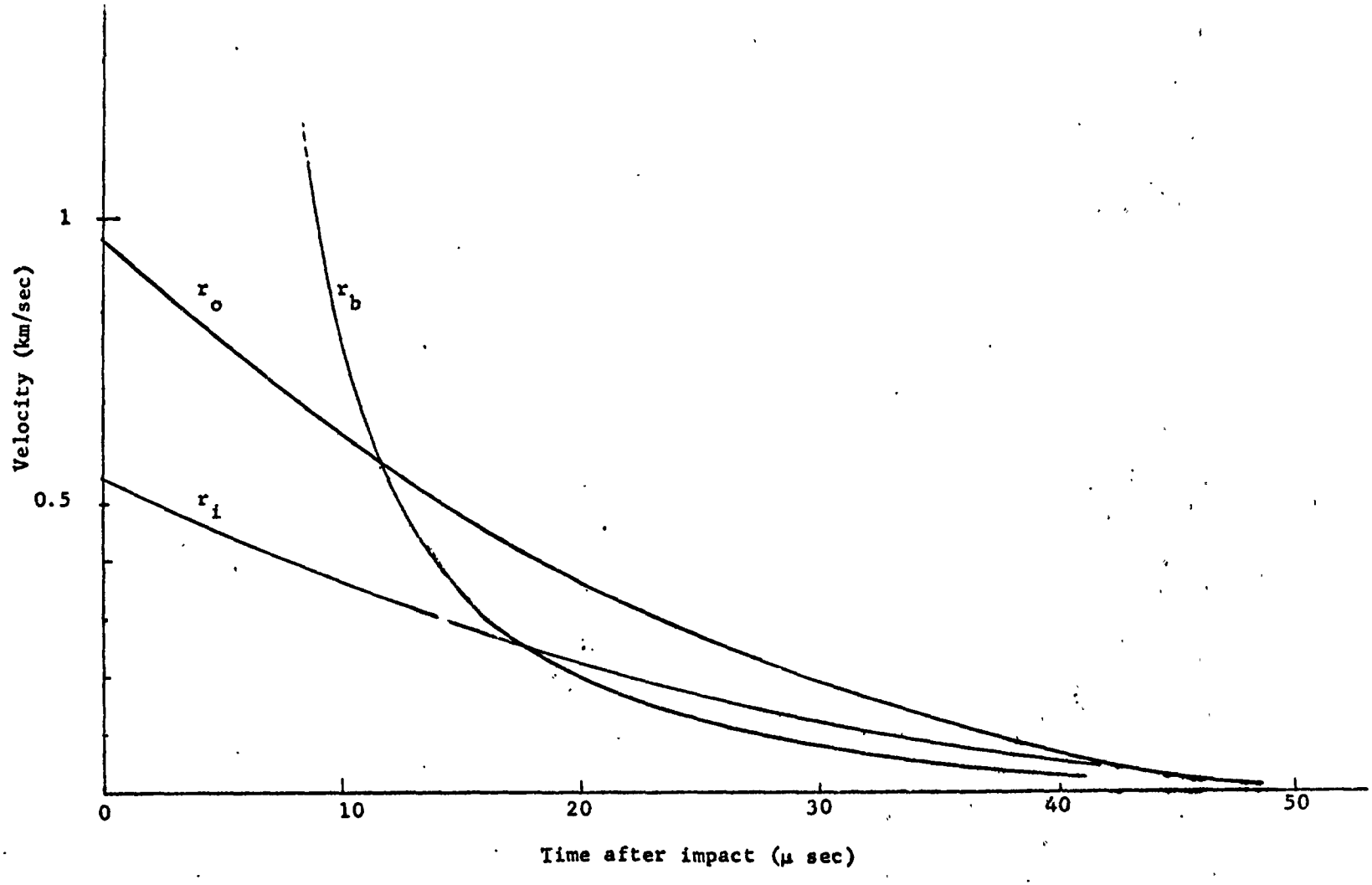

Fig. 12. Surface wave-velocities at various time for 0.425 inch target.

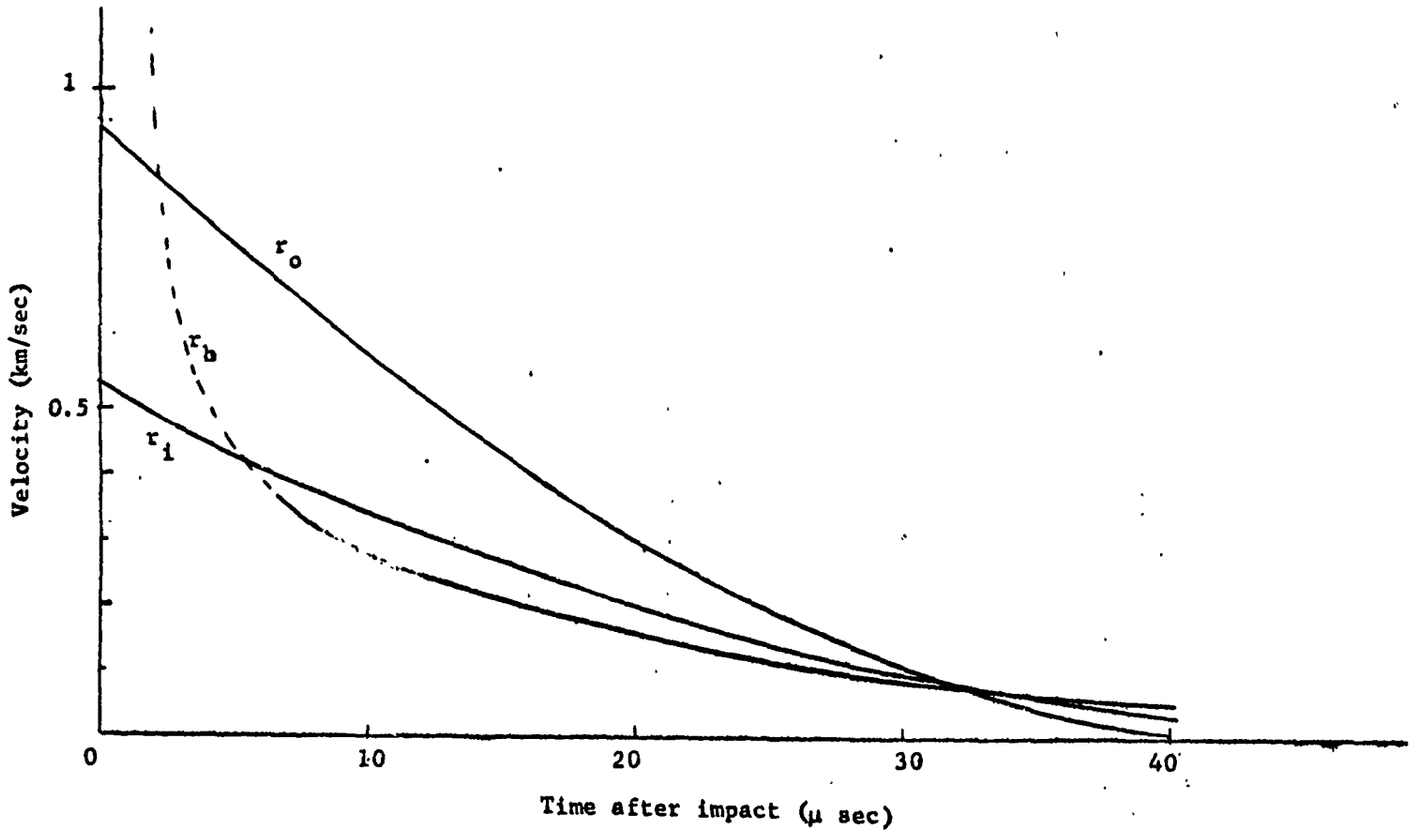

Fig. 23. Surface wave velocities at various time for 0.266 inch target.

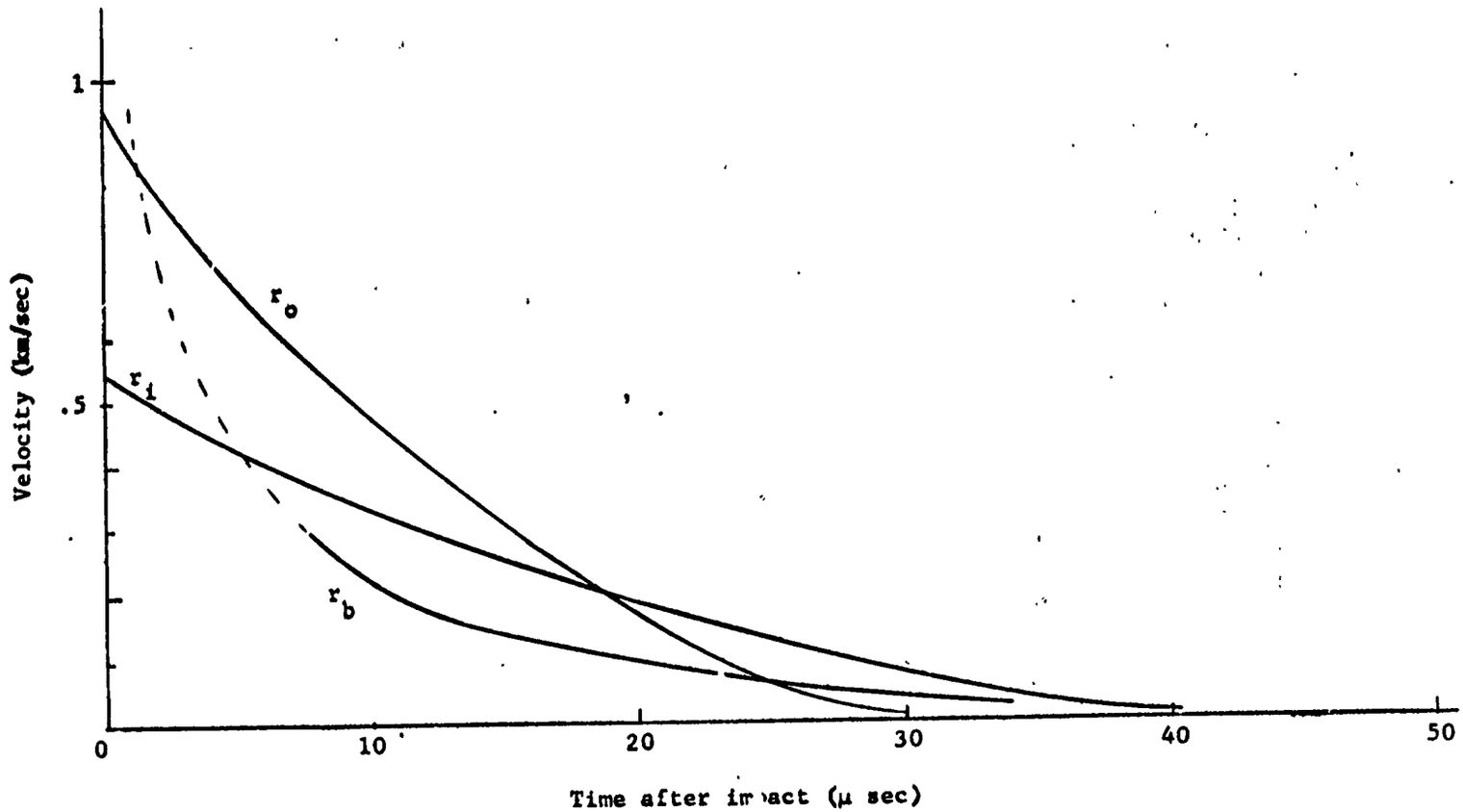

Fig. 24. Surface wave velocities at various time after impact for 0.132 inch target.

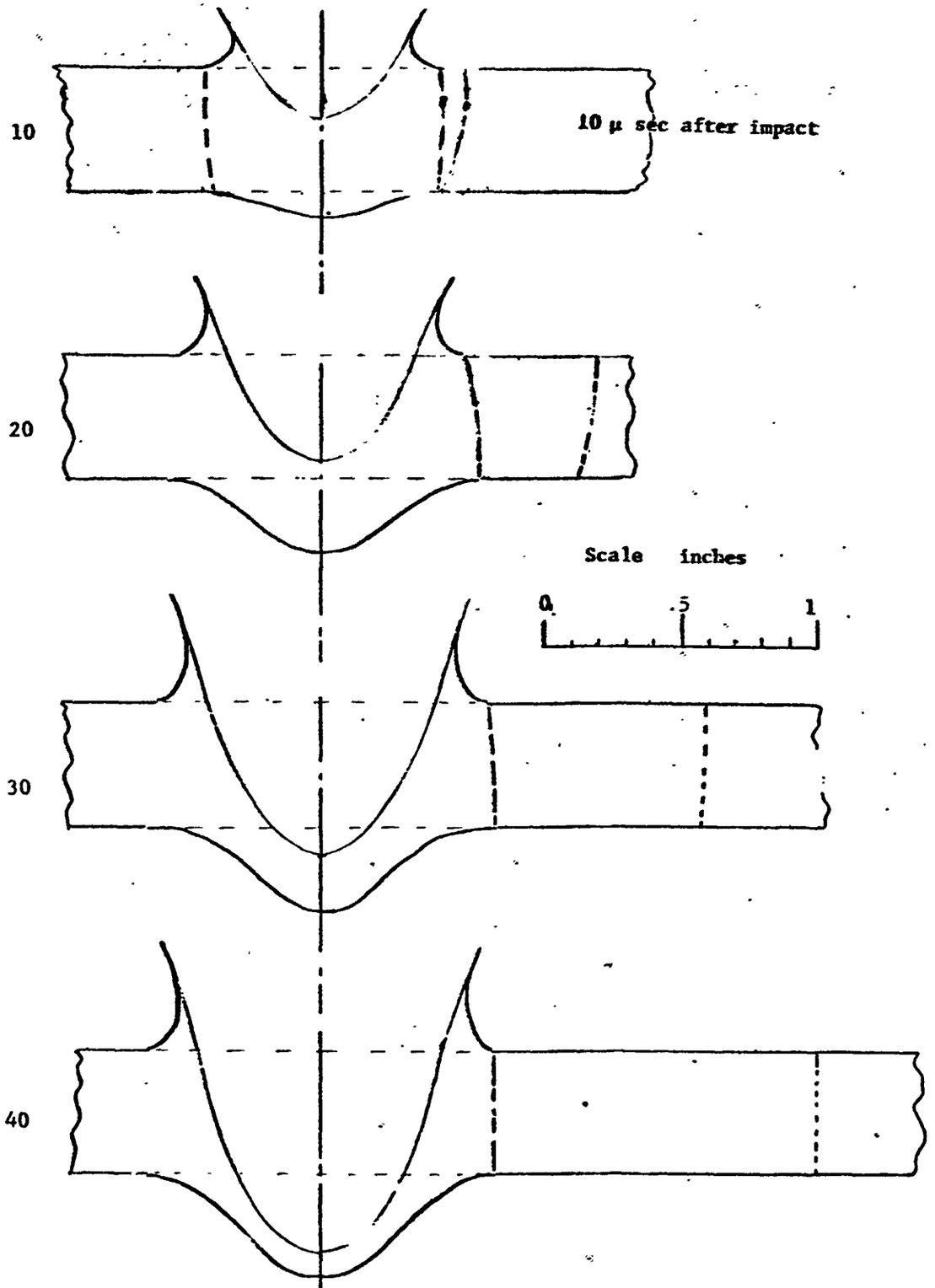

Fig. 25. Flow and wave propagation for 0.426 inch target.

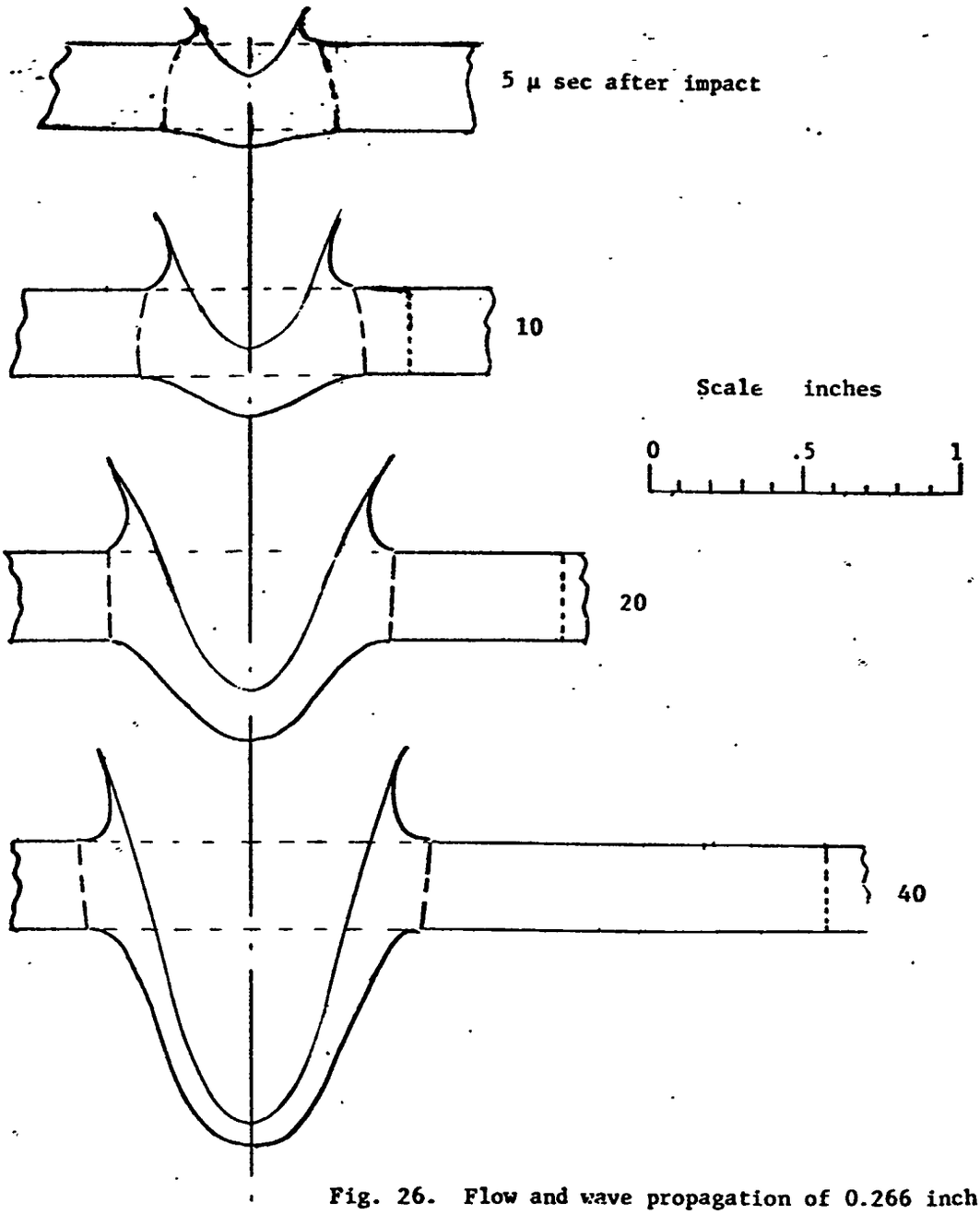

Fig. 26. Flow and wave propagation of 0.266 inch target.

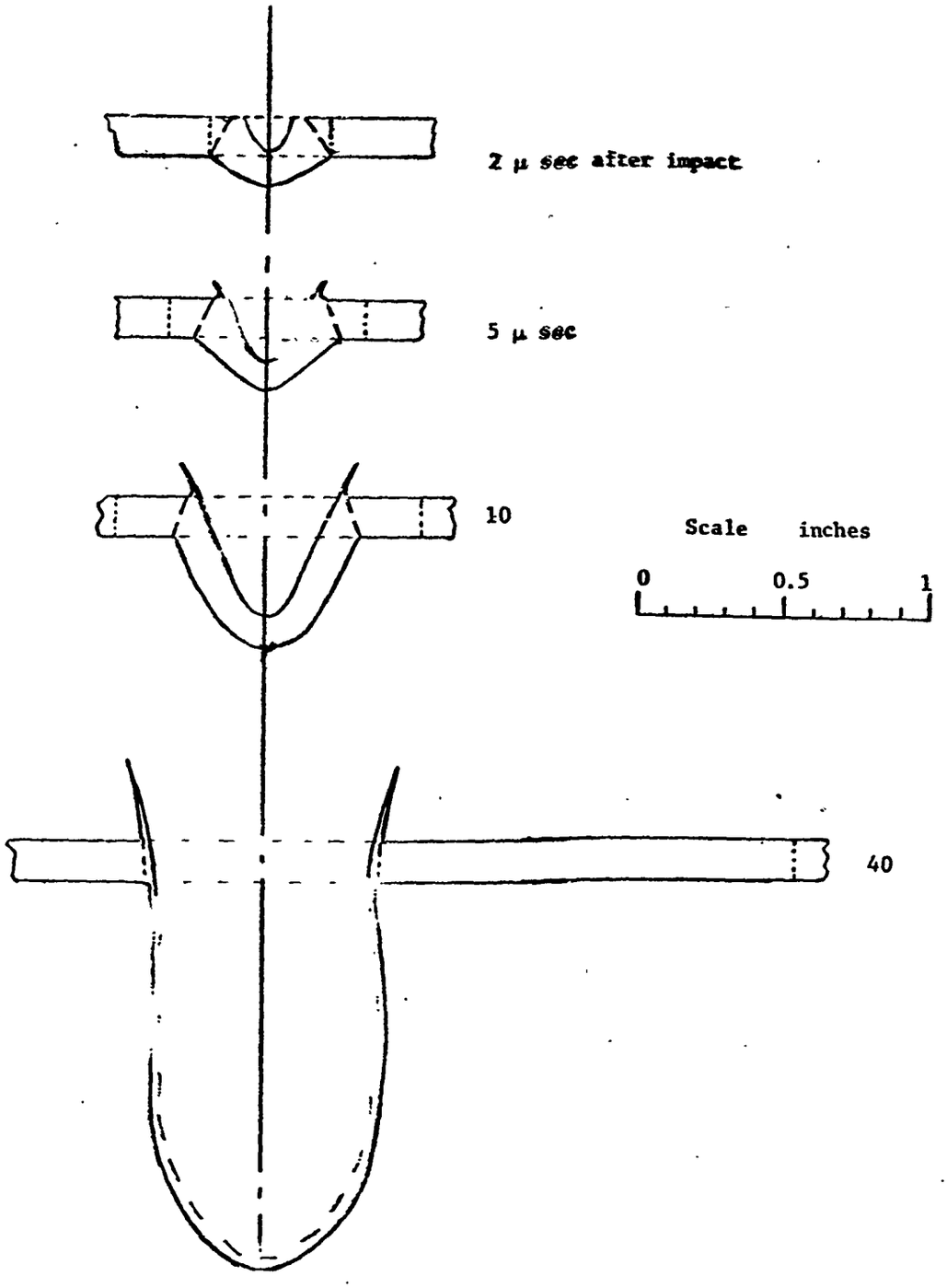

Fig. 27. Flow and wave propagation of 0.132 inch target.

V. SUMMARY AND CONCLUSIONS

A study of the perforation process was made by carefully observing a sequence of shadowgraph pictures. The initial spray velocity from the front of the target was measured and found to vary from 1.5 to 10 km/sec. These velocities are much higher than those reported previously. The difference is due to the fact that the initial spray is observed here and was neglected in earlier work. Shock wave propagation was observed and from measured free-surface velocities, the shock pressure was computed. Pressure was found to decay more rapidly than 1/r. Plastic flow was observed and its propagation measured. Considerable time lag was observed between the passage of the initial wave and the beginning of large-scale flow.

This work should be extended to other materials and different velocities. The results obtained illustrate the utility of the techniques developed here and have provided preliminary data for one material. They serve as a necessary basis for any future theoretical development.

APPENDIX A

EXPERIMENTAL DATA

Shot No.	Target Thickness inch	Counter Time μ sec	Projectile Velocity km/sec	Delay Set in μ sec	Delay from impact from scope	Storage Capacitor (kv)	Vacuum (Micron Hg)	Hole Diam. (inch)	Mass Loss (gm)
1	0.4250	5320	1.535	90	-2	7.9	180	.8124	9.078
2	0.4166	5101	1.585	98	2	7.8	250	.8097	9.1077
3	0.4361	5271	1.54	100	10	7.9	170	.8251	9.8755
4	0.4458	5460	1.491	125	25	7.9	230	.8371	8.3585
5	0.4356	5609	1.46	150	50	8.0	230	.8210	11.00
6	0.4161	5429	1.501	180	80	7.9	250	.8712	7.3586
7	0.4259	5410	1.502	250	148	7.9	200	.8433	12.305
8	0.4355	5405	1.506	240	200	7.9	200	.8364	11.76
9	0.4159	5127	1.59	300	220	7.9	250	.8565	13.098
10	0.4161	5475	1.43	330	250	7.9	230	.8316	8.088
11	0.436	Not available		95	-2	8	250	.8275	10.4265
12	0.4264	Not available		105	10	8	180	.8339	9.062
13	0.2655	5420	1.502	100	0.1	7.8	250	0.7826	9.9318
14	0.2711	5416	1.501	105	2	7.8	250	0.7688	9.587
15	0.2665	5407	1.508	103	4	8	210	0.7692	9.0526
16	0.2694	5326	1.532	117	15	8	180	0.7665	8.695
17	0.2696	5286	1.545	120	20	7.8	230	0.7916	9.9318
18	0.2701	5402	1.510	170	70	8	270	0.7931	9.2073
19	0.2661	5401	1.510	180	80	7.8	200	0.7891	9.2005
20	0.2650	5403	1.51	215	110	7.8	270	0.7760	9.4673
21	0.2652	5428	1.502	220	115	8	200	0.7782	9.4607
22	0.2648	5411	1.501	230	135	7.8	200	0.7895	9.4650
23	0.2665	5355	1.52	250	150	7.9	220	0.7826	9.0447
24	0.2652	5204	1.555	330	230	8	150	0.7698	10.1280
25	0.2672	5267	1.55	135	Not Avail.	8	190	0.7723	8.476
26	0.2661	5485	1.49	190	Not Avail.	8	250	0.7804	10.4818
27	0.1319	5216	1.551	100	2	7.8	200	0.6332	3.3140

EXPERIMENTAL DATA (cont.)

Shot No.	Target Thickness inch	Counter Time μ sec	Projectile Velocity km/sec	Delay Set in μ sec	Delay from impact from scope	Storage Capacitor (kv)	Vacuum Micron Hg	Hole Diam. (inch)	Mass Loss (gm)
28	0.1326	5313	1.535	110	12	7.9	180	0.6405	3.6083
29	0.1318	5248	1.56	130	27	7.9	200	0.6390	3.494
30	0.1322	5252	1.552	145	48	7.9	200	0.6490	3.5383
31	0.1319	5298	1.54	170	75	8	200	0.6501	3.43
32	0.1319	5288	1.544	180	90	8	250	0.6591	3.4705
33	0.1312	5200	1.568	240	130	7.9	270	0.6010	3.4175
34	0.1314	5291	1.54	250	145	8	180	0.0461	3.6265
35	0.1315	5401	1.51	330	235	8	270	0.6472	3.3410
36	0.1328	5290	1.54	300	200	8	280	0.6471	3.7090
37	0.1311	5460	1.492	----		8	210	0.6469	3.6480

BIBLIOGRAPHY

1. Werner Goldsmith, Impact, Edward Arnold LTD., London, 1960.

2. Don Humes, R. N. Hopko, and W. H. Kinard, "An Experimental Investigation of Single Aluminum 'Meteor Bumpers'," Proceedings of the Fifth Hypervelocity Impact Symposium, Vol. 1, Part 2, 1962, p 61.

3. J. H. Kineke, Jr., "Observations of Crater Formation in Duetile Materials," Proceedings of the Fifth Hypervelocity Impact Symposium, Vol. 1, Part 2, p. 339.

4. E. P. Palmer, "Perforation of Multi-Layer Plates," First and Second Quarterly Reports, Contract AF 04(694)-259, High Velocity Laboratory, University of Utah, Salt Lake City, Utah, Sept., Dec. 1962.

5. R. W. Watson, "The Perforation of Thin Plates by High Velocity Fragments," Proceedings of the Fifth Hypervelocity Impact Symposium, Vol. 1, Part 2, 1962, p. 581.

6. R. Vitali, K. R. Becker, and R. W. Watson, "Perforation of Finite Targets by High Velocity Projectles," Proceedings of the Fifth Hypervelocity Impact Symposium, Vol. 1, Part 2, 1962, p. 593.

7. Wm. S. Partridge, C. R. Morris, and M. D. Fullmer, "Perforation and Penetration Effects of Thin Targets," Proceedings of Third Symposium on Hypervelocity Impact, Vol. 1, 1959, p. 83.

8. C. E. McDermott, E. T. Cannon, and R. W. Grow, "Temperature Studies and Effects in Perforation of Thin Aluminum Targets," Technical Report UU-3, University of Utah, May 15, 1959.

9. E. P. Palmer, Third Quarterly Report, Contract AF 04(694)-259, High Velocity Laboratory, University of Utah, March 1963.

10. J. M. Walsh, M. H. Rice, R. G. McQueen, and F. L. Yarger, "Shock Wave Compression of Twenty-Seven Metals. Equation of State of Metals," Phys. Rev. Vol. 108, 1957, p. 196.

11. G. E. Durall, "Some Properties and Applications of Shock Waves in Metals," Response of Metals to High Velocity Deformation, P. G. Shewmon and V. G. Zackay, Interscience Publishers, New York, July 1960.

12. F. S. Minshall, "The Dynamic Response of Iron and Iron Alloys to Shock Waves," Ibid. p. 10, July 1960.

13. W. L. Brown, "Precision Photography of High-Velocity Impact," A Bachelor's Thesis, Department of Electrical Engineering, University of Utah, 1963.

14. E. P. Palmer, N. P. Bailey, C. E. McDermott, G. H. Turner, E. Moreno, S. M. Taylor, and J. C. Bryner, "Fourth Quarterly Report and Final Report, Contract AF 04(647)-942," Technical Report UU-9, University of Utah, High Velocity Laboratory, June 1962, p. 30.

15. J. H. McMillen, "Shock Waves Pressures in Water Produced by Impact of Small Spheres," The Physical Review, Vol. 68, No. 9-10, November 1945, p. 198.

16. E. Moreno, "Pressure and Density Measurement in the Crater Region," A master's thesis, Department of Electrical Engineering, University of Utah, June 1962.